UNIVERSITY OF HOHENHEIM

Institute of Crop Science (340)

AG Cropping Systems and Modelling

Prof. Dr. Simone Graeff-Hönninger

Combining Remote Sensing and Crop Modeling Techniques to Derive a Nitrogen Fertilizer Application Strategy

Dissertation submitted in fulfillment of the regulations to acquire the degree "Doctor scientiarum agriculturae" (Dr.sc.agr. in Agricultural Sciences) to the Faculty of Agricultural Sciences

by

Georg Röll

Born in Regensburg, Germany

Stuttgart

October 2020

This thesis was accepted as a doctoral thesis (Dissertation) in fulfillment of the regulations to acquire the doctoral degree “Doctor scientiarum agriculturae” by the Faculty of Agricultural Sciences at University of Hohenheim on **April 1, 2020.**

Dean Faculty of Agricultural Science: Prof. Dr. Ralf Vögele

Date of the oral examination: August 6, 2020

Examination Committee

Chairperson of the oral examination: Prof. Dr.-Ing. Stefan Böttinger

Supervisor: Prof. Dr. Simone Graeff-Hönninger

Co-Supervisor: Prof. Dr. Hans-Peter Kaul

Additional examiner: Prof. Dr. Torsten Müller

Table of contents

List of abbreviations and acronyms

%	Percent
°C	Degree centigrade
°E	Degree east, longitude
°N	Degree north, latitude
DSSAT	Decision Support System for Agrotechnology Transfer
DüV	Fertilizer Application Ordinance
EC_a	Soil Electrical Conductivity
ha	Hectare
L.	Linné
LAI	Leaf area Index
MM	Multi-Modeling
N	Nitrogen
NAPS	Nitrogen Application Prescription System
PAR	Photosynthetically active radiation
PF	Precision Farming
PLSR	Partial Least Squares Regression
RMSE	Root mean square error
t	Ton
VI	Vegetation Index

List of figures

1 Introduction

1.1 Current Status and Future Challenges for Food Production

Global warming is one of the greatest challenges mankind will face in the future and the effects are widely acknowledged in the scientific community [1]. In the Paris agreement, the goal was defined to limit the increase in temperature to 1.5° C above the preindustrial level [2]. This goal collides with the steady increase in energy demand, for example for daily living or for food production [3] (artificial nitrogen fixation) met by burning fossil fuel, and therefore, it seems to be out of reach [4]. Several researchers projected an increase in the global average temperature by 3.0°C by the end of the century, if the current greenhouse gas emissions continued [5]. If this scenario becomes reality, it will have a strong effect on species extinction, environmental degradation, and food security [6, 7]. This will lead to enormous environmental problems that range from rising sea levels due to glacier meltdowns [6], which will threaten one billion people in cities near the coast and will destroy up to one-third of all farmland on earth [8]. Changes in rainfall pattern and the increase of the maximum temperature will lead to a decrease in yield and production of agricultural goods. Moreover, during the winter period, the temperature increase [9, 10] will cause more favorable conditions for insects and diseases consequently reducing crop yield [11, 12].

Besides these challenges, the world's population is rising and expected to reach 9.8 billion by 2050 [13]. This will result in an increased food demand [14]. To put it in numbers: This will lead to an human population-to-land ratio of 1.96 persons per agricultural-hectare, which will be doubled compared to 1800, if the agricultural land stays at the 2010 level [14]. At the same time, an increase in wealth results in a diet change to higher resource-consuming food production, which means that the consumption changes from grains, legumes, fruits, and vegetables to processed food such as meat, refined sugars, alcohols, refined fats, and oils [15]. Consequently, the requirements for current and future human population causes an increasing pressure on agricultural production [16]. This vicious circle leads to the expansion of the cropland area by deforestation in the tropical regions for cost-efficient production of oil palm [17], soybean [18] or for cattle ranching [19]. These regions are the home of fragile natural habitats and biodiversity [20, 21]. Finally, deforestation itself results in major carbon emissions [22] and amplifies global environmental changes [23]. There are many studies that propose different measures against carbon emission such as afforestation and large-scale renewable energy production mitigating the effects of global warming [24, 25]. These measures can play a critical role in preserving carbon in the soil; however, the problem of ensuring food security [26] remains to be resolved.

Increasing agricultural production will have a more severe environmental impact [27]. Today, agricultural production is responsible for 35% of global greenhouse gas emissions [27], threatens land degradation [28] and freshwater [29] due to excessive land use and over-fertilization [30].

In the USA, China, Northern India, and Western Europe there is still an excessive application of nutrients [31]. There are reports, that 10% of the world’s croplands release more than 30% of the global nitrogen (N) and 40% of the phosphorus unused in the environment [27]. These losses

are the results of an increase of 500% since 1940 in fertilizer use [32, 33] and the doubling of land irrigation [34].

Beyond these negative environmental implications, global crop production increased extensively in the last couple of decades due to the green revolution, which has started in the mid-1960 [27,35]. The characteristics of the green revolution are new breeding techniques, the use of mineral fertilizers and the application of pesticides to increase crop yield [36]. This key technology has enabled farmers to produce cheap food with less labor and to reduce the magnitude of people suffering from hunger and undernourishment by 50% since the 1960s [37]. The use of agrochemicals, breeding, irrigation, management [38] and the extension of land area used for production [35, 39] were the most important factors for increasing yield in the last 50 years. However, the following figures show that these procedures have reached their limits. Between 1965 and 1985, the global crop production increased by 56% [27]. In the equivalent period from 1985 to 2005, crop production only increased by 20% [27]. In the last few years, there were several reports of stagnation of yield and production in different regions around the world [40–44]. The reasons for stagnation are often suspected to be the reaching of an upper limit to genetic improvements [45], reduction in fertilizer application due to environmental policy [41], pesticide resistance, a lack of new compounds [46] and the negative effects of climate change [12].

Especially, an increase in fertilizer application seems feasible at first glance to increase crop production, but it is clearly connected to environmental issues such as N leaching [32], and N oxides release from soils [47] which is considered as an important source of N oxides emissions. Globally more than 75% of N_2O emissions are related to N losses from the agricultural sector and it is suspected that one-third of these gas emissions occur after loss due to leaching or other factors from agricultural systems [48]. These side effects can be mitigated by adjusting the amount of fertilizers applied and the timing of the application [49]. Ma et al. [49] reported that an increase in fertilizer application rates from 90 to 150 kg ha^{-1} N resulted in a slight increase in yield but doubled N_2O emissions. However, despite this knowledge, there are reports of N application ranging over 360 kg ha^{-1} N for winter wheat in the North China Plain [50] whereas rates of around 130 kg ha^{-1} N seem to be optimal [51]. Asia is growing very fast and around 50% of the global ammonia production is used in that region, which results in an increasing environmental burden [52]. This is also realized by several scientists who are looking for high-yield crops with less environmental impact [53].

The problem of eutrophication is also prominent in the United States where increased riverine N contents lead to a degradation of ecosystems in most estuaries [54]. A national management goal and an action plan were released in order to reduce by 45% the riverine N discharge transported by the Mississippi and Atchafalaya River Basins into the Gulf [55,56]. These problems were realized by national governments and Bills for protecting the environment were introduced by China and the United States of America [57].

The European Union is also facing problems of escaping N in the environment through leaching into the ground and surface water. In the last 30 years, different strategies such as the Water Framework Directive 2000/60/EC [58] and Nitrates Directive 91/676/EEC [59] were developed to counteract these problems. The main source of nitrate pollution has agricultural

origin [60]. Measures were developed and included in the directives aiming at the reduction of escaping nitrate in ground and surface water by limiting the maximum N application and establishing a limit of 50 mg l^{-1} nitrate for drinking water [60]. Almost three decades after these directives were issued, no significant reduction in nitrate release into groundwater occurred. More than 26% of the groundwater bodies in the EU showed an increasing trend in N pollution [61]. In Germany, the main problem is nitrate pollution of groundwater in the areas of Bavaria, Lover Saxony and North Rhine-Westphalia [62].

In 2007, the national Fertilizer Application Ordinance (DüV) was adopted in order to meet the requirements of the EU Nitrogen Directive, [62]. New rules for regulating the limits on organic and mineral fertilizers were developed within the DüV and they came into force in 2017. This ordinance included the maximum organic N at 170 kg N ha^{-1} and an exception of 230 kg N ha^{-1} for winter wheat crops. The nutrient balance of N application is limited to 50 kg N ha^{-1} and has to consider a fertilizer planning to meet the obligation of the Nitrate Directive [63, 64].

Nonetheless, these measures for the reduction of N pollution failed and Germany was unable to achieve the objectives of the Nitrogen Directive. An official warning letter was sent in July 2019 to the German ministry of environment by the European Commission. This letter represents a new chapter in an ongoing dispute between the European Commission and the German Government over the alarming quantity of nitrate present in water bodies [65]. There are reports that in 2015 only 7% of all water bodies in Germany were in good or very good eco-friendly conditions as defined by the directive [65]. Germany is now facing an accusation by the European Court of Justice of having violated the Nitrate Directive, which could have end up in the country paying a €850,000 fine per day [62, 65, 66]. New ideas are discussed to adapt N application to soil conditions in order to reduce the potential of leaching. This will result in a reduction of N application by maintaining the current yield level. However, new regulations and measures came into force in May 2020 to avoid a penalty from the EU. In conclusion, this clearly shows that agriculture in Germany, the EU and worldwide is at a crossroads and that new measures for environmental friendly crop production, and especially for fertilizer application, have to be taken to enhance crop production without harming the environment.

To encounter these environmental issues, the German Federal Environment Foundation (Deutsche Bundesstiftung Umwelt – DBU) funded this solution-oriented research project and the evolved dissertation within the foundation's special program "Reduction of the emissions of N-containing substances in environmental compartments."

Environmental pollution due to the emission of N-containing substances outshines other environmental problems. Despite the fact that N is an irreplaceable nutrient for living organisms, its escape into different environmental compartments has to be avoided. Currently, the surplus of the German agriculture is around 100 kg ha^{-1} per year. The aim of this special is to develop a variety of measures in order to address the reduction of different N emissions sources.

Within the framework of this special program research the following areas are funded:

- Prevention of the escape of N from the barn and manure storage tanks;
- preventive actions in protein feeding of animals to reduce N emissions;
- improvement of manure application by better adjustment of timing and spatial application; and
- recovery of N-containing substances from wastewater.

In addition, the topic and the research questions of this dissertation, that is, the development of measures for an efficient use of soil-borne N and the improvement in N application on a temporal and a spatial scale, is within the scope of this special program.

1.2 New Technologies for Sustainable Food Production

The digital revolution made enormous progress in all parts of our daily life ranging from big data creation, to deep learning and artificial intelligence [67]. It also exhibits a high potential in the agricultural application called "digital agriculture," "agriculture 4.0" or "smart farming," comprising big data and precision technology systems in agriculture [68, 69]. It pays attention to the possibilities of digital agriculture by automizing of data-intensive precision technologies with the purpose of reorganizing the agricultural system towards more food production on less land and with lower inputs (especially fertilizers and pesticides application) [70,71]. Different projects are going on across the globe ranging from weed identification via unmanned aerial vehicles [72] to using Microsoft's Cortana Intelligence Suite for determination of the best planting dates for crops worldwide [73]. Digital technologies can also help to understand crop environment interaction (phenotyping), to isolate breeding traits, and to estimate crop yield [74].

In general, precision farming (PF) is within the top 10 revolutions in agriculture witnessed in the past 50 years [75]. Its applications range from assisted steering systems to yield monitoring [76], field documentation, precise manure application [77], or controlled traffic farming [78] and it is mainly based on global positioning system (GPS) and geographic information system (GIS) [79]. PF includes the management of farm inputs by applying the right management practices at the right time and the right location [80]. This leads to an improvement in crop productivity and better environmental production [79, 81]. However there are also critical reports that the environmental and economic benefits of the PF technology are not proven [82]. Primarily, PF has to take into account different types of variability within a field, which can be categorized into six groups [79] (Figure1).

In order to take account of the types of in-field variability, the field can be separated into grids that are either rectangular or in other shapes based on slope and soil elevation [83]. These grids represent the smallest units of homogeneous treatment in terms of tillage, sowing, and pesticide as well as the **fertilizer application**.

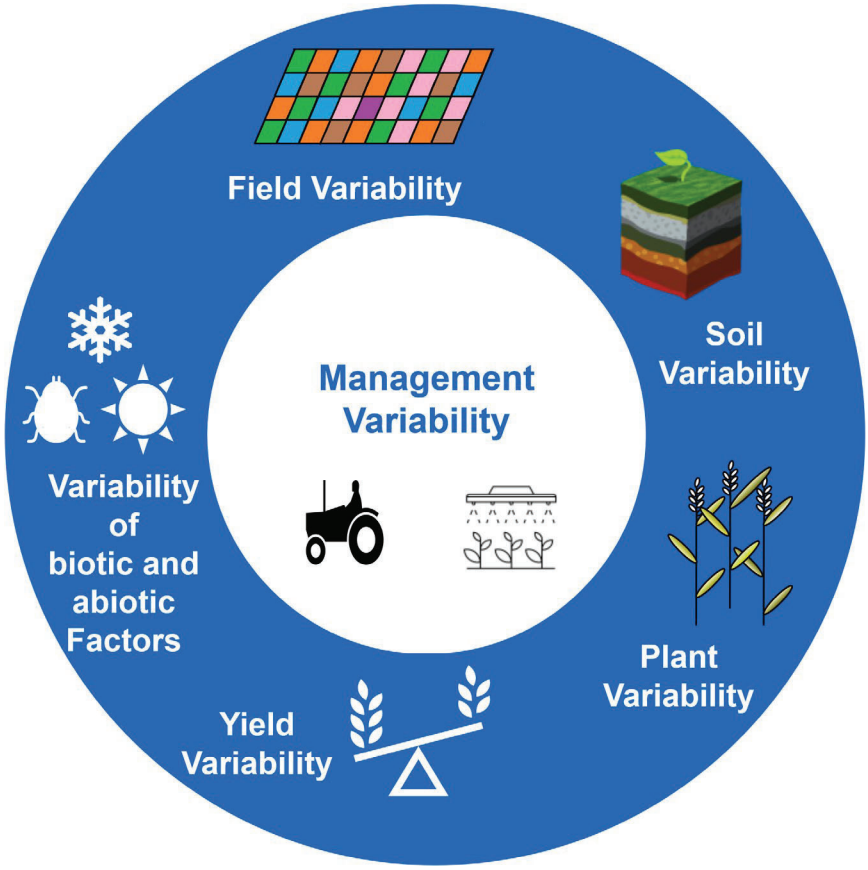

Figure 1: Different types of variability that precision farming has to consider in a field.

1.2.1 Sensor and Remote Sensing Techniques

In the last 20 years, many of sensors and techniques were developed to account for in-field variability [79]. The sensors range from soil conductivity measurements to, supersonic sensors, cameras, spectral sensors, and mass flow sensors [84–87]. For example, yield variability can be mapped within a field by mass flow sensors that are used in the combine [87]. Soil mapping by measuring electric soil conductivity also became popular in the last decades. In general, soil conductivity is strongly influenced by clay content, water content, organic matter, and cation exchange capacity, which reflect soil properties [88, 89]. In the literature, there are several existing correlations between soil properties and yield [90]. Besides these findings, there are also many reports of farmers who have been using yield monitoring for the last ten years, but do not know how to deal with these datasets, and therefore, these data are unusable for them [68, 91]. The reason for this can be seen in the fact, that measured crop yields do not always follow the trend in the soil´s chemical and physical characteristics. The spatial yield variability is strongly dependent on interactions among abiotic and biotic factors [92–94]. Therefore a suitable system should be developed in order to use yield-monitoring as well as soil data and transform these datasets into decision-making information [95]. The obstacle to dealing with all these types of variability is that they overlap and influence each other. This means that yield variability is the result of field variability, soil variability and the variability of biotic and abiotic factors that are not commonly

collected on a normal farm and may explain more than 50% of yield variability across sites and years [96, 97].

A technique for the detection of variability during the vegetation period on specific dates and measuring specific traits within the field is needed. Spectral sensors developed to measure the trait in season variability types (plant chlorophyll content, N uptake, biomass, or LAI) and can help to adjust N fertilizer applications based on their developed algorithms [98, 99].

In general, spectral sensors are non-contact devices and they are based on the electromagnetic reflectance between 300 and 2500 nm wavelength that can be categorized in multispectral or hyperspectral sensors which differ mostly in the number of spectral bands. Spectral accuracy increases from multispectral to hyperspectral and delivers more information [100].

Reflectance from vegetation is mainly characterized by the absorption of radiation due to plant pigments in the visible spectrum between 400 – 700 nm (Figure 2) [101]. The most important pigments for photosynthesis are chlorophyll a and chlorophyll b, where the maximum absorption is at 430 and 660 nm for chlorophyll a and 450 and 650 nm for chlorophyll b. In addition, pigments such as carotenoids and anthocyanins also play an important role in light absorption in the visible range [102]. Vegetation is further characterized by a high reflectance in the near-infrared region between 700 and 1000 nm (Figure 2), which is the result of canopy structure (mesophyll) and leaf density effects [103].

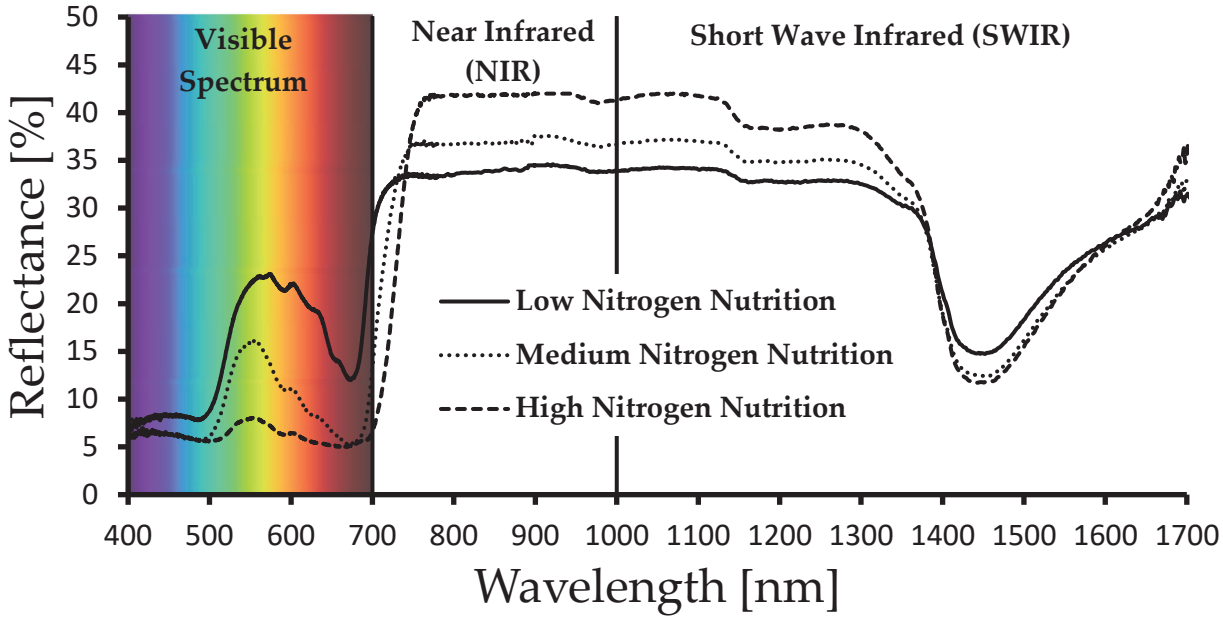

Figure 2: Reflectance spectrum of a wheat plant at three different nitrogen nutrition levels (own measurements, adapted and changed after Zhao et al. [104]).

If plants, for example, have an insufficient N supply, the reflectance normally increases in the region at 550 nm and broadens to the red edge. These changes result in a yellowing of plant leaf which is visible [105]. A different reaction can be observed in the near-infrared region where

limited N supply causes a reduction in reflectance [106] which is induced by changes in the cell structure [103] (Figure 2).

Most of the developed spectral indices focus on the so-called "red edge inflection point" where ratios (commonly known as indices) between the visible and near-infrared region are calculated [107]. Reflectance information can be collected via spaceborne, airborne or ground-borne sensors [108]. Different commercial spaceborne products, for example QuickBird or ground-borne sensors for example CropSpec, Fritzmeier Isaria, Crop Circle ACS-430 or N-Sensor, are available [109,110].

The N-Sensor (Yara, Germany), for instance, can help to adjust the N application. Several researchers obtained satisfying results by using the N-sensor technology only when N was the main growth-limiting factor [111–113]. While chlorophyll content shows a strong correlation with N availability, [114] the reflectance characteristic of the chlorophyll can also be affected by disease infection, under drought stress or under other different nutrient deficiencies [103, 115, 116]. The interpretation of spectral reflectance and the distinction between different nutrients, water status, or disease infection can be a difficult task [103]. Spectral reflectance correlates with many different effects and it is hard to reproduce the "whole picture" of the plant status within a given field.

1.2.2 Crop Models

Whereas sensor techniques are helpful in measuring current N content, crop models may be help to predict N demand. Crop models were developed during the last decades for various purposes such as analyzing yield gaps, for decision support and for shortening time-consuming and expensive field experiments [117]. In general, crop models are based on the concept of crop physiological ecology [118]. This includes the dynamic in the applicability, mechanism, and comprehensiveness, which can be used to simulate the influence of soil, weather, genetics and management on crop growth and development [119, 120]. The crop development approach encompasses the crop phenology like leaf age increment and the consecutive appearance of plant organs such as roots, leaf blades, leaf sheaths, stem internodes, tillers, and ears [121]. These processes are represented in the models as algorithms, that express the connection between plant processes such as partitioning, biomass growth, respiration, plant water uptake, photosynthesis and environmental variables like daily temperature, photoperiod, soil water availability or N [122].

These processes can be expressed in various complexities. Different crop models have been developed, ranging from simple structures like monolayer canopy to, constant specific leaf area and on daily assimilate partitioning for example CropSyst and SSM or to more complex models such as APSIM and DSSAT, where much more variables can be simulated and influenced [123, 124].

The current DSSAT 4.7 version represents a modeling platform including more than 42 models ranging from oil crops (sunflower, etc.) to legumes (soybean, etc.) and to cereals such as maize, barley, and wheat. Within this environment, all models use the same input file structure [125]. All models are based on the radiation use efficiency approach on a daily or hourly basis to

calculate the assimilate production, which can be distributed by a sink-driven approach that can be modified by temperature. Assimilates will be provided to the expanding tissue and root system and maintained. For the cereals models (CERES, NWheat, and Cropsim), the assimilation partitioning into different plant parts follows two major principles: **vegetative growth** and **grain filling period** [126].

During **vegetative growth,** shoots have a higher priority than that of roots for assimilates if sufficient water and nutrient supply is present. Under water- or nutrient limitations the roots, however, have a higher priority.

During **grain filling,** the grains are the main sink for assimilate distribution. Assimilates for filling the grains come from two pools, active photosynthesis or assimilates stored in the plant. Water or nutrient limitations have small effects on the grain filling process [126].

This model structure gives the opportunity to simulate grain yield, biomass growth, crop water, and N uptake very accurately under different environmental conditions and proves to be a useful tool for evaluation of different management strategies [127, 128]. The models were tested in the past over a wide range encompassing yield forecast during the vegetation period [129], irrigation management [130], N management optimization [131], or site-specific simulations [132]. The first attempt for coupling crop models with remote sensing was also carried out and seen as a complementary tool to understand variability within a field [133, 134]. Normally, crop models are limited by the lack of information about different variables (yield, field, soil, crop, biotic and abiotic factors, management etc.) [135]. This causes uncertainties in simulations and may reduce the overall model accuracy. Thorp et al. [135] suggested an approach of using remote sensing techniques for periodically updating the model to account for variability in the field, thus increasing modeling accuracy.

1.2.3 Coupling Remote Sensing and Crop Modeling to Address Over-Fertilization?

In general, crop models are a simplified description of the natural system which can lead to a decrease in modeling accuracy under certain circumstances [136]. By updating state variables via remote sensing, model simulation could potentially be improved. However, several researchers [134, 135, 137] showed that coupling remote sensing techniques with crop modeling was not as simple as it seemed. Crop models have to be able to simulate unique spatial units, where management, soil, and meteorological information are required on a spatial scale [135]. Crop models deal with defined growth stages and clearly defined plant N contents that have to be derived from spectral signatures. These measurements are heavily dependent on growth stages, which means that early in the season when, ground cover is very low, the measurements can lead to insufficient results [138, 139]. In addition, spectral reflectance might differ between growth stages and under different leaf angels [139]. Later on, during the season, remote sensing readings may suffer from a saturation phenomenon that can influence the results [140, 141]. This influence of measurement errors was not considered in previous combinations of remote sensing data and crop models [142, 143].

Coupling crop models and remote sensing requires the acquisition of reliable and accurate data for plant N content in order to use the latter as a "nitrogen prescription system." There is a

lack of knowledge about the determination of plant N via remote sensing techniques, especially if the differentiation between leaves and positions on different leaves is necessary. Only if these measured values were valid, would an adjustment of the crop model be useful.

An update of the model variables for more than one crop model exhibits the possibility of greater simulation accuracy and a more comprehensive understanding of spatial variability. Several crop models have been used by different researchers to evaluate the modeling performance of a multi-model (MM) simulation. MM simulations clearly show greater modeling accuracy than that obtained by using more than one model [144–146]. The most crucial part of an MM strategy is the exhaustive calibration procedure. Normally, it requires a well-trained user to insure satisfying results [147]. Developing an automated calibration procedure would eliminate the user's bias and insures a standardized calibration of the model.

While updating the plant parameters of the crop model via remote sensing for the adaptation of N application, the presence of leaf disease cannot be overlooked [148]. Leaf disease in general lowers the potential yield by modifying the photosynthetic leaf area or by "stealing" assimilates [149]. Lowering the yield potential goes hand in hand with an adjustment of N application rates. The current DSSAT Wheat crop models [125] do not have the ability to account for any disease infection. This limits the applicability of "nitrogen prescription" only to scenarios without disease infections. In reality, scenarios in field trials and on the farm level without any disease infection are very rare and can only be achieved by frequent pesticides spraying [150]. This shows the necessity of integrating a disease routine into the crop model to allow the simulation of plant leaf disease and their effects on yield.

1.3 Outline and Objectives

The overall aim of this doctoral thesis is to develop a strategy on coupling spectral sensors and crop models to obtain N prescriptions for wheat in different disease infections. Crop models are suitable tools to simulate yield while considering genetic and environmental interactions based on the calibrated datasets. Spectral reflectance sensors are able to collect current plant information. This information can be used to update model`s state variables, thereby increasing modeling accuracy.

The specific objectives of this thesis are:

(i) To test the influence of different leaves and positions on the leaf on the reflectance of wheat plants cultivated under different N levels and under drought stress;
(ii) to incorporate leaf disease into a DSSAT Wheat model to enable the simulation of the impact of leaf disease on yield;
(iii) to evaluate an automatic calibration procedure in a multi-model approach for winter wheat to increase modeling accuracy and eliminate the subjectivity factor in model calibration; and
(iv) to use a multi-model approach to improve overall modeling accuracy.

In order to achieve the above objectives, different field trials were carried out during the period 2015 – 2018 at the experimental station "Ihinger Hof" of the University of Hohenheim and they included two greenhouse trials (2018). In addition, a two-year dataset (2010 – 2011) from Argentina and a one-year dataset (2005) from "Ihinger Hof" were used to develop the necessary model algorithms.

The **first Publication** presents the influence of the leaf layer and position on the leaf for plant N content determination via spectral reflectance. It was evaluated whether remote sensing measurements were valid on the canopy scale for plant N content determination on each wheat plant leaf.

Publication two shows how disease ratings can be integrated into crop models which normally results in a change in yield and, consecutively, in a change of the N fertilizer application strategy. Disease ratings can be generated by sensors or can be done visually.

The **third Publication** deals with the development of a multi-model approach. The approach was developed and tested with three models included within the DSSAT shell by using an automated calibration method to insure objective calibration.

The presented papers in Publications I - III have been already been published. Thus, the following chapters "Publications" include the details of each publication, which provide the overall frame of the present dissertation.

2 Publications

The present cumulative thesis consists of three papers. All papers are published in international, peer-reviewed journals. The articles correspond to the Chapters I-III of the present thesis. For citations, please use the references illustrated below.

Publication I

Röll, G.; Hartung, J.; Graeff-Hönninger, S. Determination of Plant Nitrogen Content in Wheat Plants via Spectral Reflectance Measurements: Impact of Leaf Number and Leaf Position. *Remote Sens.* 2019, *11*, 2794.

Impact factor: 4.12

Publication II

Röll, G.; Batchelor, W.D.; Castro, A.C.; Simón, M.R.; Graeff-Hönninger, S. Development and Evaluation of a Leaf Disease Damage Extension in Cropsim-CERES Wheat. *Agronomy* 2019, *9*, 120.

Impact factor: 2.26

Publication III

Röll, G.; Memic, E.; Graeff-Hönninger, S. Implementation of an automatic time-series calibration method for the DSSAT wheat models to enhance multi-model approaches. *Agronomy Journal,* 2020;1-33.2020;1–22.https://doi.org/10.1002/agj2.20328.

Impact factor: 1.81

3 Publication I

Determination of Plant Nitrogen Content in Wheat Plants via Spectral Reflectance Measurements: Impact of Leaf Number and Leaf Position

Röll, G.; Hartung, J.; Graeff-Hönninger, S. Determination of Plant Nitrogen Content in Wheat Plants via Spectral Reflectance Measurements: Impact of Leaf Number and Leaf Position. *Remote Sens.* 2019, *11*, 2794.

Various publications are focusing on N determination in agricultural crops via spectral remote sensing techniques. During the past decades, a broad range of vegetation indices based on spectral reflectance were developed on the canopy scale. These developed indices do not differentiate between different leaves or leaf layers. Little information is available for shrub plants where varying chlorophyll contents in different leaf layers have been reported. For cereal plants, no information is available. This raises the question if current measurements on the canopy scale are sufficient or if differentiation between leaf layers can improve the determination of plant N content via spectral reflectance measurements.

remote sensing

MDPI

Article

Determination of Plant Nitrogen Content in Wheat Plants via Spectral Reflectance Measurements: Impact of Leaf Number and Leaf Position

Georg Röll [1,*], Jens Hartung [2] and Simone Graeff-Hönninger [1]

1 Department of Agronomy, Institute of Crop Science, University of Hohenheim, 70599 Stuttgart, Germany; Simone.graeff@uni-hohenheim.de
2 Department of Biostatistics, Institute of Crop Science, University of Hohenheim, 70599 Stuttgart, Germany; jens.hartung@uni-hohenheim.de
* Correspondence: georg.roell@uni-hohenheim.de; Tel.: +49-711 459-22380

Received: 9 September 2019; Accepted: 22 November 2019; Published: 26 November 2019

Abstract: The determination of plant nitrogen (N) content (%) in wheat via destructive lab analysis is expensive and inadequate for precision farming applications. Vegetation indices (VI) based on spectral reflectance can be used to predict plant N content indirectly. For these VI, reflectance from space-borne, airborne, or ground-borne sensors is captured. Measurements are often taken at the canopy level for practical reasons. Hence, translocation processes of nutrients that take place within the plant might be ignored or measurements might be less accurate if nutrient deficiency symptoms occur on the older leaves. This study investigated the impact of leaf number and measurement position on the leaf itself on the determination of plant N content (%) via reflectance measurements. Two hydroponic experiments were carried out. In the first experiment, the N fertilizer amount and growth stage for the determination of N content was varied, while the second experiment focused on a secondary induction of N deficiency due to drought stress. For each plant, reflectance measurements were taken from three leaves (L1, L2, L3) and at three positions on the leaf (P1, P2, P3). In addition, the N content (%) of the whole plant was determined by chemical lab analysis. Reflectance spectrometer measurements (400–1650 nm) were used to calculate 16 VI for each combination of leaf and position. N content (%) was predicted using each VI for each leaf and each position. Significant lower mean residual error variance (MREV) was found for leaves L1 and L3 and for measurement position on P3 in the N trial, but the difference of MREV between the leaves was very low and therefore considered as not relevant. The drought stress trial also led to no significant differences in MREV between leaves and positions. Neither the position on the leaf nor the leaf number had an impact on the accuracy of plant nitrogen determination via spectral reflectance measurements, wherefore measurements taken at the canopy level seem to be a valid approach.

Keywords: wheat; spectrometer; nitrogen content; hydroponics; nitrogen treatments; growth stages; vegetation index

1. Introduction

Nitrogen (N) is a key plant nutrient commonly applied to increase yield and crop quality in agricultural systems [1]. However, the production of nitrogenous fertilizer creates large amounts of greenhouse gases [2]. Environmental pollution can also occur after excessive nitrogen application if the applied fertilizer amounts exceed plant demand [3]. Under unfavorable conditions, potential greenhouse gases can escape from soils or are transported to groundwater through leaching [4]. These side effects strongly depend on the amount of N fertilizer applied [5]. In Europe, the Water

Framework Directive [6] and Nitrates Directive [7] joined forces to lower the leaching potential. This is accomplished by reducing the N amount applied and by maintaining the right amount of N under different growing conditions (drought, or well-saturated soil, for example).

Over the last 30 years, concepts of precision farming (PF) [8] have been developed that help farmers to understand yield variability within their fields in order to adjust N application. Generally, PF uses different technologies like global positions systems, yield mapping, soil conductivity measurements [9] or non-contact spectral sensors for monitoring and determination of e.g., N status of different field crops [8]. These spectral sensors are based on the principle of reflectance and changes of electromagnetic radiation between 300 and 2500 nm [10] and can be ground-borne, airborne, or space-borne [11]. Space-borne sensors are widely available [12], but data collection is affected by clouds, poor atmospheric conditions, and has to cope with atmospheric perturbation [13]. In addition, they suffer from low spectral and spatial resolution (10–60 m) [14–16]. The closer the sensor to the target, the higher the spatial resolution [17]. This is one reason why an unmanned aerial vehicle (UAV)-based, or vehicle-mounted, sensors are mainly used in agriculture (resolution 0.01 m or less) [17,18]. However, these devices also still depend on environmental conditions like wind speed, rain, or changing cloud coverage [19]. Nevertheless, the advantage is an image acquisition where measurement date and resolution can be more influenced by the user compared to satellite images. The applications range from the detection of within-field variability for yield predictions to monitoring of water- or nitrogen stress [20–22]. Several commercialized products like the Yara N-Sensor, Fritzmeier Isaria, GreenseekerTM RT 200, or Crop Circle ACS-430 are available, which are measuring the reflectance at canopy level [23]. This leads to two challenges:

The first challenge is to distinguish between soil and plant reflectance signatures [24]. Soil reflectance is affected by soil moisture, organic matter, clay minerals, or iron oxides [25]. The differentiation between soil and plants is mainly realized by using indices that adjust for soil effects [26]. The difficulty of applying such indices is the compensation for different soil albedos, which change between soil types [27]. When using remote sensing instruments, leaf reflectance is always affected by the lower leaves and the soil background, which leads to interferences. Therefore, measured reflectance in an open field is always a mixture of different diffuse reflected light and never an isolated reflectance signal, which may lead to a reduction in overall accuracy.

However, the application of these spectral indices requires a certain ground coverage of the plant to overlay soil reflectance. Hence, the application of these indices is limited to certain growing periods [12,28]. In early growing stages, when the plant has low ground cover, no sensors can be used as the soil reflectance dominates the image [29]. Later in the growing season, a saturation of indices and reflectance values makes the prediction of N status difficult [30].

The second challenge is to distinguish between different parts of the plant. Most studies focused on chlorophyll and N content of the leaves or canopy [31] and therefore did not consider the actual crop's N content, which would be more desirable for decision support systems in PF [32]. The N content within a plant is assumed to be higher in younger leaves [23,24], while a higher sensitivity to N deficiency in older leaves was reported due to translocation processes [33,34]. Wang et al. [35] showed that ignoring vertical N distribution will lead to lower accuracy and limited practical value of crop N for remote sensing. To overcome the issue of vertical N distribution, remote sensing approaches have been adopted by several researchers [34–36]. Zhao et al. [36] generated spectral information with a spectroradiometer in winter wheat by changing view zenith angles from 0° to 60°. Angles of 20 to 30° gave information about the middle leaf layers, while angels of 0 to 20° and 30–60° measured mainly the upper leaves. However, a major drawback of this approach is that each measurement contains some mixed information of all the different layers [36].

This raised the question, on which leaf layer, and at which location on the leaf itself remote sensing measurements have to be carried out to determine the N content of a plant. Measurement at canopy level has to be considered as satisfying so far if different leaves, varying leaf ages, and stress levels lead to a similar reflectance. To the best of our knowledge, there is no publication investigating the influence of the leaf layer and position of the measurement on the leaf for cereal plants. Gara et al. [37] tested spectral reflectance on different short shrubs and showed the need to account for vertical heterogeneity.

Thus, the aim of this study was to investigate a) on which leaf layer and b) at what position on the leaf itself reflectance measurements should be taken from. These measurements were then used to determine the N content (%) of the wheat plant via a range of published VI while validating the data with chemically determined N content (%).

2. Materials and Methods

2.1. Plant Growth Conditions and Experimental Design

Two hydroponic greenhouse experiments were carried out to predict N content from wheat plants (*Triticum aestivum L.*) of the cultivar "Zenon" based on spectral measurements. To achieve this goal, direct destructive lab measurements of nitrogen content (%) of whole plants and indirect spectral reflectance measurements from three positions on three leaves of the same plant were taken. In both experiments, growing conditions in the greenhouse were set at 16/8 h day/night cycle with 400–500 µmol m^{-2} s^{-1} and 20/18 °C day/night temperature. Plants were seeded in the sand and grown for two weeks. Afterward, plants were transferred to a modified Hoagland solution [38], which was continuously aerated and replaced twice a week and contained the following macro- and micronutrients in both trials: 10.0 mM CL, 7.5 mM Ca, 2.0 mM N, 1.2 mM K, 1.1 mM S, 0.6 mM Mg, 0.2 mM P, and 0.4 mM Fe (EDTA), 1.0 µM B, 0.5 µM Zn, 2.0 µM Mn, 0.3 µM Cu, 0.04 µM Mo. The concentration of the nutrient solution was gradually increased from 20% to 100% over seven days. The two experiments varied in the additional treatment factors added. In the nitrogen trial, different levels of nitrogen nutrition status were used. In the drought stress trial, different levels of water stress were induced.

2.1.1. Nitrogen Trial

In the nitrogen trial, the nitrogen fertilizer amount, and the growth stage in which the final spectral measurements took place were varied. For the former, seven different levels of N fertilizer amounts were used (with 0 mM, 0.25 mM N, 0.50 mM N, 0.75 mM N, 1 mM N, 1.5 mM N, 2.00 mM N) and applied in four replicates according to a randomized complete block design (Figure 1). This factor corresponded to the main plot factor. In total, 28 pots were used. Within each pot, five planting positions existed. At each position, a single plant was planted. A total of 140 plants were planted and harvested later (Figure 1). As plants were harvested at different growth stages, the growth stage factor corresponded to the sub-plot factor, as the randomization of the growth stage occurs within the pot. At harvest, the N content was measured by chemical lab analysis. Additionally, three spectrometer measurements from each of the last three fully developed leaves were taken directly before the harvest of each plant. This resulted in a total of 1260 reflectance measurements.

As in trials with different growth stages, the growth stage effect is confounded with either the planting date or the harvest date, a more complex design using planting dates and harvest dates as blocking factors were used. More details, a complete field plan, and a detailed description can be found in the Appendix A.

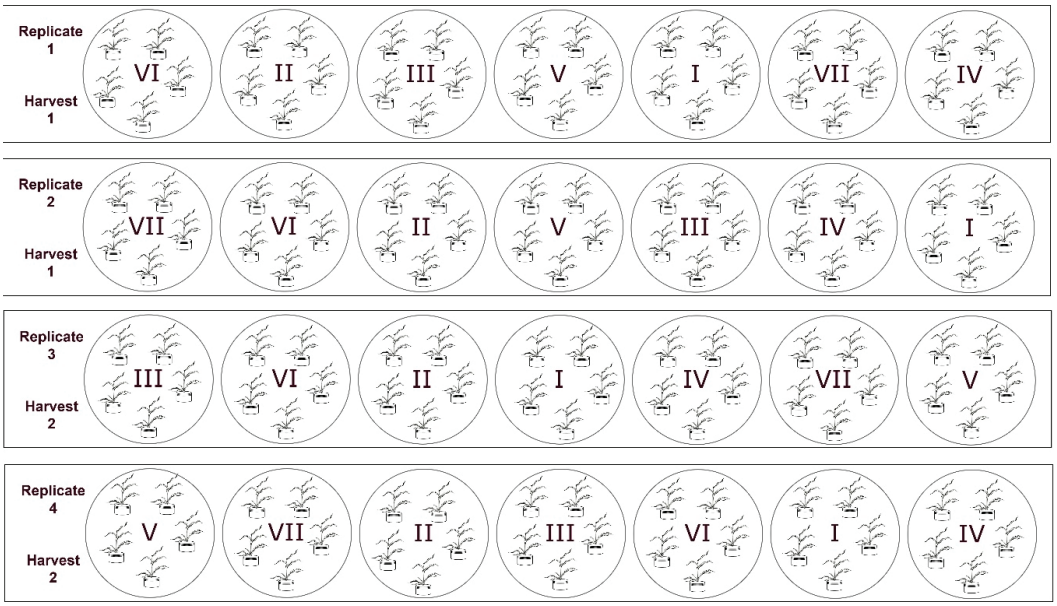

Figure 1. Experimental design of the nitrogen fertilizer trial. I–VII represents the pots of the corresponding nitrogen levels (0 mM N–2.0 mM N).

2.1.2. Drought Stress Trial

To apply drought stress to the hydroponic trials, four levels of polyethylene glycol (PEG 6000) were applied according to a randomized complete block design with three replicates. One replicate consisted of four pots with four plants per pot. Plants here correspond to repeated measures. All plants were transferred to the hydroponic solution at the same time. After one week of growing under the same conditions, the given polyethylene glycol levels (0 g l^{-1}; 36 g l^{-1}; 72 g l^{-1}; 144 g l^{-1}) were applied. The N concentration was kept constant at 2.00 mM N in all pots. After 23 days, spectrometer reflectance measurements for each combination of plant, leaf, and position (resulting in 434 measurements) were taken and harvesting was performed. Plants were then bulked per pot, and N content was determined for each pot resulting in twelve N content values. This experiment was used to test the effect of drought stress on spectral reflectance combined with an assumed N deficit due to drought stress. At the highest drought level, it was not possible to measure the L3 of each plant due to strong leaf rolling. Therefore, L3 was excluded from the evaluation in this experiment.

2.2. Spectral Reflectance Measurements

Leaf reflectance measurements were conducted using a halogen light source (HL-2000-HP-FHSA, Ocean Optics, Germany) and connected to an integrating sphere (ISP-30-6-R, Ocean Optics, Germany) to keep the measurement conditions constant. The integrating sphere was connected via bifurcated fiber (QBIF400-MIXED, Ocean Optics, Germany) to allow simultaneous measurements of two spectrometers for the wavelength range 200–1025 nm (FLAME-S-XR1-ES, Ocean Optics, Germany) and for the wavelength range 900–1700 nm (NQ512-1.7, Ocean Optics, Germany) (Figure 2).

Due to a low signal to noise ratio at both ends of the spectrum, there was an effective range of 400–950 nm at a spectral resolution of 0.4 nm for the FLAME-spectrometer and an effective range of 950–1650 nm at a spectral resolution of 1.5 nm for the NQ512-1.7 spectrometer. The integration time was adjusted at the white standard (Spectralon WS-1-SL, Ocean Optics, Germany) to ensure that enough light reached the sensor. It was set to 80%–95% of light saturation and adjusted for both spectrometers separately and gave the highest signal to noise ratio.

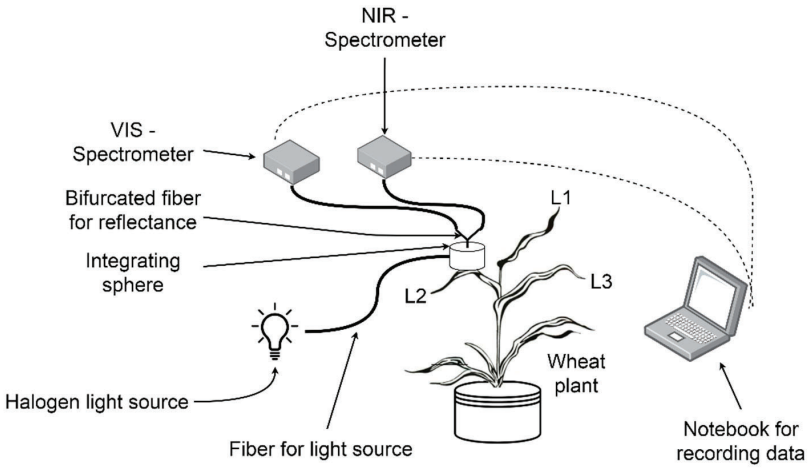

Figure 2. Setup scheme for leaf reflectance measurements under controlled conditions. The numbers indicate the order of leaves 1–3.

Leaf reflectance was calculated as a ratio between the reflected energy of the leaf and the incident energy of the light source. This incident energy was determined by using the reference measurement of the white standard.

The measurement was performed by placing the opening of the integrating sphere on the different leaves and leaf positions (Figure 2). The last fully developed leaf of the main stem was considered as the youngest leaf (L1) and was measured at three positions: leaf tip (P1), leaf center (P2), leaf base (P3) (Figure 3). The same procedure was performed for leaf two (L2) and three (L3). Note, the counting of the leaves always started at the youngest fully developed leaf downwards (Figure 3).

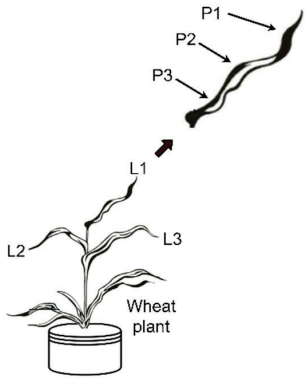

Figure 3. Scheme of the spectral measurements on the plant. P1–P3 indicates the measurement on the leaf and L1–L3 indicates the leaf number. Measurements on L2 and L3 were performed in the same way as indicated for L1.

2.3. Crop Measurements and Harvesting

After the reflectance measurements, the growth stage rating was performed based on the Zadocks scale [39] for each plant separately. Finally, plants were harvested by cutting off the stem from the roots. The stem was weighed (3100 S-G, Sartorius AG, Göttingen, Germany ± 0.01 g) and immediately dried for two days at 60 °C in a forced-air drier. After drying, the dry weight of the samples was determined; samples were ground using a hammer mill (0.5 mm, MM200, Retsch GmbH, Haan,

Germany). The chemical elementary analysis was performed, using a Vario Macro cube (Elementar Analysesysteme GmbH, Hanau, Germany) based on the method of Dumas [40].

2.4. Vegetation Indices (VI)

Information on spectral reflection measurements was explored using different VI. From a literature review, 16 VI (Table 1) with a significant correlation with plant N content or plant water content were selected and calculated for each leaf and position on each leaf [12,41,42].

Table 1. Common vegetation indices used in this study.

Index	Name	Formula	Reference
BNI	Blue nitrogen index	$\frac{R434}{(R496+R401)}$	[43]
CropSpec		$\left(\frac{R808}{R735}-1\right)\cdot 100$	[44]
GNDVI	Green normalized difference vegetation index	$\frac{(R750-R550)}{(R750+R550)}$	[45]
HVI	Hyperspectral vegetation index	$\frac{R750}{R700}$	[29]
NDVI	Normalized difference vegetation index	$\frac{(R900-R680)}{(R900+R680)}$	[46]
NDWI	Normalized difference water index	$\frac{(R860-R1240)}{(R860+R1240)}$	[47]
NIRG	Near-infrared green ratio	$\frac{R780}{R550}$	[48]
NIRR	Near-infrared red ratio	$\frac{R780}{R700}$	[48]
NWI	Normalized water index	$\frac{(R970-R900)}{(R970+R900)}$	[49]
PRI	Photochemical reflectance index	$\frac{(R531-R570)}{(R531+R570)}$	[50]
PSRI	Plant senescence reflectance index	$\frac{(R680-R500)}{(R750)}$	[51]
REIP	Red-edge inflection point	$700+40\cdot\frac{(R670+R780)/\,2-R700}{R740-R700}$	[52]
SIPI	Structure insensitive pigment index	$\frac{(R800-R445)}{(R800+R680)}$	[50]
SR 680	Simple ratio 680	$\frac{R800}{R680}$	[50]
SR 705	Simple ratio 705	$\frac{R750}{R705}$	[41]
VARI	Visible atmospherically resistant index	$\frac{(R550-R650)}{(R550+R650-R470)}$	[53]

2.5. Statistical Analysis (Mixed Model)

Data of the N trial were analyzed by a mixed model approach accounting for the two factors, nitrogen fertilizer treatment and growth stage, as well as the two blocking factors, the sowing date and harvest date (for more details of the experimental design see appendix).

The model can be described by:

$$y_{ijklmn} = \mu + \tau_m + \varphi_n + (\tau\varphi)_{mn} + h_i + s_j + r_k + t_{kl} + e_{ijklmn} \quad (1)$$

where y_{ijklmn} is the measured plant N content, μ is the intercept, τ_m is the fixed effect of the mth N treatment, φ_n is the fixed effect of the nth growth stage, and $(\tau\varphi)_{mn}$ the corresponding fixed interaction effect. h_i is the random block effect of the ith harvesting date, s_j is the random block effect of the jth sowing date, r_k is the fixed effect of the kth replicate, and t_{kl} is the random effect of the lth pot or main plot within the kth replicate. e_{ijklmn} is the error of observation y_{ijklmn}.

The model for the drought trial is similar but does not include block effects. Furthermore, only the drought stress was evaluated as an influencing variable. Thus, the model simplifies to

$$y_{klo} = \mu + r_k + t_{kl} + \rho_o + e_{klo} \quad (2)$$

where ρ_o corresponds to the oth drought stress level. In both models, VI's were added as a covariate for each of the nine combinations of leaf and position. As 16 VI were used, a total of 144 models each including different covariates were fitted. For all models, the error variance was estimated and used as evaluation criteria. It was assumed that a covariable, which correlates well with plant N content will reduce the error variance.

Error variances were stored and further analyzed with a generalized linear mixed model approach assuming a gamma distribution with a log link. The linear predictor was as follows:

$$\mu_{hpq} = \mu + l_p + p_q + (lp)_{pq} + i_h \quad (3)$$

where l_p is the effect of the pth leaf, p_q is the effect of the qth position, $(lp)_{pq}$ is the interaction effect of the pth leaf at the qth position, and i_h is the effect of the hth VI. The model allows accounting for overdispersion. If significant Wald tests were found, means were calculated using the inverse link function. For these means, a letter display was used to present the results of the Fishers LSD test created on the linked scale. All statistical evaluations were performed in the software environment SAS 9.4 by using the procedure PROC MIXED and PROC GLIMMIX.

3. Results

3.1. Nitrogen Trial

The chemically determined N content [%] showed significant differences ($p < 0.001$) and varied between 0.75% and 4.88% according to the implemented N treatments and growth stages in the N trial (Figure 4). The analysis of the residual error variance showed significant differences between leaf numbers and positions on the leaf. No significant differences were observed for the effects of the tested VI (Table 2; Figure 5). The interactions between leaf number and measurement position were found to have non-significant differences. Across all VIs, statistically significant lowest residual error variance was found at M3 and on leaf L1, and L3 (Figure 5). While the average residual error variances across VI were significantly different, almost no difference in error variance between leaf number and measurement position for the trait plant N content was observed (Figure 5).

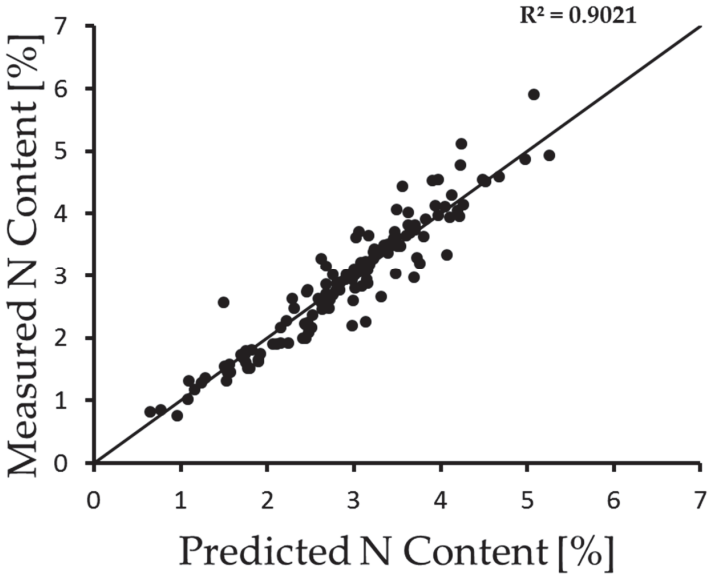

Figure 4. Scatter plot for measured and predicted nitrogen content of the nitrogen trial. The solid line indicates the 1:1.

Table 2. Results of the fixed effects of the statistical analyses of the nitrogen and drought stress trial. F values were rounded.

		Nitrogen trial		Drought stress trial	
Effect	**DF**	**F value**	**Pr > F**	**F value**	**Pr > F**
VI	15	0.49	0.9432	2.82	<0.0016
Leaf number	2	12.14	<0.0001	1.03	<0.3140
Position	2	4.34	<0.0152	1.84	<0.1657
Leaf number x Position	4	1.26	<0.2913	1.84	<0.1652

DF: degrees of freedom; Pr > F: probability level.

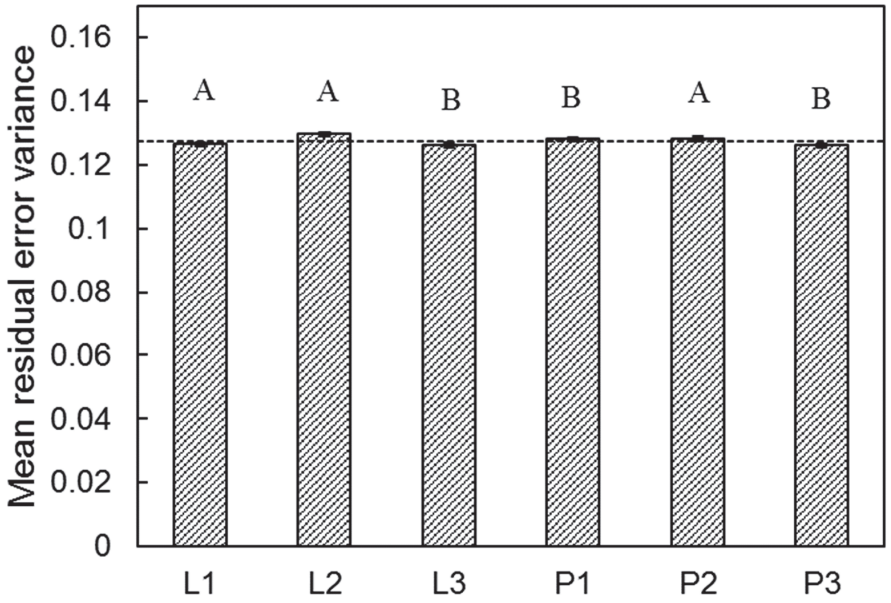

Figure 5. Mean residual error variance across VI (vegetation indices) of the nitrogen trial. L1 is considered the youngest fully developed leaf followed by the second L2 and third youngest leaf L3. P1 is the spectral reflectance measured at the leaf tip, P2 measured in the middle part of the leaf, and P3 represents the measurement taken at the leaf base of the respective leaf. The bars with the same letters within the leaves and within the positions show non-significant different residual error variances at $\alpha = 0.05$. The dotted line represents the residual error variance value without VI.

3.2. Drought Trial

Considering the drought trial (Table 2; Figure 6) where chemically determined N content varied due to the drought stress between 2.55% and 4.46%, the error variances showed significant differences ($p < 0.05$) only for VI and not for leaf number, position, and leaf number x position. Comparing the significance of different VI in the drought trial (Figure 6), the difference between PSRI, CropSpec, and BNI, indicated the highest mean residual error variance for PSRI, while BNI showed the lowest mean residual error variance.

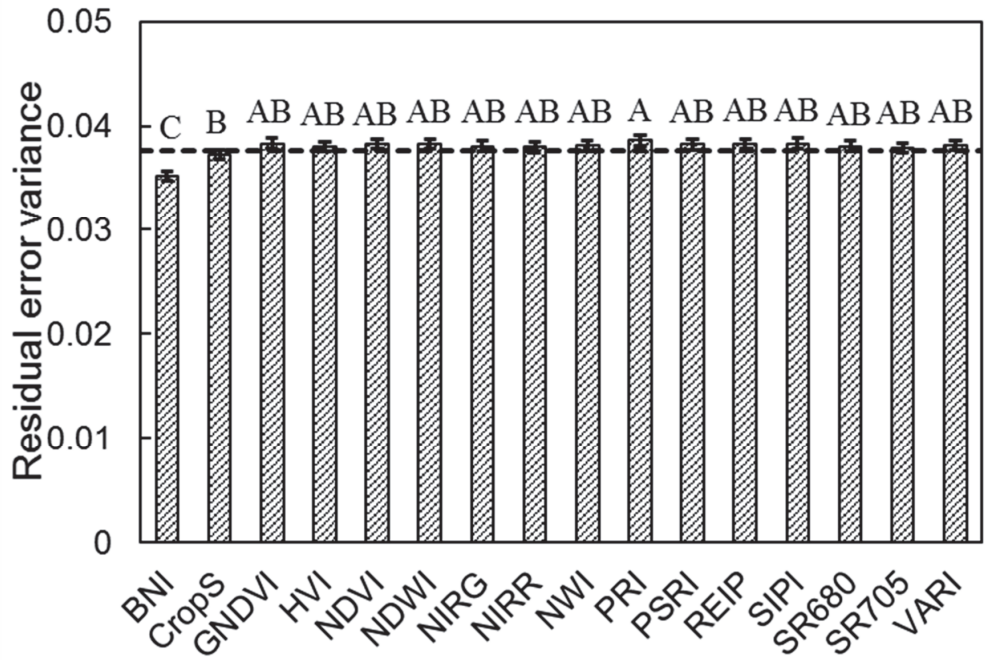

Figure 6. Different residual error variance for all used VI in the drought stress trial. The letters represent different significance groups. Indices with the same letters are not statistically different at a significance level of 0.05. The dotted line represents the residual value without using spectral reflectance measurements.

4. Discussion

This study evaluated the effect of a total of nine (three-leaf layers and three positions on each leaf) spectral reflection measurements on the prediction of N content (%) in wheat plants. To predict N content, spectral reflection measurements were used to calculate a range of published VI. Note that the aim of this study was not to optimize existing VIs, but rather to compare the nine input spectral reflection datasets and thus the impact of the leaf layer and measurement position on the accuracy of N prediction. Due to easy access and the common use of VIs in scientific and applied work [12,41,42], a range of 16 VI already published were used here. Note that each VI only used a few wavelengths. Thus, only a part of the information within the spectral reflection measurements was explored. More information can be explored when using a stepwise multiple linear regression (SMLR) and other full-spectral methods like partial least squares (PLS) [54]. These methods were tested in this study and came up with similar results as the ones presented in this paper.

Furthermore, other approaches can be used, like ridge regression [55] and neural networks [56,57], which can handle collinearity in regressions. Collinearity is common in spectral reflection data as wavelengths are measured within a narrow grid. All these alternative approaches can increase the predictability of absolute N content in plants. It was assumed that changes in absolute precision will not affect the ranking of the nine spectral reflection input measurements. This assumption was supported by results using a multiple regression approach and PLS on our data. Data are not shown here to avoid redirecting the focus of the manuscript from comparing the nine spectral reflection measurements to comparing approaches to convert wavelength measures into an N content prediction.

4.1. Leaf Number and Leaf Position

Spectral reflectance is used to detect differences in N content in plants non-destructively and to reveal the given heterogeneity in plant N supply within a field [58]. As the aim of this study was to predict plant N content within a field [42], e.g., for applying the right amount of fertilizer, effects of N level, growth stage, and drought were included in the statistical models. Thus, the statistical models can predict different N contents in plants within similar treatments averaged across these treatments. When dropping these treatment effects from the models, indices may explain well the difference between a trait (e.g., drought stress levels) not causally correlated with plant N. Note that VI explained more variance, if the treatment effect is excluded from the model. This was tested but not shown.

Considering the mixed model for all measurements in the N trial, a statistically significant higher mean residual error variance was given for L2 (Figure 5). Regarding the measurement position, a statistically significant lower value was given for the leaf base in the N trial, but differences were small. While differences were significant, they were not relevant, which was supported by the low differences between the significance groups (Figure 5). This conclusion was also reinforced by the drought stress trial, where no statistically significant difference between the leaf number and measurement position was shown. Different drought stress levels led to significantly different plant N contents. Gonzalez-Dugo et al. [59] also reported lower N contents for sunflower *(Helianthus annuus.* L) due to drought stress, based on the results of Alvarez de Toro [60]. They also showed plant N content under drought stress is dependent on the applied N. Low N application leads to a low change in plant N content, while high N application leads to a stronger plant N content reduction under drought stress. The wheat plants in this trial were cultivated under sufficient N supply, which can be seen as feasible to have significant differences between drought stress treatments.

To predict N content in wheat plants based on spectral measurements, reflectance can be measured at all positions on a leaf, at all leaves across different N treatments at different growth stages, as well as under drought stress.

4.2. Vegetation Indices and Wavelength

Regarding the residual error variance for all VI, significant differences were only determined in the drought trial for BNI (Figure 6). All other VI had no significant difference, especially the developed VI for water stress NDWI and NWI. In this trial, there was a reduction in plant N content due to drought stress observed, which was also reported by He and Dijkstra [61]. Therefore, these VI were used for the estimation of plant N under water-limited conditions. However, originally they have been developed for the estimation of water limitations in plants. In contrast, the BNI, which was developed for the estimation of plant N content showed the lowest residual error variance and seemed to be suitable for estimation of plant N content under water-limited conditions.

The BNI was the only VI out of 16 VI that used wavelengths from the blue part of the spectra. Tian et al., [43] successfully developed and tested this VI for estimation of leaf N canopy content in rice (*Oryza sativa* L.) and showed a linear relationship with canopy N content. Schlemmer et al. [62] tested different N levels in combination with drought stress in corn (*Zea mays* L.). They showed a weak influence of the reflectance spectrum under drought stress between 400 and 500 nm, if the plants were cultivated under sufficient N level. This could be the reason for the statistically lower residual error variance in the drought stress trial for all leaves and positions for BNI.

It is also important to mention that the selection criteria for the 16 VI used were based on literature, where VI were tested successfully for the determination of plant N content and drought stress [12,41,42,63,64].

This ensured that a broad range of different VI developed for N content and drought stress were tested, conceding, however, that there is a long list of VI that were not tested in the current study [32,49,65]. While we found no differences between VI in the N trial, we cannot preclude that there are no differences between VI at all. The drought stress showed the only significance for BNI, which means all VI except BNI performed in a similar way. The use of different VI sharing similar or identical wavelength ranges can be considered as not statistically independent. This can lead to the distortion of statistical results. Normally a broad range of VI focus on the red edge of the spectrum [66] leading to multiple uses of these wavelengths for calculation of various VI.

Several researchers evaluated the whole spectrum instead of using VI e.g., for plant disease detection [67] or canopy chlorophyll content [54]. These methods seem to be useful for further research where launches of hyperspectral satellite sensors are planned (e.g., EnMap, PRISMA) providing higher spectral resolution [68,69]. Other sensors like the Chinese HJ-1A [70] and the Indian Micro Satellite-1 (IMS-1) [71] also provide hyperspectral data, however, there is limited access for international scientists [69].

However current sensors including free available satellite images are normally limited to several wavelengths [72,73] and do not collect the whole spectrum in a spectral resolution like a spectrometer. This is mainly related to well tested and known VI's for the determination of N as well as a cost issue of the sensor and the necessary data processing to generate a final fertilizer recommendation. Using a spectrometer with a high spectral resolution, calculating existing VI's for nitrogen-based on the wavelength ranges seems to be a straight forward procedure to address if the differentiation between leaf and leaf positions based on existing VI's would be required.

4.3. Further Measurement Technologies, Limitations, and Future Applications

Hoel and Solhaug [74] tested the change of SPAD chlorophyll readings under shaded and fully illuminated conditions in wheat. Low changes were reported between shading and full illumination. This supports our finding of low differences between the three measured leaf layers, where L2 and L3 were shaded by L1. In comparison to spectrometer measurements, SPAD readings are limited to two wavelengths at 640 nm and 940 nm and are based on the principle of transmission of light [12]. Spectrometer readings, in contrast, focus on the reflectance of light. Comparisons of reflectance and SPAD values showed positive correlations for chlorophyll content, which also correlates very well with N content depending on different growth stages [75]. SPAD readings are contact measurements and not suitable for remote sensing applications [12].

Measuring leaf reflectance without separation of different leaves on canopy scale generally includes information of LAI, chlorophyll content or changes in plant morphology [76,77]. These lead to non-linear effects in the obtained sensor data and are not separated in commercialized products, which results in an overall mean N content [77]. Measuring at the canopy scale includes mixed information also from other parts of the plant like stem or leaf orientation [76], an aspect which was not considered in this study. It is also feasible, that differentiation between leaf layers is necessary under other nutrition deficiencies like sulfur, phosphorus, or potassium. Shaw and Royle [78] reported that early infection of lower leaf layers with *Septoria tritici* blotch (*Zymoseptoria tritici D.*) can make it necessary to differentiate between different leaves under leaf disease infections and has to be tested in further studies.

Currently, developed sensors are working on the canopy level and are not considering individual leaves or different positions on the leaf [79,80]. Nevertheless, we think, all these sensors require a minimum of spatial resolution in order to delineate the given within-field variability of plant N content on the farmer's practical scale (e.g., the width of sprayer bow). Hence, sensors for N fertilizer application in PF can only be useful if the spatial resolution of the sensor matches the N application size, which is determined by the fertilizer application technique. This has to be considered especially for satellite sensors, where spatial resolution ranges from 10–60 m [15]. Based on this study, differentiation between different leaf layers for the determination of N content can be seen as less relevant, which indicates valid measurements at the canopy scale.

5. Conclusions

The results of the study indicated that neither leaf number nor the measurement position on the leaf had an influence on the determination of plant N content, via spectral reflectance. Significant lower mean residual error variance (MREV) was found for leaves L1 and L3 and for measurement position on P3, but the difference of MREV between the leaves was very low and therefore considered as not relevant. While a broad range of different VI developed for the assessment of N content and drought stress was tested in this study, it cannot be excluded that there are no differences between VI at all and differences might exist for VI that were not tested in this study. To transfer the results to field measurements, it has to be considered that the measurements were taken under fully controlled lab conditions. Field measurements will be influenced by different effects like the reflection from soil, stem, or other plant parts, which can lead to weaker performance of spectral reflection measurements compared to lab conditions. In addition, other stress factors (e.g., diseases, other nutrient deficiencies) might occur in parallel in the field and interfere with spectral reflectance.

Author Contributions: Conceptualization, G.R., J.H., and S.G.-H.; methodology, G.R., J.H., and S.G.-H.; software, G.R. and J.H.; validation, G.R.; formal analysis, G.R.; investigation, G.R.; resources, G.R.; data curation, G.R.; writing—original draft preparation, G.R.; writing—review and editing, G.R., J.H., and S.G.-H.; visualization, G.R.; supervision, S.G.-H.; project administration, S.G.-H.; funding acquisition, S.G.-H.

Funding: This research was funded by the German Federal Environmental Foundation (DBU) (ProjectNr. 33143/01).

Acknowledgments: Many thanks to the hema electronic company for providing the spectrometer measurement equipment and Thomas Schwarzbäck for supporting the measurements and the device selection.

Conflicts of Interest: The authors declare no conflict of interest. The funders had no role in the design of the study; in the collection, analyses or interpretation of data; in the writing of the manuscript or in the decision to publish the results.

Appendix A

In the nitrogen trial, 140 plants were planted and harvested (Figures A1 and A2). As seven N fertilizer treatments were used, each N fertilizer treatment was applied to four pots; each pot contained five plants. Thus, the fertilizer treatment corresponded to the main plot factor and was allocated to pot according to the randomized complete block design. Within a pot, plants of different growth stages were tested. To generate plants of different growth stages, plants can be planted at different times and measured at a single harvest date or can be planted at the same time, but harvested at different time points. In both cases, the growth stage effect is confounded with the planting or harvest day. To handle this confounding, a more complex experimental design was used. The general idea behind this design was that planting date and harvest date were used as block factors. Within a block, as many growth stages as possible were measured. In our experiment, six planting dates and two harvest dates were used. This resulted in measuring plants of the same planting date at two different growth stages and measuring plants of five growth stages at the same harvest day (Figure A1).

With plants planted at six dates and harvested at two dates, five different growth stages can be observed. Thus, the design is complete as all growth stages occur in each pot. The experiment was performed as follows: wheat seeds were seeded at six different sowing dates (three weeks with two staring dates per week) (Figure A2). Plants from the first sowing date were randomly planted to one of the positions within each pot of replicate 1 and 2. Thus, 14 plants were planted at the first planting date. Plants from the second sowing date were seeded randomly to one of the remaining positions in each pot of replicate 1 + 2, and to one position in replicate 3 + 4. Plants from the third, fourth, and fifth sowing dates were planted randomly to one of the remaining positions in each pot in replicate 1–4. Finally, plants from the sixth sowing date were seeded in the remaining positions of replicate 3 and 4. Note that plants of the first sowing date were 14 or 17 days older (two or two and a half week), compared to plants of the fifths or sixth sowing date, respectively. Furthermore, replicate 1 and 2 were measured and harvested first (H1) followed by replicates 3 and 4 half a week later (H2).

Thus, a plant sown at the third date measured at H1 has the same growth stage as a plant sown at the fourth sowing date and measured at H2 (indicated by the length of arrows in Figure A2).

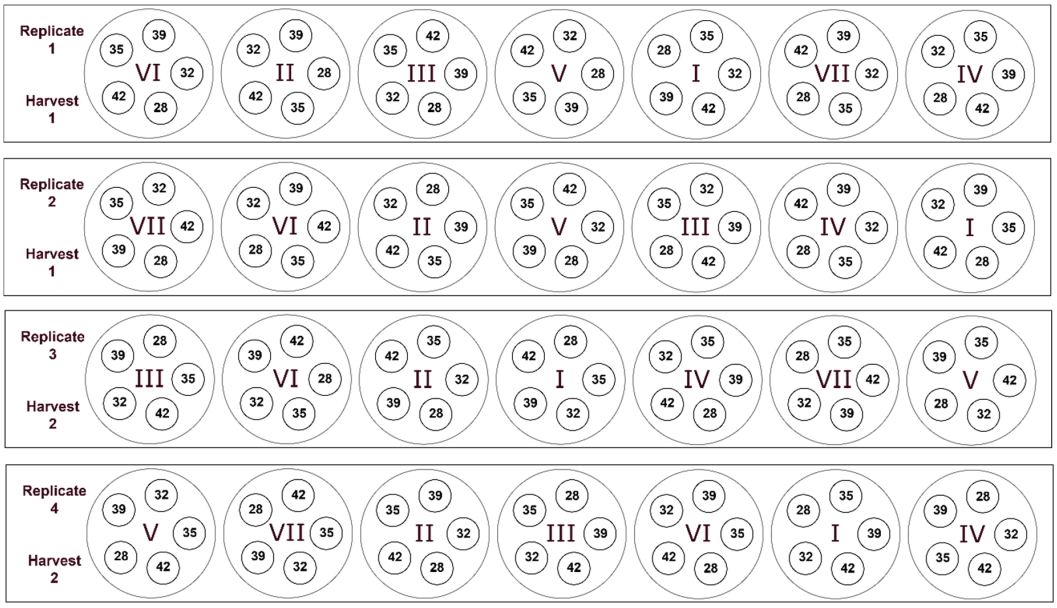

Figure A1. Experimental design of the nitrogen fertilizer trial. I–VII represents the pots for the corresponding nitrogen levels (0 mM N–2.0 mM N). Numbers 28–24 represents the growing days (from seeding until harvest) of the respective plant.

As mentioned above, the fertilizer treatment corresponded to the main plot factor and was allocated to pot according to the randomized complete block design. Growth stages were randomized to plants within a pot and thus can be seen as sub-plot factor. The design can be seen as a kind of split-plot design with two additional block factors (sowing date and harvest date). To model such type of data, the effects for both treatment factors (N treatment and growth stage) should be separated from the two blocking factors.

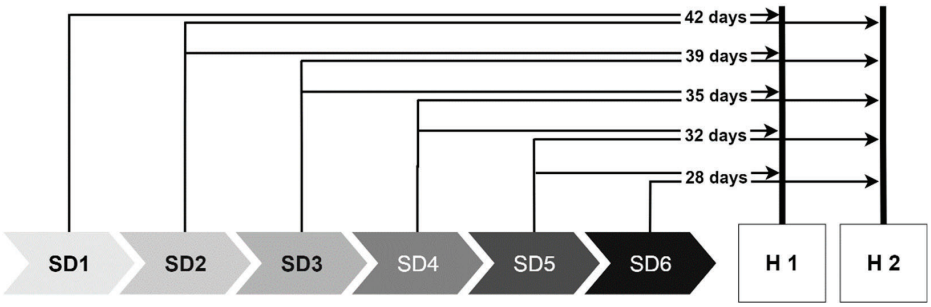

Figure A2. Scheme of different sowing dates (SD) and the corresponding harvest dates (H) of the nitrogen trial. The duration indicates the growing time (from sowing to harvest) in the experiment for each sowing date.

References

1. Ladha, J.K.; Pathak, H.; Krupnik, T.J.; Six, J.; Van Kessel, C. Efficiency of fertilizer nitrogen in cereal production: Retrospects and prospects. *Adv. Agron.* **2005**, *87*, 85–156.

2. Rafiqul, I.; Weber, C.; Lehmann, B.; Voss, A. Energy efficiency improvements in ammonia production—Perspectives and uncertainties. *Energy* **2005**, *30*, 2487–2504. [CrossRef]
3. Kim, H.; Kim, S.; Dale, B.E. Biofuels, Land Use Change, and Greenhouse Gas Emissions: Some Unexplored Variables. *Environ. Sci. Technol.* **2009**, *43*, 961–967. [CrossRef]
4. Gruber, N.; Galloway, J.N. An Earth-system perspective of the global nitrogen cycle. *Nature* **2008**, *451*, 293. [CrossRef]
5. Kim, S.; Dale, B.E. Effects of Nitrogen Fertilizer Application on Greenhouse Gas Emissions and Economics of Corn Production. *Environ. Sci. Technol.* **2008**, *42*, 6028–6033. [CrossRef]
6. European Commission. Directive 2000/60/EC of the European Parliament and of the Council of 23 October 2000 establishing a framework for Community action in the field of water policy. *Off. J. Eur. Union* **2000**, *327*, 193.
7. European Commission. Council Directive 91/676/EEC of 12 December 1991 concerning the protection of waters against pollution caused by nitrates from agricultural sources. *Off. J. Eur. Union* **1991**, *375*, 12.
8. Webber, H.; Heyd, V.; Horton, M.; Bell, M.; Matthews, W.; Chadburn, A. Precision farming and archaeology. *Archaeol. Anthropol. Sci.* **2019**, *11*, 727–734. [CrossRef]
9. Carter, L.M.; Rhoades, J.D.; Chesson, J.H. Mechanization of soil salinity assessment for mapping. *Am. Soc. Agric. Eng.* **1993**. Available online: https://www.ars.usda.gov/arsuserfiles/20360500/pdf_pubs/P1305.pdf (accessed on 8 September 2019).
10. Jackson, R.D.; Pinter, P.J. Spectral response of architecturally different wheat canopies. *Remote Sens. Environ.* **1986**, *20*, 43–56. [CrossRef]
11. Selige, T.; Böhner, J.; Schmidhalter, U. High resolution topsoil mapping using hyperspectral image and field data in multivariate regression modeling procedures. *Geoderma* **2006**, *136*, 235–244. [CrossRef]
12. Muñoz-Huerta, R.F.; Guevara-Gonzalez, R.G.; Contreras-Medina, L.M.; Torres-Pacheco, I.; Prado-Olivarez, J.; Ocampo-Velazquez, R.V. A Review of Methods for Sensing the Nitrogen Status in Plants: Advantages, Disadvantages and Recent Advances. *Sensors* **2013**, *13*, 10823–10843. [CrossRef] [PubMed]
13. Moran, M.S.; Inoue, Y.; Barnes, E.M. Opportunities and limitations for image-based remote sensing in precision crop management. *Remote Sens. Environ.* **1997**, *61*, 319–346. [CrossRef]
14. Mulla, D.J. Twenty five years of remote sensing in precision agriculture: Key advances and remaining knowledge gaps. *Biosyst. Eng.* **2013**, *114*, 358–371. [CrossRef]
15. Chemura, A.; Mutanga, O.; Odindi, J.; Kutywayo, D. Mapping spatial variability of foliar nitrogen in coffee (*Coffea arabica* L.) plantations with multispectral Sentinel-2 MSI data. *ISPRS J. Photogramm. Remote Sens.* **2018**, *138*, 1–11. [CrossRef]
16. Hank, T.B.; Berger, K.; Bach, H.; Clevers, J.G.P.W.; Gitelson, A.; Zarco-Tejada, P.; Mauser, W. Spaceborne Imaging Spectroscopy for Sustainable Agriculture: Contributions and Challenges. *Surv. Geophys.* **2019**, *40*, 515–551. [CrossRef]
17. Xue, J.; Su, B. Significant Remote Sensing Vegetation Indices: A Review of Developments and Applications. *J. Sensors* **2017**, *2017*, 1–17. [CrossRef]
18. Thompson, A.L.; Thorp, K.R.; Conley, M.M.; Elshikha, D.M.; French, A.N.; Andrade-sanchez, P.; Pauli, D. Comparing Nadir and Multi-Angle View Sensor Technologies for Measuring in-Field Plant Height of Upland Cotton. *Remote Sens.* **2019**. [CrossRef]
19. Ramana, M.V.; Ramanathan, V.; Kim, D.; Roberts, G.C.; Corrigan, C.E. Albedo, atmospheric solar absorption and heating rate measurements with stacked UAVs. *Q. J. R. Meteorol. Soc.* **2007**, *133*, 1913–1931. [CrossRef]
20. Yao, H.; Huang, H. Remote sensing applications to precision farming. In *Remote Sensing of Natural Resources*; CRC Press: New York, NY, USA, 2013; pp. 333–352.
21. Bégué, A.; Todoroff, P.; Pater, J. Multi-time scale analysis of sugarcane within-field variability: Improved crop diagnosis using satellite time series? *Precis. Agric.* **2008**, *9*, 161–171. [CrossRef]
22. Baret, F.; Houlès, V.; Guérif, M. Quantification of plant stress using remote sensing observations and crop models: The case of nitrogen management. *J. Exp. Bot.* **2007**, *58*, 869–880. [CrossRef] [PubMed]
23. Link, A.; Reusch, S. Implementation of site-specific nitrogen application—Status and development of the YARA N-Sensor. *NJF Semin.* **2006**, *390*, 37–41.
24. Vigneau, N.; Ecarnot, M.; Rabatel, G.; Roumet, P. Potential of field hyperspectral imaging as a non destructive method to assess leaf nitrogen content in Wheat. *Field Crop. Res.* **2011**, *122*, 25–31. [CrossRef]

25. Thomasson, J.A.; Sui, R.; Cox, M.S.; Al-Rajehy, A. Soil reflectande sensing for determining soil properties in precision agriculture. *Trans. ASAE* **2001**, *44*, 1445. [CrossRef]
26. Haboudane, D.; Miller, J.R.; Tremblay, N.; Zarco-Tejada, P.J.; Dextraze, L. Integrated narrow-band vegetation indices for prediction of crop chlorophyll content for application to precision agriculture. *Remote Sens. Environ.* **2002**, *81*, 416–426. [CrossRef]
27. Sripada, R.P.; Heiniger, R.W.; White, J.G.; Weisz, R. Aerial Color Infrared Photography for Determining Late-Season Nitrogen Requirements in Corn. *Agron. J.* **2005**, *97*, 1443. [CrossRef]
28. Schepers, J.S.; Francis, D.D.; Vigil, M.; Below, F.E. Comparison of corn leaf nitrogen concentration and chlorophyll meter readings. *Commun. Soil Sci. Plant Anal.* **1992**, *23*, 2173–2187. [CrossRef]
29. Thenkabail, P.S.; Smith, R.B.; De Pauw, E. Hyperspectral Vegetation indices and their relationships with agricultural crop characteristics. *Remote Sens. Environ.* **2000**, *71*, 158–182. [CrossRef]
30. Gitelson, A.A. Wide Dynamic Range Vegetation Index for Remote Quantification of Biophysical Characteristics of Vegetation. *J. Plant Physiol.* **2004**, *161*, 165–173. [CrossRef]
31. Haboudane, D.; Tremblay, N.; Miller, J.R.; Vigneault, P. Remote Estimation of Crop Chlorophyll Content Using Spectral Indices Derived From Hyperspectral Data. *IEEE Trans. Geosci. Remote Sens.* **2008**, *46*, 423–437. [CrossRef]
32. Li, F.; Miao, Y.; Hennig, S.D.; Gnyp, M.L.; Chen, X.; Jia, L.; Bareth, G. Evaluating hyperspectral vegetation indices for estimating nitrogen concentration of winter wheat at different growth stages. *Precis. Agric.* **2010**, *11*, 335–357. [CrossRef]
33. Bertheloot, J.; Andrieu, B.; Martre, P. Light–nitrogen relationships within reproductive wheat canopy are modulated by plant modular organization. *Eur. J. Agron.* **2012**, *42*, 11–21. [CrossRef]
34. Wang, Z.; Wang, J.; Zhao, C.; Zhao, M.; Huang, W.; Wang, C. Vertical Distribution of Nitrogen in Different Layers of Leaf and Stem and Their Relationship with Grain Quality of Winter Wheat. *J. Plant Nutr.* **2005**, *28*, 73–91. [CrossRef]
35. Wang, Z. Prediction of Canopy Nitrogen Distribution and Grain Quality Using Remote Sensing in Winter Wheat (*Triticum aestivum* L.). Ph.D. Thesis, China Agricultural University, Beijing, China, 2004.
36. Zhao, C.J.; Huang, W.J.; Wang, J.H.; Liu, L.Y.; Song, X.Y.; Ma, Z.H.; Li, C. Extracting winter wheat chlorophyll concentration vertical distribution based on bidirec-tional canopy reflected spectrum. *Trans. Chin. Soc. Agric. Eng.* **2006**, *22*, 104–109.
37. Gara, T.W.; Skidmore, A.K.; Darvishzadeh, R.; Wang, T. Leaf to canopy upscaling approach affects the estimation of canopy traits. *GIScience Remote Sens.* **2019**, *56*, 554–575. [CrossRef]
38. Hoagland, D.R.; Arnon, D.I. The water-culture method for growing plants without soil. *Circ. Calif. Agric. Exp. Stn.* **1950**, *347*, 32.
39. Zadoks, J.C.; Chang, T.T.; Konzak, C.F. A decimal code for the growth stages of cereals. *Weed Res.* **1974**, *14*, 415–421. [CrossRef]
40. Dumas, A. Stickstoffbestimmung nach Dumas (N-determination according to Dumas). In *Die Praxis des Organischen Chemikers*; Gattermann, L., Wieland, H., Eds.; De Gruyter: Berlin, Geramny, 1962; pp. 45–51.
41. Sims, D.A.; Gamon, J.A. Relationships between leaf pigment content and spectral reflectance across a wide range of species, leaf structures and developmental stages. *Remote Sens. Environ.* **2002**, *81*, 337–354. [CrossRef]
42. Zecha, C.; Link, J.; Claupein, W. Fluorescence and Reflectance Sensor Comparison in Winter Wheat. *Agriculture* **2017**, *7*, 78. [CrossRef]
43. Tian, Y.C.; Yang, J.; Yao, X.; Zhu, Y.; Cao, W.X. A newly developed blue nitrogen index for estimating canopy leaf nitrogen concentration of rice. *Chin. J. Appl. Ecol.* **2010**, *24*, 966–972.
44. Reusch, S.; Jasper, J.; Link, A. Estimating crop biomass and nitrogen uptake using CropSpec TM, a newly developed active crop-canopy reflectance sensor. In Proceedings of the 10th International Conference on Precision Agriculture, Denver, CO, USA, 18–21 July 2010.
45. Gitelson, A.A.; Kaufman, Y.J.; Merzlyak, M.N. Use of a Green Channel in Remote Sensing of Global Vegetation from EOS-MODIS. *Remote Sens. Environ.* **1996**, *58*, 289–298. [CrossRef]
46. Rouse, W.; Haas, H.; Schell, J.; Deering, D. Monitoring vegetation systems in the great plains with ERTS. In Proceedings of the 3rd ERTS Symposium; NASA SP-351. Freden, S.C., Becker, M.A., Eds.; NASA: Washington, DC, USA, 1973; pp. 309–317.

47. Gao, B. NDWI—A normalized difference water index for remote sensing of vegetation liquid water from space. *Remote Sens. Environ.* **1996**, *58*, 257–266. [CrossRef]
48. Bausch, W.C.; Duke, R.H. Remote Sensing of Plant Nitrogen Status in Corn. *Trans. ASAE* **1996**, *39*, 1869–1875. [CrossRef]
49. Babar, M.A.; Reynolds, M.P.; van Ginkel, M.; Klatt, A.R.; Raun, W.R.; Stone, M.L. Spectral Reflectance to Estimate Genetic Variation for In-Season Biomass, Leaf Chlorophyll, and Canopy Temperature in Wheat. *Crop Sci.* **2006**, *46*, 1046. [CrossRef]
50. Peñuelas, J.; Gamon, J.A.; Fredeen, A.L.; Merino, J.; Field, C.B. Reflectance Indices Associated with Physiological Changes in Nitrogen-and Water-Limited Sunflower Leaves. *Remote Sens. Environ.* **1994**, *146*, 135–146. [CrossRef]
51. Merzlyak, M.N.; Gitelson, A.A.; Chivkunova, O.B.; Yu, V.; Campus, S.B. Non-destructive optical detection of pigment changes during leaf senescence and fruit ripening. *Physiol. Plant.* **1999**, *106*, 135–141. [CrossRef]
52. Horler, D.N.H.; Dockray, M.; Barber, J. The red edge of plant leaf reflectance. *Int. J. Remote Sens.* **1983**, *4*, 273–288. [CrossRef]
53. Kaufman, Y.J.; Tanrd, D. Strategy for Direct and Indirect Methods for Correcting the Aerosol Effect on Remote Sensing: From AVHRR to EOS-MODIS. *Remote Sens. Environ.* **1992**, *55*, 65–79. [CrossRef]
54. Atzberger, C.; Guérif, M.; Baret, F.; Werner, W. Comparative analysis of three chemometric techniques for the spectroradiometric assessment of canopy chlorophyll content in winter wheat. *Comput. Electron. Agric.* **2010**, *73*, 165–173. [CrossRef]
55. Hoerl, A.E.; Kennard, R.W. Ridge Regression: Biased Estimation for Nonorthogonal Problems. *Technometrics* **1970**, *12*, 55–67. [CrossRef]
56. Haykin, S. *Neural Networks: A Comprehensive Foundation*; Macmillan College Publishing: Englewood Cliffs, NJ, USA, 1994; ISBN 0023527617.
57. Sarle, W.S. Neural Networks and Statistical Models. In Proceedings of the 19th Annual SAS Users Groups International Conference, Cary, NC, USA; 1994; pp. 1538–1550.
58. Thorp, K.R.; Wang, G.; Bronson, K.F.; Badaruddin, M.; Mon, J. Hyperspectral data mining to identify relevant canopy spectral features for estimating durum wheat growth, nitrogen status, and grain yield. *Comput. Electron. Agric.* **2017**, *136*, 1–12. [CrossRef]
59. Gonzalez-Dugo, V.; Durand, J.L.; Gastal, F. Water deficit and nitrogen nutrition of crops. *Sustain. Agric.* **2009**, *2*, 557–575. [CrossRef]
60. De Toro, A. *Respueta del Girasol (Helianthus annuus L.) a un Suministro Variable de Agua de Reigo y de Nitrogeno*; University of Cordoba: Cordoba, Spain, 1987.
61. He, M.; Dijkstra, F.A. Drought effect on plant nitrogen and phosphorus: A meta-analysis. *New Phytol.* **2014**, *204*, 924–931. [CrossRef] [PubMed]
62. Schlemmer, M.R.; Francis, D.D.; Shanahan, J.F.; Schepers, J.S. Remotely Measuring Chlorophyll Content in Corn Leaves with Differing Nitrogen Levels and Relative Water Content. *Agron. J.* **2005**, *97*, 106. [CrossRef]
63. Hansen, P.M.; Schjoerring, J.K. Reflectance measurement of canopy biomass and nitrogen status in wheat crops using normalized difference vegetation indices and partial least squares regression. *Remote Sens. Environ.* **2003**, *86*, 542–553. [CrossRef]
64. Zhao, D.; Huang, L.; Li, J.; Qi, J. A comparative analysis of broadband and narrowband derived vegetation indices in predicting LAI and CCD of a cotton canopy. *ISPRS J. Photogramm. Remote Sens.* **2007**, *62*, 25–33. [CrossRef]
65. Hatfield, J.L.; Gitelson, A.A.; Schepers, J.S.; Walthall, C.L. Application of spectral remote sensing for agronomic decisions. *Agron. J.* **2008**, *100*, 117–131. [CrossRef]
66. Antille, D.L.; Lobsey, C.R.; McCarthy, C.L.; Thomasson, J.A.; Baillie, C.P. A review of the state of the art in agricultural automation. Part IV: Sensor-based nitrogen management technologies. In *An ASABE Meeting Presentation, Proceedings of the Annual International Meeting, Detroit, MI, USA, 29 July–1 August 2018*; American Society of Agricultural and Biological Engineers: St. Joseph, MI, USA, 2018.
67. Thomas, S.; Wahabzada, M.; Kuska, M.T.; Rascher, U.; Mahlein, A.-K. Observation of plant–pathogen interaction by simultaneous hyperspectral imaging reflection and transmission measurements. *Funct. Plant Biol.* **2017**, *44*, 23. [CrossRef]

68. Labate, D.; Ceccherini, M.; Cisbani, A.; De Cosmo, V.; Galeazzi, C.; Giunti, L.; Melozzi, M.; Pieraccini, S.; Stagi, M. The PRISMA payload optomechanical design a high performance instrument for a new hyperspectral mission. In Proceedings of the 59th International Astronautical Congress IAC, Glasgow, UK, 29 September–3 October 2008; pp. 2637–2643. [CrossRef]
69. Guanter, L.; Kaufmann, H.; Segl, K.; Foerster, S.; Rogass, C.; Chabrillat, S.; Kuester, T.; Hollstein, A.; Rossner, G.; Chlebek, C.; et al. The EnMAP spaceborne imaging spectroscopy mission for earth observation. *Remote Sens.* **2015**, *7*, 8830–8857. [CrossRef]
70. Zhao, X.; Xiao, Z.; Kang, Q.; Li, Q.; Fang, L. Overview of the Fourier Transform Hyperspectral Imager (HSI) boarded on HJ-1A satellite. *2010 IEEE International Geosci. Remote Sens. Symp.* **2010**, 4272–4274. [CrossRef]
71. Kumar, A.; Saha, A.; Dadhwal, V.K. Some issues related with sub-pixel classification using HYSI data from IMS-1 satellite. *J. Indian Soc. Remote Sens.* **2010**, *38*, 203–210. [CrossRef]
72. Platnick, S.; King, M.D.; Ackerman, S.A.; Menzel, W.P.; Baum, B.A.; Riédi, J.C.; Frey, R.A. The MODIS cloud products: Algorithms and examples from terra. *IEEE Trans. Geosci. Remote Sens.* **2003**, *41*, 459–472. [CrossRef]
73. Forkuor, G.; Dimobe, K.; Serme, I.; Tondoh, J.E. Landsat-8 vs. Sentinel-2: Examining the added value of sentinel-2's red-edge bands to land-use and land-cover mapping in Burkina Faso. *GIScience Remote Sens.* **2018**, *55*, 331–354. [CrossRef]
74. Hoel, B.O.; Solhaug, K. Effect of Irradiance on Chlorophyll Estimation with the Minolta SPAD-502 Leaf Chlorophyll Meter. *Ann. Bot.* **1998**, *82*, 389–392. [CrossRef]
75. Zhou, G.; Yin, X. Assessing nitrogen Nutritional status, Biomass and Yield of Cotton with NDVI, SPAD and Petiole SAP Nitrate concentration. *Exp. Agric.* **2018**, *54*, 531–548. [CrossRef]
76. Schepers, J.; VanToai, T.; Major, D.J.; Baumeister, R.; Touré, A.; Zhao, S. Methods of Measuring and Characterizing the Effects of Stresses on Leaf and Canopy Signatures. *ASA Spec. Publ.* **2003**, *66*, 81–93. [CrossRef]
77. Li, H.; Zhao, C.; Huang, W.; Yang, G. Non-uniform vertical nitrogen distribution within plant canopy and its estimation by remote sensing: A review. *Field Crop. Res.* **2013**, *142*, 75–84. [CrossRef]
78. Shaw, M.W.; Royle, D.J. Estimation and validation of a function describing the rate at which Mycosphaerella graminicola causes yield loss in winter wheat. *Ann. Appl. Biol.* **1989**, *115*, 425–442. [CrossRef]
79. Rodriguez-Moreno, F.; Zemek, F.; Kren, J.; Pikl, M.; Lukas, V.; Novak, J. Spectral monitoring of wheat canopy under uncontrolled conditions for decision making purposes. *Comput. Electron. Agric.* **2016**, *125*, 81–88. [CrossRef]
80. Filella, I.; Serrano, L.; Serra, J.; Penuelas, J. Evaluating Wheat Nitrogen Status with Canopy Reflectance Indices. *Crop Sci.* **1995**, *35*, 1400–1405. [CrossRef]

4 Publication II

Development and Evaluation of a Leaf Disease Damage Extension in Cropsim-CERES Wheat

Röll, G.; Batchelor, W.D.; Castro, A.C.; Simón, M.R.; Graeff-Hönninger, S. Development and Evaluation of a Leaf Disease Damage Extension in Cropsim-CERES Wheat. *Agronomy* 2019, *9*, 120.

Spectral sensors and crop models are useful tools to develop an N application strategy. While crop models have to account for different crop managements and biotic and abiotic stresses, the wheat models included within the DSSAT environment are not capable of simulating the effects of disease infection on growth and yield parameters. Extending the model to account for disease creates, the ability to simulate disease damage on the wheat crop including reduction in yield due to reduction in assimilate production. As a consequence, N application may have to be adjusted if a disease occurs and leads to yield limitations.

agronomy

MDPI

Article

Development and Evaluation of a Leaf Disease Damage Extension in Cropsim-CERES Wheat

Georg Röll [1,*], William D. Batchelor [2], Ana Carolina Castro [3,4], María Rosa Simón [3,5] and Simone Graeff-Hönninger [1]

1 Department of Agronomy, Institute of Crop Science, University of Hohenheim, 70599 Stuttgart, Germany; Simone.graeff@uni-hohenheim.de
2 Biosystems Engineering Department, Auburn University, Auburn, AL 36849, USA; wdb0007@auburn.edu
3 Cerealicultura, Facultad de Ciencias Agrarias y Forestales, Universidad Nacional de La Plata, Av. 60 y 119, La Plata 1900, Argentina; ana.castro@agro.unlp.edu.ar (A.C.C.); mrsimon@agro.unlp.edu.ar (M.R.S.)
4 Consejo Nacional de Investigaciones Científicas y Técnicas (CONICET), Centro Científico Tecnológico (CCT), La Plata 1900, Argentina
5 Comisión de Investigaciones Científicas, Pcia. de Buenos Aires, 526, 10 y 11, La Plata 1900, Argentina
* Correspondence: georg.roell@uni-hohenheim.de; Tel.: +49-711-459-22380

Received: 10 January 2019; Accepted: 1 March 2019; Published: 2 March 2019

Abstract: Developing disease models to simulate and analyse yield losses for various pathogens is a challenge for the crop modelling community. In this study, we developed and tested a simple method to simulate septoria tritici blotch (STB) in the Cropsim-CERES Wheat model studying the impacts of damage on wheat *(Triticum aestivum* L.) yield. A model extension was developed by adding a pest damage module to the existing wheat model. The module simulates the impact of daily damage on photosynthesis and leaf area index. The approach was tested on a two-year dataset from Argentina with different wheat cultivars. The accuracy of the simulated yield and leaf area index (LAI) was improved to a great extent. The Root mean squared error (RMSE) values for yield (1144 kg ha^{-1}) and LAI (1.19 m^2 m^{-2}) were reduced by half (499 kg ha^{-1}) for yield and LAI (0.69 m^2 m^{-2}). In addition, a sensitivity analysis of different disease progress curves on leaf area index and yield was performed using a dataset from Germany. The sensitivity analysis demonstrated the ability of the model to reduce yield accurately in an exponential relationship with increasing infection levels (0–70%). The extended model is suitable for site specific simulations, coupled with for example, available remote sensing data on STB infection.

Keywords: wheat; disease; yield; septoria tritici blotch; leaf area index; crop modelling; decision support system for agrotechnology transfer (DSSAT); Cropsim-CERES Wheat

1. Introduction

Wheat *(Triticum aestivum* L.) is the second most important staple food crop for human nutrition. It is grown worldwide on approximately 220 million hectares under different climatic conditions. It is projected that wheat production must increase by 1.6% annually to meet the expected global demand by 2050 [1]. However, increasing temperatures and changing global rainfall patterns will likely influence breeding, management, fertilization and crop protection strategies for wheat [2] and also influence disease patterns [3,4]. Hence, crop protection measures will play an important role under future climate change, as rising temperatures and changes in rainfall pattern, will cause more favourable conditions for pests and diseases, especially in the warming north, where wheat production is predominant [2].

On a global scale, there are approximately 50 diseases and pests, which have the potential to damage wheat and reduce farmer's income [5–7]. On a global level, the most widely adapted wheat

fungal diseases are leaf rust caused by "*Puccinia triticina* E.," stripe rust caused by "*Puccinia striiformis* W.," stem or black rust caused by "*Puccinia graminis* E.," powdery mildew caused by "*Blumeria graminis* P." and septoria tritici blotch (STB) caused by "*Zymoseptoria tritici* D." [1]. The infection by "*Zymoseptoria tritici* D." is the most economically damaging wheat disease worldwide [8]. It can cause yield reductions of 50% to 60% [9] by creating leaf lesions resulting in defoliation and reduced photosynthesis. It has been estimated that 70% of the annual usage of fungicides in Europe is related to the treatment of this disease [10].

During the past decade, there has been an increasing resistance of STB to azole and strobilurin fungicides in Europe [9–11]. Breeding for STB disease resistance is complicated, due to the variability of the pathogen reproduction cycle [12,13]. Researchers have studied different strategies including tillage, crop rotation, delayed sowing, fungicide application and a proper level of fertilizer application to reduce or control the infection of STB [14]. It appears that moderate fungicide application coupled with the right amount of fertilizer is a strategy that holds promise for environmentally friendly wheat production, while reducing at the same time STB infection.

Crop models are suitable for decision support and contribute to a better understanding in the development of new wheat production strategies. They can play a vital role in understanding plant growth processes, the impact of different weather scenarios as well as management strategies on disease outbreak, final yield and grain quality. Hence, crop models might help to spread the production of wheat in more economic and sustainable ways.

Crop models can also provide an insight into yield losses due to pests and diseases, including STB. Several mechanistic wheat crop growth models have been developed over the last several decades, including APSIM [15], WheatGrow [16], STICS [17], Sirius [18] and DSSAT [19]. These models were developed to study crop-environment interaction and to evaluate optimum management strategies.

The Cropsim-CERES-Wheat (CCW) model [20–22] included in the DSSAT version 4.6 [23] was developed to study the impact of genetics, management, weather and climate change on wheat growth and yield. The model simulates daily plant development based on daily maximum and minimum temperature, daylength and vernalisation requirements. Growth is computed on a daily basis using a radiation use efficiency approach. Carbon is allocated daily to different plant parts based on the development stage. The CCW model has been linked with remote sensing data [24] and was successfully tested with different cultivars, soil characteristics as well as in different climatic conditions including Canada [25], Argentina [26], Southern Italy [27] and the United Kingdom [28]. Currently the CCW model does not account for damage due to weeds, pests or diseases [29]. As a consequence, inaccurate simulations of crop growth and yield result when simulating datasets that include pests and diseases [30,31].

Developing and incorporating a disease damage extension would expand the use of the CCW model to simulate and study the impact of disease damage on crop growth and yield. Batchelor et al. [32] incorporated a pest damage into the CROPGRO [33] family of models distributed with the DSSAT [34]. In their approach, they defined pest coupling points as daily rate and state variable modifiers to simulate the impact of daily pest damage on leaf, stem, seed, shell and root state variables and daily photosynthesis rate based on daily inputs of pest damage. They tested this approach for different pest damage types for peanut and soybean crops. They evaluated this approach using a dataset to simulate the impact of velvetbean caterpillar on soybean.

Using the same approach, the purpose of this work was to: (i) develop a disease model extension for the simulation of STB in wheat, to (ii) evaluate the model performance using a dataset from Argentina; and (iii) to conduct a sensitivity analysis for the impact of different disease progress curves on leaf area index and yield using a dataset from Germany.

2. Materials and Methods

2.1. Model Development

Currently the CCW model does not account for competition with weeds, pests or diseases. To solve this problem, modifications of the current CCW version are necessary to include the impact of leaf diseases on final crop yield.

Plant dry matter accumulation and yield can be expressed as a function of leaf area index (LAI), radiation use efficiency and the loss of assimilates due to respiration. Pathogens can modify both leaf area index and daily photosynthesis [35].

The primary damage resulting from STB is defoliation, which reduces both leaf area and leaf photosynthetic rate [36,37].

To apply the damage theory, it was necessary to integrate the pest damage module [32] structure into the current CCW wheat model (Figure 1). These changes included the adding and linkage of the following subroutines to the original version: PEST.for, LINDM.for, PESTCP.for, VEGDM.for and OPPEST.for. A pest damage definition file was created to define the coupling point "leaf area" for the leaf disease STB (Figure 1), where daily damage could be applied to state and rate variables in the model. Percent cumulative leaf area destroyed (PCLA) was chosen as major coupling point in the model.

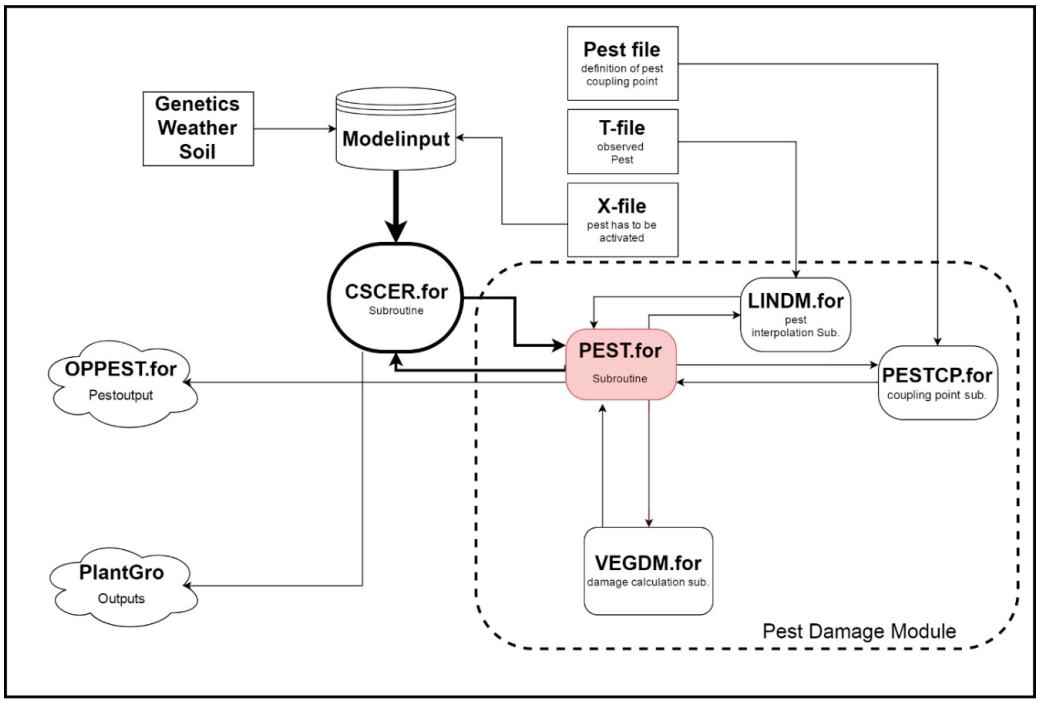

Figure 1. A simplified diagram of the Cropsim-CERES-Wheat (CCW) model with the pest damage module incorporated.

Field observed damage levels were entered in the time series file, referred to as File T in the DSSAT family of models. In this file, the year and day of year (DOY) are entered, along with STB infection in percent. Observed disease infection was linked to the percent cumulative leaf area destroyed (PCLA) coupling point. This damage type (i.e., PCLA) is defined in the pest damage definition model input file, which links field observed damage type and levels to the internal model pest damage coupling point. The model uses a linear interpolation to compute daily damage from periodic field observations. In this work, it was assumed that STB infection began ten days before the first infection symptoms were

observed in the field. This assumption was made, based on Sánchez-Vallet et al. [38] who reported a latent period for STB between day 8 and 14 after infection depending on the environmental conditions. The daily percentage of damage (N_{pt}) was calculated between field observations using

$$N_{pt} = P_{rt*} + \frac{(P_{rt} - P_{rt*})}{(D_{pt} - D_{pt*})} \times (D_s - D_{pt*}) \quad (1)$$

N_{pt} = daily reported damage for damage type p at time t; D_{pt} = DOY of next field observation of damage (P_{rt}); D_{pt*} = DOY of previous field observation of damage (P_{rt*}); D_s = day of current simulation; P_{rt} = damage level reported in the next field observation; P_{rt*} = damage level reported in the previous field observation.

The daily damage calculation, which was applied to the leaf area coupling point (P_{it}) is calculated in the PESTCP. for subroutine (Figure 1) by Equation (2):

$$P_{it} = (N_{pt})(C_{ip}) \quad (2)$$

The pest coefficient (C_{ip}) allows the model to convert units of damage into units used for the model state or rate variable that is being damaged.

After calculating the daily damage to be applied to the diseased leaf area based on interpolations from field observations, the daily damage (D_{ipt}) to be applied to the leaf area state variable (defoliated leaf area) is calculated by the following equation:

$$D_{ipt} = X_{it}{}^* - (Xt_{it} - Xs_{it}) \times \left(1 - \frac{P_{it}}{100}\right) \quad (3)$$

X_{it}* = state or model variable i on day t, before application of damage; X_{it} = state or model variable i on day t, after application of damage; Xt_{it} = cumulative amount of coupling point I; Xs_{it} = cumulative senescence of coupling point I; D_{ipt} = amount of damage applied on state or model variable i on day t; P_{it} = coupling point leaf area.

Finally, the model state or rate variable is adjusted by subtracting the computed defoliation from the leaf area state variable by Equation (4):

$$X_{it} = X_{it}{}^* - D_{ipt} \quad (4)$$

X_{it} = state or model variable i on day t, after application of damage; X_{it}* = state or model variable i on day t, before application of damage; D_{ipt} = amount of damage applied on state or model variable i on day t.

2.2. Field Trials

In this study, datasets from two different locations were used for model development. The first dataset was recorded on the Experimental Station Julio Hirschhorn in La Plata (34°56′ S, 57°57′ W, 15 m above sea level, 16.3 °C average temperature; 946 mm mean annual precipitation) National University of La Plata in Argentina. The second experiment was carried out at the Experimental Station Ihinger Hof (48°44′ N, 8°55′ E; 480 m above sea level, mean annual temperature 9.1 °C and 714 mm mean annual precipitation) University of Hohenheim in Germany.

The trial in Argentina was conducted in two consecutive years (2010 and 2011) and published by Castro and Simón [39]. The objective of this trial was to test the tolerance of ten different Argentinean wheat cultivars (*Triticum aestivum* L.) for STB and to evaluate the disease impact on grain yield and grain quality. The sowing dates were on 15th of July in 2010 and 16th of June in 2011. The soil type was a silty loam. Nitrogen was applied as urea at 100 kg N ha^{-1} at sowing and 80 kg N ha^{-1} at the end of tillering. Three different inoculation levels with *Zymoseptoria tritici* D. were performed. The first level was the control treatment, the second was considered to be a low inoculation level (with 5×10^5

spores mL^{-1} suspension), while the third treatment was considered as high inoculation treatment (5×10^6 spores ml^{-1} suspension). All inoculations were performed at growth stage 22 (beginning of tillering) [40] and at growth stage 39 (flag leaf emergence). For model development weather data (daily temperature, rainfall, solar radiation) from the weather station La Plata (34°56′ S, 57°57′ W), disease severity ratings (%) from three growth stages (GS 39, 60, 82), leaf area index (LAI) which was calculated from the green leaf area (GLAI) plus non-green leaf area (NGLAI), yield, soil properties and management information were collected.

The second trial in Germany was conducted in 2006 using the cultivar Monopol with three inoculation levels (control treatment; low inoculation 50%; high inoculation 100%) of *Zymoseptoria tritici*. Inoculation was imposed by spraying 50% or 100% of a spore suspension (1×10^6 spores per mL, strain CBS 292.69) onto the plots at growth stage 32 [41]. The sowing date was 22nd of October 2005 on a silty clay soil. Nitrogen in form of ammonium nitrate was applied at three growth stages: 100 kg N ha^{-1} at GS 30, 80 kg N ha^{-1} at GS 32 and 40 kg N ha^{-1} at GS 49. The objective of this field trial was to use different vegetation indices to determine the occurrence of plant diseases in winter wheat (*Triticum aestivum* L.). For model sensitivity analysis, data including temperature, rainfall and solar radiation from the weather station Ihinger Hof, as well as growth stages, yield monitoring data, disease severity ratings and the LAI at growth stages GS 31, 34 and 49 were collected. Further information on the trial layout can be found in Gröll [41].

2.3. Model Calibration and Evaluation

The modified CCW model extension was incorporated into the DSSAT 4.6 software. Model inputs were created for both datasets from Argentina and Germany. The dataset from La Plata of 2010, which included phenological, yield, soil data (Table 1) and weather data, was used for calibration to test the ability of the model to simulate the impact of STB on wheat growth and yield.

Table 1. Soil properties for experiments in La Plata and Ihinger Hof used in the simulation.

Location La Plata	Clay Content %	Sand Content %	Silt Content %	LLL *	DUL **	SAT ***
0–30 cm	20.7	28.9	50.4	0.226	0.457	0.561
30–60 cm	20.7	28.9	50.4	0.226	0.457	0.561
60–90 cm	20.7	28.9	50.4	0.226	0.457	0.561
Location Ihinger Hof						
0–30 cm	43.3	9.9	46.8	0.247	0.412	0.467
30–60 cm	43.3	9.9	46.8	0.247	0.412	0.467
60–90 cm	25.0	18.8	56.2	0.142	0.313	0.503

* Lower limit ≙ permanent wilting point (pF 4.2). ** Drained upper limit ≙ field capacity (pF 1.8). *** Saturated ≙ saturated water content (pF 0).

Genetic coefficients for growth and development were calibrated using the 2010 dataset and the control treatment for each cultivar. Calibration was performed by sequentially adjusting the genetic coefficients (Table 2) to minimize the error between measured and simulated values [19]. The existing species file was set as default and the existing ecotype UKWH01 as well as the cultivar file were modified. Coefficients for phenological development (P1V, P1D, P1–P5 and PHINT) were calibrated in the first step, followed by crop growth coefficients (G1, G2 and G3). The RMSE, index of agreement (d-Index) and modelling efficiency (EF) statistics were used to assess the quality of the calibration (see section statistical evaluation). After calibration of individual cultivars, the percentage infection with STB of the low and high inoculation was applied to test the model response. The dataset from La Plata of 2011 was used for model validation.

Table 2. Cultivar coefficients in Cropsim-CERES-Wheat (CCW) model used to simulate crop development, crop growth and crop yield for different cultivars.

Parameter	Definition	Ihinger Hof		La Plata					
		Monopol	ACA801	B75 Aniversario	Buck Brasil	Buck Guapo * Baguette 10 * Klein Zorro * Relmó Centinela *	Klein Escorpion	Klein Flecha	Klein Chaja
Cultivar file									
P1D	Percentage reduction in development rate in a photoperiod 10 h shorter than the threshold relative to that at the threshold	110	100	100	100	100	100	100	100
P1V	Days at optimum vernalizing temperature required to complete vernalisation	90	20	20	20	20	20	20	20
G1	Kernel number per unit canopy weight at anthesis (kernels g^{-1})	15	25	25	20	22	22	22	25
G2	Standard kernel size under optimum conditions (mg)	48	25	30	30	30	35	30	39
G3	Standard, non-stressed dry weight of a single tiller at maturity (g)	2.0	4.0	4.0	4.0	4.0	4.0	4.0	4.0
P5	Duration of the grain filling phase (°C d)	600	420	430	420	420	420	420	420
PHINT	Interval between successive leaf tip appearances (°C d)	90	92	92	92	92	80	93	92
Ecotype file									
P1	Duration of phase end juvenile to terminal spikelet	350	350	350	350	350	350	350	350
P2	Duration of phase from double ridges to the end of leaf growth (°C d)	200	250	250	250	250	250	250	250
P3	Duration of phase from the end of leaf growth to the end of spike growth (°C d)	300	220	220	220	220	220	220	220
P4	Duration of phase from the end of spike growth to the end of the grain fill lag (°C d)	380	300	300	300	300	300	300	300
PARUE	Conversion rate from photosynthetically active radiation to dry matter before the last leaf stage (g MJ^{-1})	2.3	2.7	2.7	2.7	2.7	2.7	2.7	2.7
SLAS	Specific leaf area, standard first leaf (cm^2/g)	400	450	450	450	450	450	450	450

* various wheat cultivars with the same cultivar coefficients.

The second dataset from Ihinger Hof was used for sensitivity analysis to test the model on a different location to proof the concept and to test the responsiveness of the model of different STB infection levels. The calibration was performed in the same way as in La Plata with the control treatment by modifying the necessary cultivar coefficients (Table 2). We applied 0%, 10%, 20%, 30%, 50% and 70% damage rates at maximum LAI (GS 39) and started the damage application at growth stage GS 31 to estimate the corresponding yield loss. The different damage rates were used to test the model responsiveness on a broad disease range, which typically starts to impact yield after growth stage 31 [42].

Statistical Evaluation

The statistical model evaluation was conducted by comparing the simulated and observed LAI and yield of the different inoculation treatments (dataset from La Plata).

For statistical analysis, the root mean squared error (RMSE. Equation (5)), the index of agreement (d-Index, Equation (6)) [43] and the modelling efficiency (EF, Equation (7)) were used. The RMSE was used to quantify the amount of variation between simulated and measured values on a metric scale. The d-Index shows if the model is under -or over-estimating the measurements. The EF parameter compares simulated values with the average of the measurements. For a perfect fit between simulated and observed data, the RMSE should be at 0 and the d-Index and EF parameter should have a value of 1.0.

The statistical evaluation was done for simulation runs of the original CCW version and the modified CCW for LAI and yield from both years (2010; 2011) on the location La Plata over all cultivars and inoculation treatments.

Root mean square error (RMSE):

$$RMSE = \left[\frac{1}{n}\sum_{i=1}^{n}(S_i - O_i)^2\right]^{0.5} \quad (5)$$

Index of agreement (d):

$$d = 1 - \left[\frac{\sum_{i=1}^{n}(S_i - O_i)^2}{\sum_{i=1}^{n}\left(|S_i - \overline{O}| + |O_i - \overline{O}|\right)^2}\right] \quad (6)$$

Modelling efficiency (EF):

$$EF = 1 - \left[\frac{\sum_{i=1}^{n}(S_i - O_i)^2}{\sum_{i=1}^{n}\left(O_i - \overline{O}\right)^2}\right] \quad (7)$$

where: O_i = observed values; S_i = simulated values; n = numbers of samples; $\overline{O}$ = mean of observed data

3. Results and Discussion

3.1. Model Calibration for La Plata

3.1.1. Leaf Area Index

The calibration was performed on the 2010 dataset by fitting the relevant genetic coefficients (Table 2) for phenology and growth. One essential prerequisite for model development is an accurate simulation of growth stages. In this study, growth stages (GS 39; GS 60; GS 82) were predicted by the model conclusively: For all ten cultivars the flowering date (GS 65) was documented approximately 110 days after sowing (DAS), the model simulated this growth stage 115 DAS. A similar result was obtained by comparing observed and simulated DAS of the early dough stage (GS 82) (observed approximately at 131 DAS, simulated 132 DAS).

The main focus of this model calibration was on the adjustment of leaf area as a major coupling point for disease damage. Figures 2 and 3 illustrate the simulated and the observed values for leaf area index and grain yield across different inoculation treatments along with the statistics (Table 3).

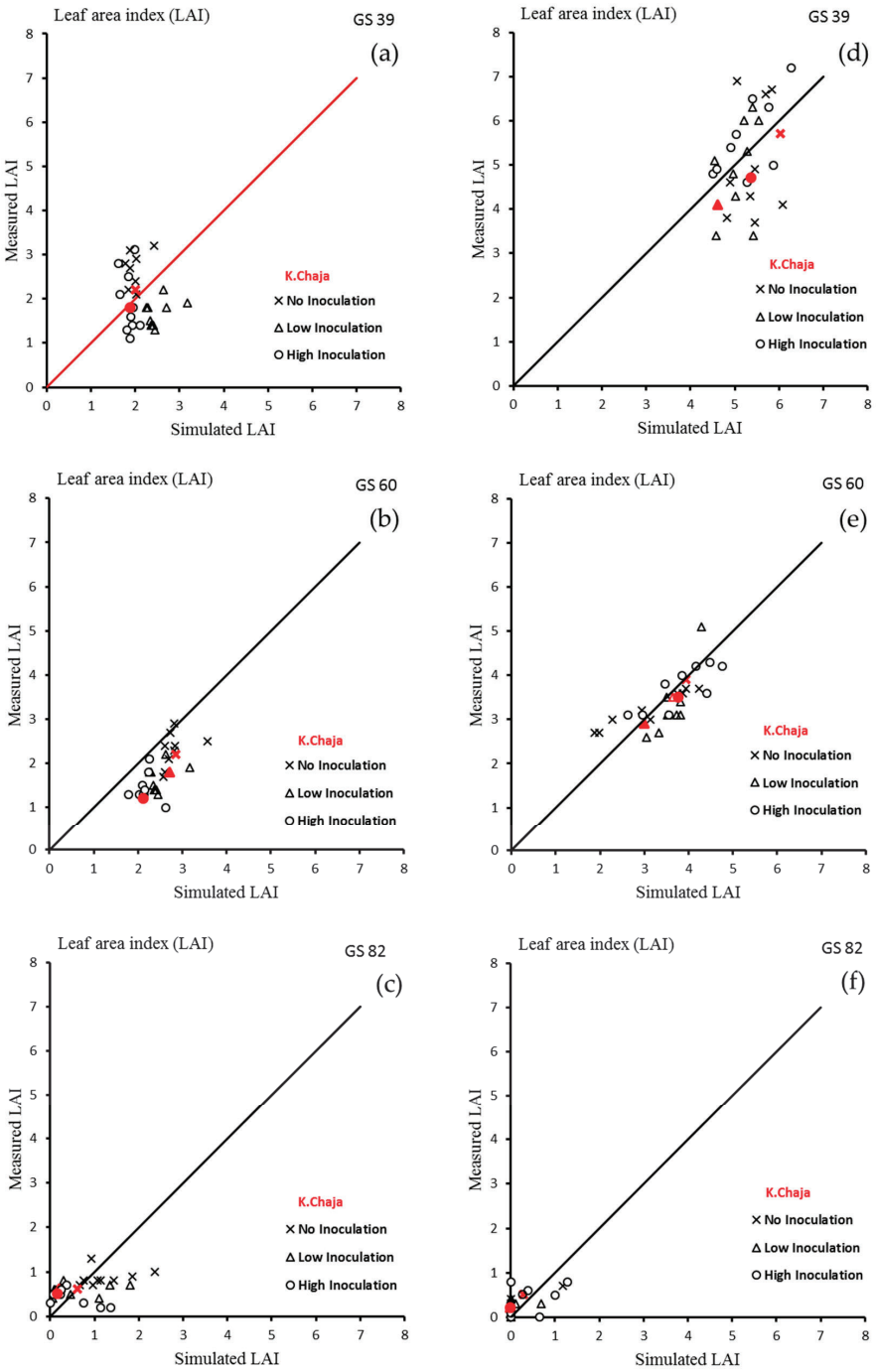

Figure 2. Simulated vs. measured leaf area index (LAI) for calibration (year 2010 **a**–**c**) and validation (year 2011 **d**–**f**) for all ten cultivars on the location La Plata. Different symbols represent the different inoculation treatments where × = No Inoculation; Δ = Low Inoculation and O = High Inoculation.

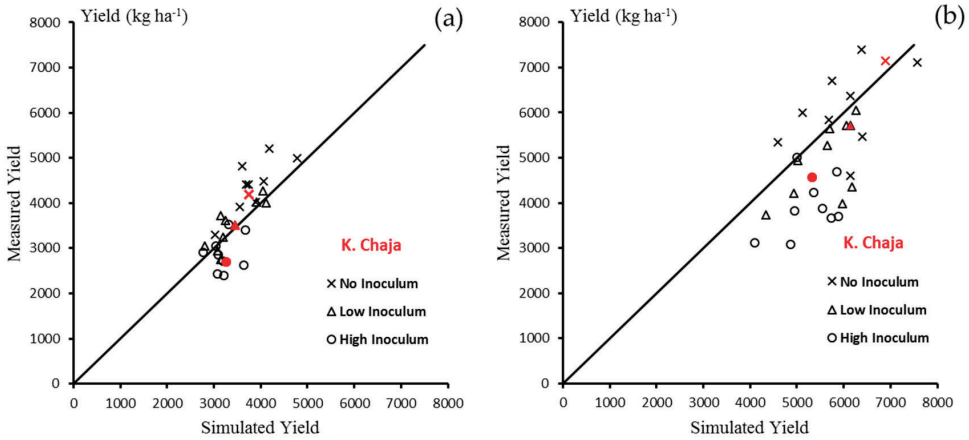

Figure 3. Simulated vs. measured yield (kg DM ha^{-1}) for calibration and validation for all ten cultivars on the location La Plata 2010 (**a**) and La Plata 2011 (**b**).

Table 3. Statistical evaluation of the simulation of leaf area index and grain yield of the original CCW model and the developed CCW model extension for diseases using root mean square error (RMSE), Willmott's d statistic (d-Index) and modelling efficiency (EF).

		Original CCW			Modified CCW		
Variable	**Experiment**	**RMSE**	**d-Index**	**EF**	**RMSE**	**d-Index**	**EF**
Leaf area index	La Plata 2010	1.19	0.33	−2.69	0.69	0.51	−1.07
	La Plata 2011	2.88	0.24	−0.98	1.11	0.70	0.68
Yield	La Plata 2010	1144	0.47	−1.19	499	0.81	0.58
	La Plata 2011	1755	0.50	−1.19	1285	0.66	−0.18

For demonstration of the overall model behaviour in regard to LAI changes induced by three different STB inoculation treatments over time, the wheat cultivar K. Chaja was selected. This cultivar was considered to be highly susceptible to STB infection [39]. Figure 4a shows the impact of disease infestation on LAI according to different inoculation treatments 90 days after sowing. All three simulation runs reached the maximum LAI at day 100. For the control treatment a maximum LAI of 3.5 was simulated. A difference of 0.5 LAI was found between the control and the high-inoculation treatment. Comparing simulated and observed LAI values, the model predicted the LAI over the vegetation period in an accurate manner (RMSE 0.47, d-Index 0.9).

Similar results are displayed in Figure 2a–c, which illustrates the simulated versus observed LAI across three different inoculation treatments for different cultivars. Regardless of susceptibility, in GS 39 all ten cultivars showed a homogenous distribution of all data points around the 1:1 line with no strong outliers. A slight tendency for an overestimation of LAI was given at GS 39 in the low and high inoculation treatments, whereas for the control treatment a slight underestimation was shown over all cultivars. In GS 60 and GS 82, a slight overestimation of LAI was found for all inoculation treatments.

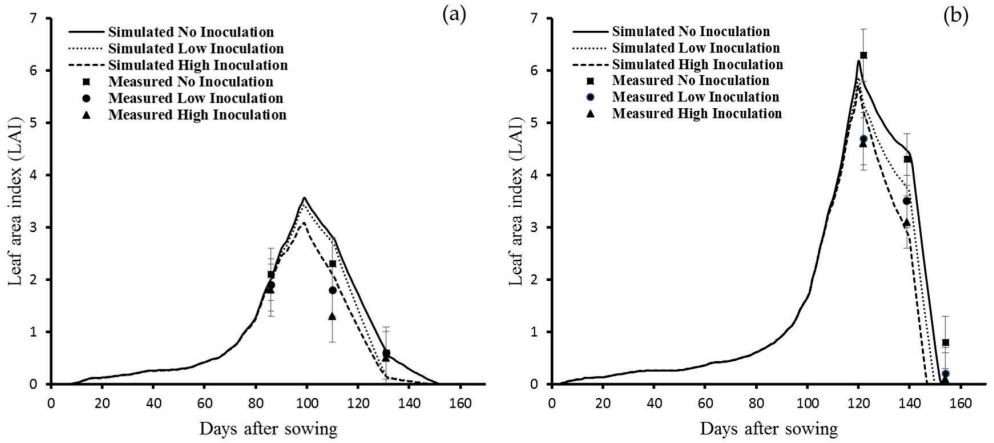

Figure 4. Simulated and measured leaf area index values for cultivar K. Chaja, year 2010 (**a**) and 2011 (**b**) including different inoculation treatments with septoria tritici blotch (STB). The error bars demonstrate the LSD of the leaf area index.

Finally, the modified CCW model (RSME 0.69; d-Index 0.51) performed better compared to the original CCW model (RSME 1.19; d-Index 0.33), as indicated by the corresponding statistics. Outliers in Figure 2a–c can be explained by the LSD ranging from 0.4 to 1.0 depending on the sampling date, reported from Castro and Simón [39].

Nevertheless, the model was able to account for all ten cultivars representing different tolerance levels to STB at different growth stages and disease severities accurately.

3.1.2. Yield

A reduction in LAI after infection with STB also leads to a reduction in yield (Figure 5a). Yield formation started for the cultivar K. Chaja (Figure 5a) on day 122 and was negatively correlated with the inoculation treatment. Yield of the control treatment (3800 kg ha^{-1}) was slightly underestimated and the high inoculation treatment (3400 kg ha^{-1}) showed a slight overestimation.

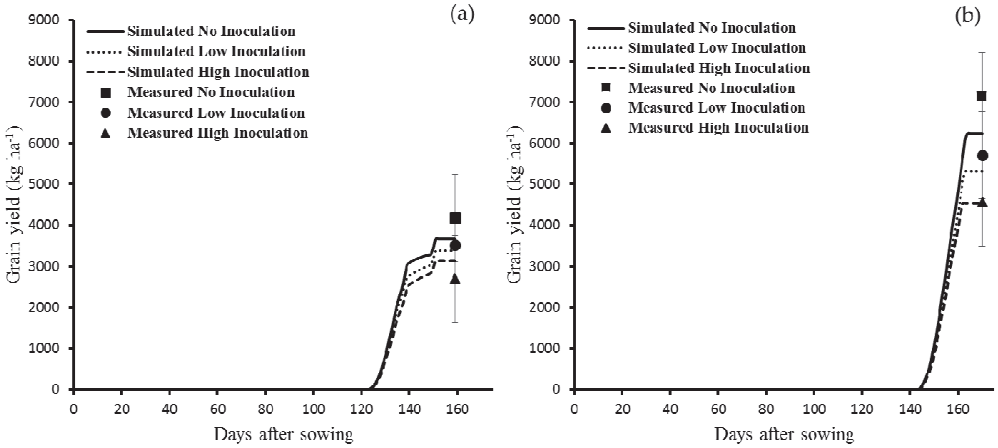

Figure 5. Simulated and measured grain yield values for cultivar K. Chaja year 2010 (**a**) and 2011 (**b**) including different inoculation treatments with STB. The error bars demonstrate the LSD of the yield.

Figure 3a represents the observed versus the simulated yield for all ten cultivars and showed a dense clustering of the different inoculation treatments around the 1:1 line. Overall, it indicated

the highest simulated yield for the control and the lowest yield for the high inoculation treatment. The results illustrated the capability of the modified CCW model to account for disease damage. This is expressed in the statistical evaluation (Table 3), where a reduction of the RMSE from 1144 (original version) to 499 (modified version) was observed. The d-Index also underlined these findings, which increased from 0.47 (original version) to 0.81 (modified version).

The modification of the existing CCW showed very good results in LAI and yield simulation (Table 3). It indicated a clear improvement for all statistical parameters compared with the existing CCW included in the current DSSAT version. The calibration successfully minimized the error between measured and simulated data for both, LAI and yield.

3.2. Model Validation for La Plata

3.2.1. LAI

Illustrating LAI (Figure 2d–f) and yield (Figure 3b) for the cultivar K. Chaja and all cultivars in the validation year 2011.

In 2011, a maximum LAI of 6.3 was observed in the control treatment for K. Chaja (Figure 4b) at day 120. The model simulated a maximum LAI of 6.2 for the control treatment on the same day. For the low-inoculation treatment, a maximum LAI of 4.7 was observed, whereas the model simulated a maximum LAI of 5.8. Regarding the highest inoculation treatment, a LAI of 4.6 was observed in the field experiment. The model simulated for the same treatment a maximum LAI of 5.7. The model was capable to simulate the maximum LAI for the control treatment exactly but it slightly overestimated the maximum LAI both for the lowest and highest inoculation treatment.

In general LAI was higher in 2011 than in 2010 independent of cultivars, growth stages and inoculation treatments (Figure 2). For 2011 and GS 39, the 1:1 plot showed no strong outliers and a slight overestimation for the control treatment and a slight underestimation for the highest inoculation treatment. This can be caused by an earlier onset of disease in the inoculated treatments which was not reported and cause a slightly underestimation in the model. For GS 60 and GS 82 the model predicted the observed LAI values accurately.

3.2.2. Yield

Yield formation started 140 days after sowing for K. Chaja (Figure 5b), while full maturity was reached on day 165. A maximum yield of 6000 kg ha^{-1} was reached in the control treatment compared with the lowest yield of 5400 kg ha^{-1} in the high inoculation treatment. The corresponding error bars of the measured values were met by the simulated curves, which indicated a high accuracy of the simulation. Under consideration of all cultivars and inoculation treatments (Figure 3b) data points scattered around the 1:1 line on a broader range compared to the calibration (Figure 3a). An inverse relationship between inoculation level and yield was shown (Figure 5).

Overall, the developed model extension was able to account for STB disease damage. This is also shown by the statistics (Table 3), where a 30% improvement of the RMSE in the modified CCW version was achieved compared with the original model. This improvement was also shown by the d-Index and EF values. Further, the calibration showed a higher model accuracy when compared with the validation. Jing et al. [44] and Attia et al. [45] also reported a slightly weaker simulation accuracy regarding the validation dataset.

For 2010, a 20 days shorter growing period due to a 30 days later sowing date and a 130 mm lower precipitation compared to 2011 [39] was reported. Both factors resulted in a reduction of LAI and yield in 2010. Despite these differences the model performed very well for each inoculation treatment and showed its robustness when growing conditions differ between years. Measured yields in the inoculation treatments were simulated quite accurately, while the measured mean value of the control showed a 5% off-set. An explanation for this offset might be given in the way the disease ratings were performed and represented in the model. The model used the mean values from the disease

ratings of all repetitions and did not represent each individual plot. It is also possible that the trials had a slight infection of other diseases, which were not measured and caused a slight model offset. Another conceivable reason is the defined onset of disease ten days before disease rating was reported. This assumption was made because of the reported latent period for STB between day 8 and 14 after infection from Sánchez-Vallet et al. [38].

For 2010 and 2011, the d-Index values of the original CCW version are in a similar range for both LAI and yield. In the developed model extension, the d-Index, which represents the model accuracy, increased strongly even though in different intensities for each year. This may point to one possible shortcoming of the current model extension, as it does not account for spore disposal [46]. Spore disposal model use different leaf layers, rain intensity thresholds, droplets, sporulation and concentrations of starting spore pools and can therefore extend the simulation accuracy further.

Nevertheless, other STB models show a strong performance, if a minimum dataset is provided, in which more inputs like leaf wetness are included [47] or in which the initial state of infection of the first leaves is known [46]. Magarey et al. [47] also reported the necessity of hourly weather data for many disease models. In previous datasets this information is not given [48] and they cannot be used for disease modelling, which is literally a loss of information for agricultural decision making. This clearly shows the advantage of the developed CCW extension, in which only the percentage of disease rating, weather- and soil data is needed as a minimum dataset. This leads to a more accurate simulation as shown in Table 3 and makes the CCW applicable for a broader use.

3.3. Sensitivity Analysis

In order to test the general responsiveness of the developed model extension, a sensitivity analysis was carried out by comparing different inoculation treatments with the corresponding disease infections [41]. The model was calibrated by using an independent dataset with disease infections from Germany [41]. The disease infections varied between 4%, 13% and 15%. Disease infection started in GS 31 (DAS 200). Figure 6a depicts the simulated curves for the three different inoculation treatments. A maximum LAI of 7.3 was reached 40 days after GS 31. Simulated curves illustrate a clear separation between the 4%, 13% and the 15% disease infection. A maximum LAI of 7.2, 6.3, 6.1 was reached at day 240 at 4%, 13% and the 15% disease infection rating. Comparing simulated infection scenarios with measured values, the model simulated the LAIs of the three different disease infection levels accurately.

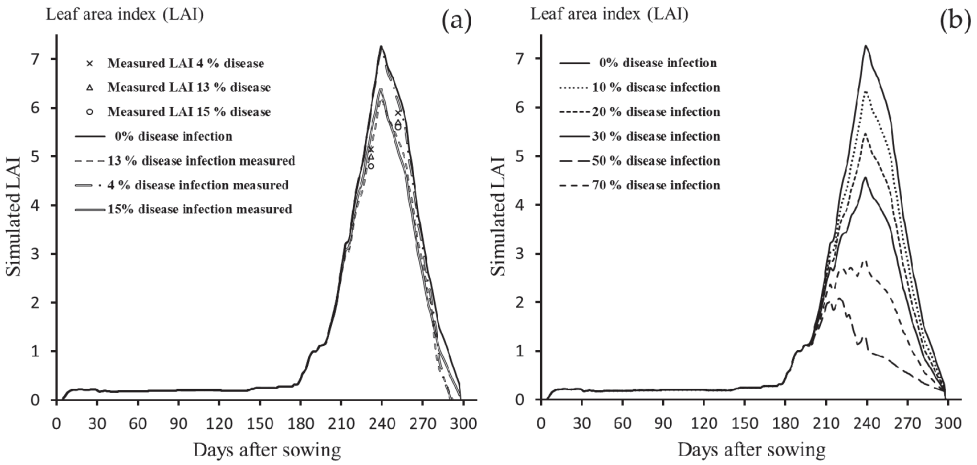

Figure 6. Sensitivity analysis of the CCW disease extension for measured disease infections (4%; 13%; 15%) (**a**) and for five infection scenarios (0%; 10%; 20%; 30%; 50%; 70% disease infection) (**b**) with STB at the location Ihinger Hof.

In the next step an artificial disease infection level of up to 70% was applied (Figure 6b) to test the general responsiveness and the boundaries of the developed model and to test the leaf damage theory on the leaf area coupling point (PCLA).

In Figure 6a a maximum LAI of 7.3 was reached 40 days after GS 31 in the control treatment. LAI increased almost linearly from day 200 to day 240 before the onset of senescence led to a constant decrease in LAI up to final harvest date. For the depicted disease infection scenarios of 10%, 20%, 30% and 50 % a maximum LAI of 7.3, 6.2, 5.4, 4.6, 2.9 and 1.3 was reached at day 240 (Figure 6b). The 70% disease infection scenario showed that a maximum LAI of 2.0 was reached earlier at 220 DAS (Figure 6b). Due to the massive destruction of leaf area, a shortage of assimilate production occurred, which affected in a next step the growth of new leaves. Simulated LAI reduction for maximum LAI in the different disease levels followed the magnitude of 12.5 % (10% diseased LAI), 24.8% (20% diseased LAI), 37.1% (30% diseased LAI), 60.3% (50% diseased LAI) and 82.4% (70% diseased LAI) (Table 4).

Table 4. Yield evaluation of the sensitivity analysis from the Ihinger Hof dataset, by comparing the percentage disease infection with STB and the corresponding simulated percentage yield reduction in kg DM ha^{-1} for the cultivar Monopol.

% Disease Infection	Simulated Yield kg ha^{-1}	Measured Yield kg ha^{-1}	% Yield Reduction	% LAI Reduction at Maximum LAI
0	4384		0	0
4 *	4332	4409	1.2	0.8
10	4190		4.4	12.5
13 *	4159	3934	5.1	14.5
15 *	4124	3965	5.9	12.0
20	3990		9.0	24.8
30	3737		14.8	37.1
50	3242		26.0	60.3
70	2380		45.7	82.4

* measured disease infection.

Table 4 shows the corresponding yields of the applied and measured disease infection levels. The maximum observed yield obtained with the disease infection level of 4% was 4409 kg ha^{-1}. Higher disease infection levels (13%; 15%) resulted in lower yield (3934 kg ha^{-1}; 3965 kg ha^{-1}). Simulated yield decreased gradually with higher infection levels. The control treatment resulted in a maximum yield of 4384 kg ha^{-1}, while the 70% disease infection level resulted in a total grain yield of 2380 kg ha^{-1} which corresponded to a 45.7% yield reduction. Over all tested disease infection levels, the simulated yield reduction followed an exponential shape, indicating that yield reductions became more severe and are more than doubled at higher disease infection levels. An exponential relationship between yield loss and disease infection was also shown by King et al. [49].

Comparing simulated and measured yield, the model showed a slightly underestimation for the 4% level and a slight overestimation for the 13% and 15% disease infection level. These variations are in an acceptable range.

Regarding the accuracy of the current simulation, similar results for yield reduction based on the occurrence of leaf diseases are reported by Ziv and Eyal [50]. Ziv and Eyal [50] tested different inoculation treatments in different spring wheat cultivars and reported yield losses of up to 53% at a disease infection of 73%. The developed CCW model extension gave comparable results to a previous study of Bhathal et al. [51] also at lower infection level scenarios. Bhathal et al. [51] tested different inoculation treatments in wheat to evaluate the relationship between disease infection and yield. Notably, they showed an onset of the disease as it was used in the sensitivity analysis of this study, at GS 31 and demonstrated a 10% yield loss due to a natural disease infection of 26%. King et al. [49], also confirmed this model theory on an independent dataset from the United Kingdom carried out at four different locations. Similar observations and an exponential yield loss curve due to STB disease were obtained. In addition, a yield loss of 30% by a disease infection of 55.1% as well as a yield

reduction of 8% by a disease infection of 14.5% occurred. This confirmed the model theory and clearly showed the capability to simulate leaf disease infection with STB by using the coupling point leaf area (PCLA).

3.4. Future Model Applications

Despite the good simulation results, the developed model concept can currently only be used for STB. The concept was not tested on other wheat diseases like stripe rust caused by "*Puccinia striiformis* W.," stem or black rust caused by "*Puccinia graminis* E." or powdery mildew caused by "*Blumeria graminis* P." It can be assumed that this concept will also work for other diseases, by changing the pest coefficient in the pest file to account for different damage types. Bastiaans [52] showed a ß–value for STB, which represents the correlation between visible affected leaf area and the affected photosynthetic rate. A ß–value > 1 indicates a stronger effect on photosynthetic rate as it visually appears. For STB this value is close to 1 wherefore the pest coefficient in the CCW model extension was set to 1. Bastiaans [52] reported a ß–value of 8.7 for "*Erisyhe graminis*" or 1.3 for "*Puccinia recondita*" in winter wheat. It is assumed, that the pest coefficient has to be increased in a similar manner but it has to be proven by real data. However, the structure of the model extension is set up in a flexible way and has the possibility to be transferred to other leaf diseases.

Further, the disease extension routine can suite as a gateway between crop models and remote sensing data, like it was published by Thorp et al. [53]. Thorp et al. [53] showed an improvement of simulation results by updating the plant leaf area state variable with green LAI generated by remote sensing. This offers the opportunity to simulate a given field on a site-specific scale, which means the CCW model extension can be updated by the percentage diseased leaf area detected by for example, remote sensing. In this way, the model could serve as decision support tool to give farmers an economic advise on a field level as Ficke et al. [54] proposed.

4. Conclusions

In this study a disease extension for the CCW model was developed to simulate the damage effect of STB disease on LAI and yield in wheat. The model was tested successfully in a sensitivity analysis on a German dataset and on a dataset obtained from La Plata, Argentina. Results of the study clearly showed the effect of the implementation of the coupling point "PCLA" and on the corresponding LAI and yield for different locations. For the location La Plata, the obtained simulation results of the modified CCW model indicated a higher model accuracy which almost doubled and clearly showed an improved model behaviour. Especially for the cultivar K. Chaja, the CCW model extension showed a high modelling accuracy. The LAI and yield were simulated very accurate in both years. Furthermore the sensitivity analysis also displayed the flexibility of the CCW model extension to account for disease damage over a broad range between 0 and 70% of STB disease infection.

Nevertheless, further research is needed to test the developed model on other leaf diseases like leaf rust, powdery mildew or stripe rust in wheat. The model extension could be used in future studies as decision support system for example, coupled with remote sensing technologies to obtain the necessary disease ratings for the model input files.

Author Contributions: Conceptualization, G.R., W.D.B. and S.G.-H.; methodology, W.D.B., G.R. and S.G.-H.; software, G.R. and W.D.B.; validation, G.R.; formal analysis, G.R.; investigation, G.R., A.C.C. and M.R.S.; resources, G.R., A.C.C. and M.R.S.; data curation, G.R.; writing—original draft preparation, G.R.; writing—review and editing, G.R., W.D.B. and S.G.-H.; visualization, G.R.; supervision, W.D.B. and S.G.-H.; project administration, S.G.-H.; funding acquisition, S.G.-H.

Funding: This research was funded by German Federal Environmental Foundation (DBU) (ProjectNr. 33143/01) and by the National Institute of Food and Agriculture, U.S. Department of Agriculture, Hatch project (ALA-14-1-16016).

Acknowledgments: The authors would like to thank the Universitätsbund Hohenheim e.V. for supporting the journey to Auburn University, Alabama.

Conflicts of Interest: The authors declare no conflict of interest. The funders had no role in the design of the study; in the collection, analyses or interpretation of data; in the writing of the manuscript or in the decision to publish the results.

References

1. Singh, R.P.; Singh, P.K.; Rutkoski, J.; Hodson, D.P.; He, X.; Jørgensen, L.N.; Hovmøller, M.S.; Huerta-Espino, J. Disease Impact on Wheat Yield Potential and Prospects of Genetic Control. *Annu. Rev. Phytopathol.* **2016**, *54*, 303–322. [CrossRef] [PubMed]
2. Olesen, J.E.; Trnka, M.; Kersebaum, K.C.; Skjelvåg, A.O.; Seguin, B.; Peltonen-Sainio, P.; Rossi, F.; Kozyra, J.; Micale, F. Impacts and adaptation of European crop production systems to climate change. *Eur. J. Agron.* **2011**, *34*, 96–112. [CrossRef]
3. Eigenbrode, S.D.; Binns, W.P.; Huggins, D.R. Confronting Climate Change Challenges to Dryland Cereal Production: A Call for Collaborative. *Prod. Engagem.* **2018**, *5*. [CrossRef]
4. Ahanger, R.A.; Bhat, H.A.; Bhat, T.A.; Ganie, S.A.; Lone, A.A.; Wani, I.A.; Ganai, S.A.; Haq, S.; Khan, O.A.; Junaid, M.J.; Bhat, T.A. Impact of Climate Change on Plant Diseases. *Int. J. Modern Plant & Anim. Sci. USA* **2013**, *3*, 105–115.
5. Weiss, M.V. *Compendium of Wheat Diseases*, 2nd ed.; APS Press: St. Paul, MN, USA, 1987.
6. Forrer, H.R.; Zadoks, J.C. Yield reduction in wheat in relation to leaf necrosis caused by Septoria tritici. *Neth. J. Plant Pathol.* **1983**, *89*, 87–98. [CrossRef]
7. Eyal, Z. The septoria tritici and stagonospora nodorum blotch diseases of wheat. *Eur. J. Plant Pathol.* **1999**, *105*, 629–641. [CrossRef]
8. Bearchell, S.J.; Fraaije, B.A.; Shaw, M.W.; Fitt, B.D.L.; Cowling, E.B. Wheat Archive Links Long-Term Fungal Pathogen Population Dynamics to Air Pollution. *Proc. Natl. Acad. Sci. USA* **2005**, *102*, 5438–5442. [CrossRef] [PubMed]
9. Eyal, Z.; Amiri, Z.; Wahl, I. Physiological Specialization of Septoria tritici. *Phytopathology* **1973**, *63*, 1087–1091. [CrossRef]
10. Fones, H.; Gurr, S. The impact of Septoria tritici Blotch disease on wheat: An EU perspective. *Fungal Genet. Biol.* **2015**, *79*, 3–7. [CrossRef] [PubMed]
11. Fraaije, B.; Cools, H.J.; Fountaine, J.; Lovell, D.J.; Motteram, J.; West, J.S.; Lucas, J. A Role of Ascospores in Further Spread of QoI-Resistant Cytochrome b Alleles (G143A) in Field Populations of Mycosphaerella graminicola. *Phytopathology* **2005**, *95*, 933–941. [CrossRef] [PubMed]
12. Estep, L.K.; Torriani, S.F.F.; Zala, M.; Anderson, N.P.; Flowers, M.D.; Mcdonald, B.A.; Mundt, C.C.; Brunner, P.C. Emergence and early evolution of fungicide resistance in North American populations of Zymoseptoria tritici. *Plant Pathol.* **2015**, *64*, 961–971. [CrossRef]
13. Simón, M.R.; Cordo, C.A.; Castillo, N.S.; Struik, P.C.; Börner, A. Population Structure of Mycosphaerella graminicola and Location of Genes for Resistance to the Pathogen: Recent Advances in Argentina. *Int. J. Agron.* **2012**, *2012*, 680275. [CrossRef]
14. Rodrigo, S.; Cuello-Hormigo, B.; Gomes, C.; Santamaria, O.; Costa, R.; Poblaciones, M.J. Influence of fungicide treatments on disease severity caused by Zymoseptoria tritici, and on grain yield and quality parameters of bread-making wheat under Mediterranean conditions. *Eur. J. Plant Pathol.* **2014**, *141*, 99–109. [CrossRef]
15. Keating, B.A.; Carberry, P.S.; Hammerb, G.L.; Probert, M.E.; Robertson, M.J.; Holzworth, D.; Huth, N.I.; Hargreaves, J.N.G.; Meinke, H.; Hochman, Z.; et al. An overview of the crop model APSIM. *Eur. J. Agron.* **2003**, *18*, 267–288. [CrossRef]
16. Lv, Z.; Liu, X.; Cao, W.; Zhu, Y. Agricultural and Forest Meteorology Climate change impacts on regional winter wheat production in main wheat production regions of China. *Agric. For. Meteorol.* **2013**, *171–172*, 234–248. [CrossRef]
17. Brisson, N.; Gary, C.; Justes, E.; Roche, R.; Mary, B.; Ripoche, D.; Zimmer, D.; Sierra, J.; Bertuzzi, P.; Burger, P.; et al. An overview of the crop model Stics. *Eur. J. Agron.* **2003**, *18*, 309–332. [CrossRef]
18. Jamieson, P.D.; Semenov, M.A.; Brooking, I.R.; Francis, G.S. Sirius a mechanistic model of wheat respinse to environmental variation. *Eur. J. Agron.* **1998**, *8*, 161–179. [CrossRef]

19. Jones, J.W.; Hoogenboom, G.; Porter, C.H.; Boote, K.J.; Batchelor, W.D.; Hunt, L.A.; Wilkens, P.W.; Singh, U.; Gijsman, A.J.; Ritchie, J.T. The Dssat Cropping System Model. *Eur. J. Agron.* **2003**, *18*, 235–265. [CrossRef]
20. Hunt, L.A.; Pararajasingham , S. CROPSIM—WHEAT: A model describing the growth and development of wheat. *Can. J. Plant Sci.* **1995**, 619–632.
21. Ritchie, J.T.; Singh, U.; Godwin, D.C.; Bowen, W.T. Cereal growth, development and yield. *Underst. Opt. Agric. Prod.* **1998**, 79–98. [CrossRef]
22. Ritchie, J.T.; Otter, S. Description and performance of CERES-Wheat: A user-orientes wheat yield model. *ARS Wheat Yield Proj.* **1985**, *38*, 159–175.
23. Hoogenboom, G.; Jones, J.W.; Wilkens, P.W.; Porter, C.H.; Boote, K.J.; Hunt, U.S.; Lizaso, J.I.; White, J.W.; Uryasev, O.; Ogoshi, R.; et al. *Decision Support System for Agrotechnology Transfer (DSSAT) [CD-ROM]*; University of Hawaii: Honululu, HI, USA, 2015.
24. Thorp, K.R.; Hunsaker, D.J.; French, A.N.; White, J.W.; Clarke, T.R. Evaluation of the CSM-CROPSIM-CERES-Wheat Model as a Tool for Crop Water Management. *Trans. ASABE* **2010**, *53*, 1–17. [CrossRef]
25. Chipanshi, A.C.; Ripley, E.A.; Lawford, R.G. Large-scale simulation of wheat yields in a semi-arid environment using a crop-growth model. *Agric. Syst.* **1999**, *59*, 57–66. [CrossRef]
26. Savin, R.; Satorre, E.H.; Hall, A.J.; Slafer, G.A. Assessing strategies for wheat cropping in the monsoonal climate of the Pampas using the CERES-Wheat simulation model. *Field Crops Res.* **1995**, *42*, 81–91. [CrossRef]
27. Sardinia, S.; Dettori, M.; Cesaraccio, C.; Motroni, A.; Spano, D.; Duce, P. Field Crops Research Using CERES-Wheat to simulate durum wheat production and phenology. *Field Crops Res.* **2011**, *120*, 179–188. [CrossRef]
28. Bannayan, M.; Crout, N.M.J.; Hoogenboom, G. Application of the CERES-Wheat model for within-season prediction of winter wheat yield in the United Kingdom. *Agron. J.* **2003**, *95*, 114–125. [CrossRef]
29. Gbegbelegbe, S.; Cammarano, D.; Asseng, S.; Robertson, R.; Chung, U.; Adam, M.; Abdalla, O.; Payne, T.; Reynolds, M.; Sonder, K.; et al. Baseline simulation for global wheat production with CIMMYT mega-environment specific cultivars. *Field Crops Res.* **2017**, *202*, 122–135. [CrossRef]
30. Batchelor, W.D.; Jones, J.W.; Boote, K.J.; Porter, C.H. *Pest and Disease Damage Module*; University of Florida: Gainsville, FL, USA, 2004.
31. Boote, K.J.; Bennet, J.M.; Jones, J.W.; Jowers, H.E. On-farming testing of peanut and soybean models in north Florida. *Paper Am. Soc. Agric. Eng. USA* **1989**. Available online: http://agris.fao.org/agris-search/search.do?recordID=US9165910 (accessed on 10 January 2019).
32. Batchelor, W.D.; Jones, J.W.; Boote, K.J.; Pinnschmidt, H.O. Extending the use of crop models to study pest damage. *Trans. Am. Soc. Agric. Eng. Gen. Ed.* **1993**, *36*, 551–558. [CrossRef]
33. Boote, K.J.; Jones, J.W.; Hoogenboom, G.; Pickering, N.B. The CROPGRO model for grain legumes. In *Understanding Options for Agricultural Production*; Tsuji, G.Y., Hoogenboom, G., Thornton, P.K., Eds.; Springer: Dordrecht, The Netherlands, 1998; pp. 99–128. ISBN 978-94-017-3624-4.
34. Andarzian, B.; Hoogenboom, G.; Bannayan, M.; Shirali, M.; Andarzian, B. Determining optimum sowing date of wheat using CSM-CERES-Wheat model. *J. Saudi Soc. Agric. Sci.* **2015**, *14*, 189–199. [CrossRef]
35. Waggoner, P.E.; Berger, R.D. Defoliation, Disease, and Growth. *Phytopathology* **1987**, *77*, 1495–1497.
36. Robert, C. Analysis and modelling of effects of leaf rust and Septoria tritici blotch on wheat growth. *J. Exp. Bot.* **2004**, *55*, 1079–1094. [CrossRef] [PubMed]
37. Robert, C.; Bancal, M.O.; Lannou, C.; Ney, B. Quantification of the effects of Septoria tritici blotch on wheat leaf gas exchange with respect to lesion age, leaf number, and leaf nitrogen status. *J. Exp. Bot.* **2006**, *57*, 225–234. [CrossRef] [PubMed]
38. Sánchez-Vallet, A.; McDonald, M.C.; Solomon, P.S.; McDonald, B.A. Is Zymoseptoria tritici a hemibiotroph? *Fungal Genet. Biol.* **2015**, *79*, 29–32. [CrossRef] [PubMed]
39. Castro, A.C.; Simón, M.R. Effect of tolerance to Septoria tritici blotch on grain yield, yield components and grain quality in Argentinean wheat cultivars. *Crop Prot.* **2016**, *90*, 66–76. [CrossRef]
40. Zadoks, J.C.; Chang, T.T.; Konzak, C.F. A decimal code for the growth stages of cereals. *Weed Res.* **1974**, *14*, 415–421. [CrossRef]
41. Gröll, K. *Use of Sensor Technologies to Estimate and Assess the Effects of Various Plant Diseases on Crop Growth and Development*; Universty of Hohenheim: Stuttgart, Germany, 2008; Available online: http://opus.uni-hohenheim.de/volltexte/2008/296/ (accessed on 10 January 2019).

42. Thomas, M.; Cook, R.; King, J. Factors affecting development of Septoria tritici in winter wheat and its effect on yield. *Plant Pathol.* **1989**, 246–257. [CrossRef]
43. Willmott, C.J. Some Comments on the Evaluation of Model Performance. *J. Appl. Phys.* **1982**, *36*, 1309–1313. [CrossRef]
44. Jing, Q.; Qian, B.; Shang, J.; Huffman, T.; Liu, J.; Pattey, E.; Dong, T.; Tremblay, N.; Drury, C.F.; Ma, B.L.; et al. Assessing the options to improve regional wheat yield in eastern canada using the csm–ceres–wheat model. *Agron. J.* **2017**, *109*, 510–523. [CrossRef]
45. Attia, A.; Rajan, N.; Xue, Q.; Nair, S.; Ibrahim, A.; Hays, D. Application of DSSAT-CERES-Wheat model to simulate winter wheat response to irrigation management in the Texas High Plains. *Agric. Water Manag.* **2016**, *165*, 50–60. [CrossRef]
46. Robert, C.; Fournier, C.; Andrieu, B.; Ney, B. coupling a 3D virtual wheat (Triticum aestivum) plant model with a Septoria tritici epidemic model (Septo3D): A new approach to investigate plant-pathogen interactions linked to caonpy architecture. *Funct. Plant Biol.* **2008**, *35*, 997–1013. [CrossRef]
47. Magarey, R.D.; Sutton, T.B.; Thayer, C.L. A Simple Generic Infection Model for Foliar Fungal Plant Pathogens. *Phytopathology* **2005**, *95*, 92–100. [CrossRef] [PubMed]
48. Donatelli, M.; Magarey, R.D.; Bregaglio, S.; Willocquet, L.; Whish, J.P.M.; Savary, S. Modelling the impacts of pests and diseases on agricultural systems. *Agric. Syst.* **2017**, *155*, 213–224. [CrossRef] [PubMed]
49. King, J.E.; Jenkins, J.E.E.; Morgan, W.A. The estimation of yield losses in wheat from severity of infection by Septoria species. *Plant Pathol.* **1983**, *32*, 239–249. [CrossRef]
50. Ziv, O.; Eyal, Z. Assessment of Yield Component Losses Caused in Plants of Spring Wheat Cultivars by Selected Isolates of Septoria tritici. *Phytopathology* **1977**, *68*, e796. [CrossRef]
51. Bhathal, J.S.; Loughman, R.; Speijers, J. Yield reduction in wheat in relation to leaf disease from yellow (tan) spot and septoria nodorum blotch. *Eur. J. Plant Pathol.* **2003**, *109*, 435–443. [CrossRef]
52. Bastiaans, L. Ecology and Epidemiology Ratio Between Virtual and Visual Lesion Size as a Measure to Describe Reduction in Leaf Photosynthesis of Rice Due to Leaf Blast. *Phytopathology* **1991**, *81*, 611–615. [CrossRef]
53. Thorp, K.R.; Hunsaker, D.J.; French, A.N. Assimilating leaf area index estimates from remote sensing into the simulations of a cropping systems model. *Trans. ASABE* **2010**, *53*, 251–262. [CrossRef]
54. Ficke, A.; Cowger, C.; Bergstrom, G.; Brodal, G. Understanding Yield Loss and Pathogen Biology to Improve Disease Management: Septoria Nodorum Blotch—A Case Study in Wheat. *Plant Dis.* **2018**, *102*, 696–707. [CrossRef] [PubMed]

5 Publication III

Implementation of an automatic time-series calibration method for the DSSAT wheat models to enhance multi-model approaches

Röll, G.; Memic, E.; Graeff-Hönninger, S. Implementation of an automatic time-series calibration method for the DSSAT wheat models to enhance multi-model approaches. *Agronomy Journal*, 2020;1-33.2020;1–22.https://doi.org/10.1002/agj2.20328.

Linking spectral measurements and crop models by adjusting the state variables within a crop model, might lead to improvements in model prediction. In addition, the use of more than one model can also provide higher modeling accuracy as various, model structures are involved. However, using more than one model necessitates extensive model calibration. In fact, this exercise would require an exhausting manual calibration procedure that is not feasible in combination with remote sensing data on a spatial scale. Therefore, an automatic calibration method was used to calibrate the DSSAT models under different N application rates.

Received: 7 March 2020 | Accepted: 10 June 2020

DOI: 10.1002/agj2.20328

Agronomy Journal

ARTICLE

Biometry, Modeling, & Statistics

Implementation of an automatic time-series calibration method for the DSSAT wheat models to enhance multi-model approaches

Georg Röll | **Emir Memic** | **Simone Graeff-Hönninger**

Department of Agronomy, Institute of Crop Science, University of Hohenheim, Stuttgart 70599, Germany

Correspondence
Georg Röll, Department of Agronomy, Institute of Crop Science, University of Hohenheim, Stuttgart, 70599, Germany.
Email: georg.roell@uni-hohenheim.de

Funding information
German Federal Environmental Foundation (DBU), Grant/Award Number: 33143/01

Abstract

Multi-modeling (MM) approaches allow increasing modeling accuracy through a combination of different modeling structures for the simulation of plant growth and yield. The Decision Support System for Agrotechnology Transfer (DSSAT) 4.7 modeling platform currently includes three different wheat (*Triticum aestivum* L.) models (CERES, N-Wheat, and Cropsim). However, the main obstacle for using an MM approach is the calibration procedure. Calibration is time consuming and complex, especially if the user is not familiar with all three models. It results in a subjective calibration optimum and might discriminate models if the user is less trained. To avoid these conflicts, an automated calibration program which optimizes cultivar coefficients based on the root means square error (RMSE) of time-series data was developed to ensure objective calibration results across three different wheat models and to highlight the potential of MM approaches for decision support in the future. Model calibration was performed on a 4-yr nitrogen wheat fertilizer trial (0–240 kg ha^{-1} N) in southwest Germany. The evaluation mean showed satisfying results for the calibration (d-index = .93) and evaluation dataset (d-index = .81). By comparing different years, the MM approach improved modeling accuracy in most cases. Especially in the drought season of 2018, the MM approach revealed higher modeling accuracy for yield (d-index = .61) in contrast to a single simulation of CERES (d-index = .34) and Cropsim (d-index = .39). This demonstrated the advantage of an MM approach as different modeling structures could compensate for errors that occur in single modeling approaches.

1 | INTRODUCTION

Various crop growth models were developed over the last 30 yr along with APSIM (Keating et al., 2003), WheatGrow (Yan, Cao, Luo, & Jiang, 2000), STICS (Brisson et al., 2003), Sirius (Jamieson, Semenov, Brooking, & Francis, 1998),

Abbreviations: AMC, automated model calibration; DAP, days after planting; DSSAT, Decision Support System for Agrotechnology Transfer; GLUE, generalized likelihood uncertainty; LAI, leaf area index; MM, multi-modeling

CropSyst (Stöckle, Donatelli, & Nelson, 2003), and Decision Support System for Agrotechnology transfer (DSSAT; Jones et al., 2003) for capturing crop–environment interactions which lead to optimization of crop production. In general, these models were developed to examine the implication of management practices, nutrient dynamics, genetics, weather, and climate change on wheat (*Triticum aestivum* L.) growth and yield (Thorp, Hunsaker, French, White, & Clarke, 2010). Plant growth and development is simulated on a daily time step based on a daily maximum and minimum temperature, day length, and vernalization requirements (Hunt et al., 2003). The daily plant growth is computed on a radiation use efficiency concept (Ritchie, Singh, Godwin, & Bowen, 1998).

Different crop models have different strengths and complexities (Ahmed et al., 2016) under different environmental conditions, which makes the selection of the proper model for the right task difficult. Grenouillet, Buisson, Casajus, and Lek (2011) showed the advantages of using model ensembles instead of a single model. Higher model accuracy was also reported when calculating the mean of different models (Rötter et al., 2012). However, the challenge remains when using different models in the calibration procedure. The calibrations strongly depend on user knowledge (Botterweg, 1995). The results of the calibration can vary between users especially if the user is more experienced in one model compared to other models (Confalonieri et al., 2016). This can lead to an inadequate (nonrepresentative) multi-model (MM) approach.

Martre et al. (2015) used 27 different wheat models in an MM ensemble. The calibration was guided by separate researcher groups that were well trained in the respective models. A similar calibration procedure was used for testing nine different barley (*Hordeum vulgare*) models at various study sites across Europe. In total, 44 growing seasons were evaluated (Rötter et al., 2012). Although the studies indicated that the model simulations greatly improved when using a MM approach and were worth the effort in terms of improved outputs, the required intensive calibration (Eckhardt, Fohrer, & Frede, 2005) is often a deterrent for users.

Duan, Sorooshian, and Gupta (1992) mentioned the importance of proper model calibration for a successful model application. A user-friendly, automated calibration process could overcome the existing MM calibration bottleneck and ensure a user-independent model calibration while enabling more users to apply an MM approach to their studies.

All models have specific calibration requirements that are not always easy or straightforward. In order to improve model outputs, an increase in complexity is required, which leads to even more complex models with complex calibration procedures. An often-cited example in this context is the calibration of cultivar coefficients (Botterweg, 1995). Due to the complexity and mathematical factors, different coefficient combinations can result in optimal and statistically satisfactory solutions (Duan et al., 1992) for the same calibration task. To remove subjectivity from the calibration procedure, a calibration program is needed that selects the optimum cultivar coefficient combination based on mathematical criteria that should enable nonbiased model results.

Core Ideas

- Manual calibration is time consuming and complex even for well-trained users.
- Development of an automated calibration method that can cope with time-series data.
- The DSSAT 4.7 uses three wheat models in a tailor-made multi-modeling combination with AMC.

The current DSSAT 4.7 (Jones et al., 2003) modeling platform includes three wheat models: CERES, Cropsim, and NWheat. These models were developed during the last 30 yr and tested in a wide range of environments (Bannayan, Crout, & Hoogenboom, 2003; Chipanshi, Ripley, & Lawford, 1999; Sardinia et al., 2011; Savin, Satorre, Hall, & Slafer, 1995) for yield estimation for different purposes, such as using for remote sensing (Thorp et al., 2010), under elevated CO_2 (Tubiello et al., 1999), leaf disease (Röll, Batchelor, Castro, Simón, & Graeff-Hönninger, 2019), or under different nitrogen (N) strategies (Kassie, Asseng, Porter, & Royce, 2016; Singh, Tripathy, & Chopra, 2008). Within the DSSAT environment, all models use the same soil, weather, and management file structures and are thus suitable for an MM approach. In a previous MM approach, these models were tested in Egypt (Asseng et al., 2018) for future wheat yield predictions. The calibration was performed in a manual user adjustment of cultivar coefficients (trial and error method) and showed acceptable results between the simulated and measured values.

In the current DSSAT 4.7 release, two different tools are available for automatic calibration of cultivar coefficients: GENCALC (Hunt et al., 1993) and generalized likelihood uncertainty estimation (GLUE; Jones et al., 2011). In both tools, similar target variables can be optimized, such as phenological events (onset of flowering, physiological maturity, etc.) and growth-related parameters (grain yield, aboveground biomass, max leaf area index [LAI], etc.) based on different optimization methods. In GENCALC and GLUE, only one observation per crop growing season can be used for optimizing target variables

(maximum LAI, biomass at maturity, grain weight at maturity, etc.). This procedure can be sufficient for optimizing phenological events. However, when it comes to growth-related in-season rates, the coefficient optimization (e.g., optimization of cultivar coefficients influencing aboveground biomass, LAI, etc.), the use of more than one in-season observation is beneficial (Boote, 2019).

Furthermore, when considering grain yield, a constant (linear) growth rate is typically observed after flowering and represented in crop growth models as linear growth function. The reason for this is that grain number is computed before the beginning of the grain growth, resulting in grain growth rate (defined through G3 coefficient) to be linear, unless affected by water or N stress. In the specific case of grain yield, one observation per season (yield at harvest) can potentially be a good indicator for model performance evaluation in whether phenology was simulated correctly (i.e., correct initialization of reproductive stage).

However, the same patterns are not observed for traits like aboveground biomass, LAI, etc. Thus, one observation at the end of the season cannot be used for the evaluation of crop model performance. The same obstacle is given for the estimation of corresponding cultivar coefficients influencing in-season biomass accumulation rates (leaf and stem weight), wherefore time-series data are mandatory.

Since the existing tools within DSSAT are not able to estimate cultivar coefficients based on time-series observations, crop model performance is usually manually evaluated by using in-season observations. The coefficients are subsequently adjusted if the existing optimization tools (GENCALC and GLUE) did not deliver desired results. In order to overcome these current limitations, a cultivar coefficient optimization tool that relays on in-season time-series observations for estimating cultivar coefficients is needed.

Thus, the aims of this study were (a) the development and application of an automatic calibrator for faster and user-independent model calibration of cultivar coefficients of all three wheat models within the DSSAT environment, and (b) the evaluation of the potential of an MM approach based on the automatic calibrator for the simulation of wheat yields under different N application rates based on a 4-yr dataset.

2 | MATERIALS AND METHODS

2.1 | Field experiments

Field data were obtained from N fertilizer trials carried out in winter wheat during the 2014–2015, 2015–2016, 2016–2017, and 2017–2018 seasons. Field trials were conducted at the Experimental Station Ihinger Hof (48°44′N, 8° 55′E; 480 m asl, mean annual temperature 9.1 °C, and 714-mm mean annual precipitation) of the University of Hohenheim in Germany. Previous crops were winter barley in 2014–2015, 2015–2016, and 2017–2018, and oilseed rape (*Brassica napus* L.) in 2016–2017. The sowing dates for cultivar JB Asano were on 3 Nov. 2014, 14 Oct. 2015, 10 Oct. 2016, and 12 Oct. 2017 with a row spacing of 0.15 cm and a sowing density of 300 seeds m^{-2}. All experiments were performed in a randomized block design with a plot size of 12 by 36 m. Calcium ammonium nitrate (CAN, 27% N) was broadcast in spring at tillering (GS 25) (Zadoks, Chang, & Konzak, 1974), at the start of stem elongation (GS 32) and at booting stage (GS 47). In total, seven different N treatments between 0 and 240 kg ha^{-1} N were implemented (Table 1). During the whole vegetation period, the plots were kept weed-, pest-, and disease-free by application of herbicides and fungicides.

TABLE 1 Seven different N application rates (kg ha^{-1}N) and the corresponding growth stages (in parentheses) at application times in the growing seasons of 2015, 2016, 2017, and 2018

Nitrogen rates total	1st application (GS 25)[a]	2nd application (GS 32)[b]	3rd application (GS 47)[c]
kg ha^{-1} N			
0	0	0	0
40	20	20	0
80	30	30	20
120	40	40	40
160	60	60	40
200	80	80	40
240	100	100	40

[a] Application dates: 20 Feb. 2015, 18 Feb. 2016, 10 Apr. 2017, and 9 Apr. 2018.
[b] Application dates: 24 Apr. 2015, 22 Apr. 2016, 2 May 2017, and 4 May 2018.
[c] Application dates: 5 June 2015, 1 June 2016; 29 May 2017, and 29 May 2018.

Throughout the vegetation period, nondestructive LAI measurements (LAI 2000, LiCor, Lincoln, NE), fresh and dry matter of the plant, as well as N content, were obtained by harvesting 0.3 mš within each plot almost every week after the start of vegetation in March. In total, 10 sampling dates were performed in 2015 and 2016 and eight sampling dates in 2017 and 2018. Grain yield was determined by harvesting 0.6 mš by hand. All samples were weighed and immediately dried in a forced-air drier at 80 °C for 4 d. After drying the samples were weighed again, pulverized by a hammer mill (0.5 mm, MM200, Retsch GmbH, Haan, Germany), and analyzed by NIRS 5000 (Foss NIRSystem, Silver Spring, MD).

2.1.1 | Soil and weather data

The predominant soil type in this region is a stagnogleyic cambisol with the corresponding soil texture shown in Table 2.

TABLE 2 Soil properties for the field experiments on the location Ihinger Hof

Soil depth	Clay %	Sand %	Silt %	LLL[a]	DUL[b]	SAT[c]	RGF[d]
2015 Experiment (Field: Inneres Taele)							
0–30 cm	30.7	2.6	66.7	0.211	0.423	0.512	1
30–60 cm	33.9	2.0	64.1	0.214	0.411	0.443	0.638
60–90 cm	33.0	2.7	64.3	0.198	0.384	0.446	0.407
2016 Experiment (Field: Riech)							
0–30 cm	43.3	9.9	46.8	0.274	0.453	0.512	1
30–60 cm	25.0	28.8	46.2	0.170	0.345	0.443	0.638
60–90 cm	30.8	13.4	55.8	0.187	0.355	0.446	0.407
2017 Experiment (Field: Lammwirt)							
0–30 cm	30.1	10.4	59.5	0.197	0.384	0.485	1
30–60 cm	33.6	10.9	55.5	0.198	0.365	0.413	0.638
60–90 cm	38.6	9.0	52.4	0.213	0.370	0.421	0.407
2018 Experiment (Field: Lerchenberg)							
0–30 cm	22.0	24.1	53.9	0.215	0.35	0.489	1
30–60 cm	43.1	20.7	36.2	0.219	0.348	0.488	0.638
60–90 cm	27.0	15.2	57.8	0.184	0.309	0.512	0.407

[a]LLL, lower limit ≙ permanent wilting point (pF 4.2).
[b]Drained upper limit ≙ field capacity (pF 1.8).
[c]SAT, saturated ≙ saturated water content (pF 0).
[d]RGF, Root growth factor.

Soil samples for mineral N content were taken in each plot shortly before the first fertilizer application date and after harvest. The soil mineral N content was processed colorimetrically by using a flow injection analyzer (FIAstar 500 Analyzer, FOSS GmbH, Hamburg, Germany) following Bassler and Hoffmann (1997).

2.2 | Crop models

All three wheat models are written in Fortran and are included in the current DSSAT 4.7 shell. The models share common input files like weather, soil, and experimental data and use model-specific genotype files (Jones et al., 2003). This gives the user a unique possibility to set up the model input files for all three models simultaneously, enabling an easier application of the MM approach.

All three models: CERES, NWheat, and Cropsim, were developed in the 1980's by Ritchie and Otter (1985) where dry matter production is calculated on the daily solar radiation by using a radiation use efficiency coefficient (Hunt & Pararajasingham, 1995). These calculations are driven by daily temperature, water, and nutrient availability. The dry matter distribution to the different growing plant parts and the phenological development is calculated by thermal time. Differences in the duration of growth stages between species, ecotypes, and cultivars are represented by cultivar coefficients, which were used as model inputs. The progress of the life cycle depends on daily assimilate production, temperature, leaf N, and water status. A shortage of N and/or water is represented as a stress index in the models. These indices for water and N are used to modify the carbohydrate assimilation and the partitioning to different tissues as well as the availability of assimilates for new leaf growth (Hunt & Pararajasingham, 1995).

Since the early days of CERES, model development continued, and different subtypes were developed. N-Wheat is one of these subtypes that evolved out of CERES based on Australian growing conditions (Asseng et al., 1998). An important change in developing N-Wheat was the modification of the crop water uptake routine (Kassie et al., 2016). The original CERES uses a function of potential evapotranspiration and LAI. This was replaced by a critical fraction of available water and a linkage to the water demand of the biomass by using transpiration efficiency in the NWheat model (Stapper, 1984). They also included high-temperature stress effects for an acceleration of leaf senescence to account for Australian conditions (Asseng et al., 2002). This model was developed and extensively tested within the APSIM environment in different climates for agronomic studies in Western and Eastern Australia (Asseng et al., 1998; Keating, McCown, & Cresswell, 1995; Meinke, Hammer, van Keulen, Rabbinge, & Keating, 1997). For an MM approach, the crop component of N-Wheat was integrated by Kassie et al. (2016) into the DSSAT framework.

The Cropsim model is a CERES model derivative (Ritchie, 1991) with significant changes in the model structure (McMaster et al., 2008). Significant changes were made by modifying the calculation of the mean daily temperature. Cropsim uses the daily maximum and minimum temperature divided by two. The CERES model uses an approach based on a diurnal temperature cycle that follows a sinusoidal function and interpolates from daily maximum and minimum temperature (McMaster et al., 2008). Another modification was done in the vernalization approach in Cropsim (McMaster et al., 2008). The original CERES model subtracts one vernalization day from accumulated vernalization days if the daily temperature exceeds 30 °C. This approach was changed in the Cropsim model to 0.05(Tdailymax − 30) where Tdailymax represents the daily maximum temperature (McMaster et al., 2008). Within this study, almost no day exceeded the daily temperature of 30 °C in the fall. Therefore, this change is assumed to be of minor importance for the tested dataset.

2.3 | Automated Model Calibration (AMC)

The functions governing the phenological development of the plant regarding environmental and crop management practices have to be agronomically meaningful. The DSSAT crop growth model enables the use of generic algorithms for simulating phenology and growth responses of different crop species and cultivars by modifying species, ecotype, and cultivar file coefficients. Within this study, different coefficients included in the ecotype and cultivar file were modified and adjusted for the cultivar that was used in the field trial. The importance of these cultivar coefficients is enormous in attaining statistically acceptable simulations and getting the phenology, growth, and yield of the used cultivars set up in the right way. Model performance is judged based on the statistical fit of simulated outputs with observed data (Yang, Yang, Liu, & Hoogenboom, 2014).

Multiple tools and methods for the estimation of cultivar coefficients were developed in the past. At the moment within the DSSAT shell, two tools are available: GENCALC (Hunt et al., 1993) and GLUE (Jones et al., 2011). Both cultivar coefficient estimators are using the File-A for introducing the observations into the model. Here only one observation per season can be entered, either at harvest (grain weight at harvest) or during the season (maximum LAI). The GENCALC selection criteria is based on Root Mean Squared Error (RMSE), where the coefficients combination that provides the lowest difference between simulated and observed yield values is finally selected (Hunt et al., 1993). The coefficients are optimized sequentially (coefficient by coefficient). After the first coefficient is optimized and the optimal value chosen, it is saved and used during the optimization of the next coefficient until all of the coefficients are optimized step-wise (Hunt et al., 1993). During the optimization of earlier coefficients, the values of the later coefficients are set nominally. The GLUE tool uses a Bayesian estimation method based on Monte Carlo distributions sampling and Gaussian likelihood functions for determining optimal cultivar coefficients based on the simulated and observed yield values (Jones et al., 2011). The GLUE uses observations, which are passed into the model through File-A (Jones et al., 2011). Time-series observations (File-T) for the whole season of the experiment (if recorded during a season) can only be used for manual check-out (visual fit of simulated and observed) of the results and enable modification of the predefined cultivar coefficient ranges. The cultivar coefficient optimization results depend on the prior defined coefficient distributions to a great deal. One of the latest comparisons of the GENCALC and GLUE tools was carried out with the CERES-Rice model by Buddhaboon, Jintrawet, and Hoogenboom (2018). Other methods such as trial and error based on visual and statistical fit, simplex method (Grimm, Jones, Boote, & Hesketh, 1993), simulated annealing (Mavromatis et al., 2001), or K-Nearest Neighbor approach (Bannayan & Hoogenboom, 2009) have also been used in different studies for estimating cultivar coefficients.

It is important to point out that some statistical evaluation methods, even if very helpful in understanding the crop model performance, are not suitable for being implemented (in a programming context) as cultivar coefficient selection criteria (error minimization between multiple simulated and observed in-season observations). Dimensionless statistics can give a better insight in understanding model simulation outputs, especially if target variables have different absolute unit scales. If, for example, d-index (unitless measure of fit) was used for evaluating model simulation outputs based on the observed values for one target variable (such as LAI), it is easy to conclude that a coefficient combination with the highest d-index is the optimum. The problem occurs when multiple target variables are used for the optimization of the cultivar coefficients. In some cases, cultivar coefficients combinations might provide extremely satisfactory results for one target variable and extremely bad for others. In that case, a compromising solution would be sacrificing a partial statistical fit of one target variable to reach an overall statistically acceptable fit for multiple target variables.

As the compromising solution for dimensionless statistics was extremely difficult to implement in order to come up with some sort of mathematical criteria for selecting cultivar coefficient combinations providing minimum

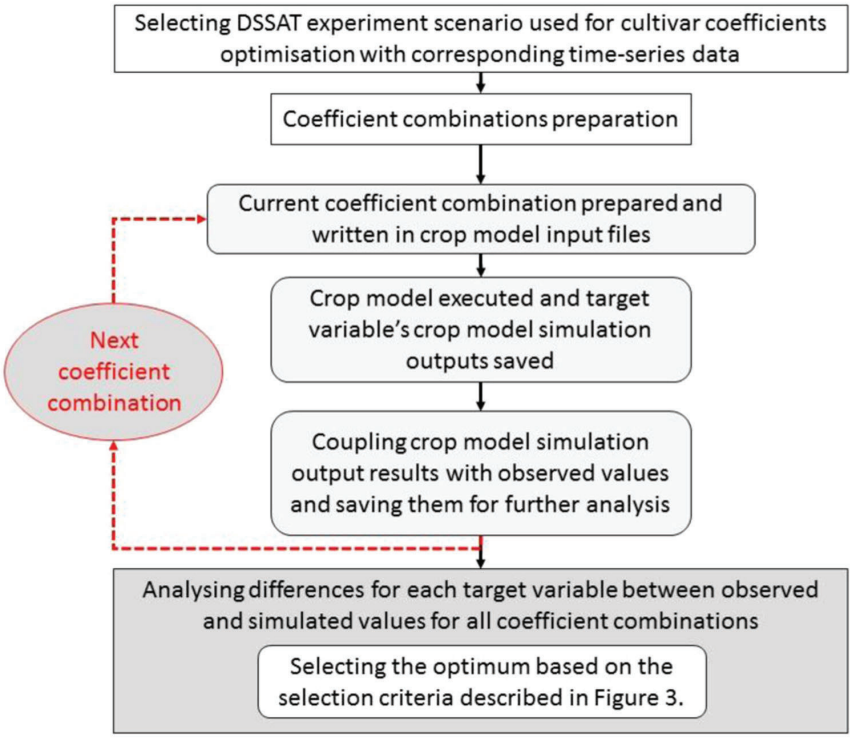

FIGURE 1 Flow chart of the developed calibrator

errors between simulated and observed values of multiple target variables, an alternative approach was developed. The method used in this study enables the user to use all available observed time-series data (File-T) from the experimental season. Multiple target variables (GSTD, growth stages; CWAD, tops weight; LAID, leaf area index; and GWAD, grain yield) can be used simultaneously for estimating cultivar coefficients responsible for the correct simulation of phenology and growth. It is very important to be able to use multiple in-season observations for determining cultivar coefficients because variables such as tops weight do not have linear growth rates throughout the season. Using a single observation at the end of the season can lead to less accuracy in the determination of cultivar coefficients, especially when they are linked to nonlinear growth rates.

The calibrator was written in Python and the estimation process of cultivar coefficients was based on an exhaustive gridding method. With this method, a specific range was defined (minimum and maximum coefficient values) for each coefficient, and optimization occurred in incremental steps. Note that exhaustive gridding is a primitive and time-consuming approach in model input coefficient optimization (Duan et al., 1992). After initializing the calibration program, the user selects the crop model experiment files (File-X) with the corresponding observed time-series data (stored in File-T) and defines the cultivar specific coefficient ranges and increment steps (Figure 1). Based on the defined coefficient ranges, a temporal coefficient combination list (set of cultivar coefficient combinations) is created, and a separate model run is executed for each combination. Within the program, simulated outputs of target variables are coupled with the available time-series observations (whole season) and saved for later analysis. After executing the model for all defined cultivar coefficient combinations, simulation outputs and observed values of target variables are saved in one file and analyzed. Based on the defined selection criteria (RMSE), the optimal combination for each model was selected (Table 3).

The implemented selection criteria were based on RMSE, like in GENCALC (Hunt et al., 1993). The RMSE statistics retain original units of the target variables. In case of having multiple target variables with different scales, a direct comparison is difficult, if not impossible. Therefore, an adapted form of normalization was introduced as selection criteria to enable the comparison of variables with different scales (e.g., LAI and tops weight). The weight coefficient (e.g., LAIDStep = 0.3) was multiplied with the mean of the observations of the target variables (normalizing the selection criteria) to form an initial mathematical

TABLE 3 Calibration coefficient of CERES, NWheat, and Cropsim

Models	Coefficient	Coefficient definition	AMC[a] estimated values
CERES	P1[b]	Duration of phase end juvenile to terminal spikelet	200
	P1V[b]	Days, optimum vernalizing temperature, required for vernalization	22
	P2[b]	Duration of phase terminal spikelet to end leaf growth	286
	P3[b]	Duration of phase end leaf growth to end spike growth	264
	P5[b]	Grain filling (excluding lag) phase duration (°C d)	228
	P1D[b]	Photoperiod response (% reduction in rate)	117
	PHINT[c]	Interval between successive leaf tip appearances (°C d)	73
	LA1S[c]	Area of standard first leaf (cm^2)	4.0
	LAFV[c]	Increase in potential area of leaves, vegetative phase (fraction per leaf)	0.05
	G3[c]	Standard, non-stressed mature tiller weight, including grain (g dry $weight^{-1}$)	22.8
	G2[c]	Standard kernel size under optimum conditions (mg)	1.2
	G1[c]	Kernel number per unit canopy weight	22.8
Nwheat	P1[b]	Thermal time from seedling emergence to the end of the juvenile phase (°C d)	500
	VSEN[b]	sensitivity to vernalization 1.0–4.0	3.5
	P5[b]	Thermal time (base 0 °C) from beginning of grain fill to maturity	530
	PPSEN[b]	sensitivity to photoperiod	4.0
	PHINT[c]	Phyllochron interval	95
	STMMX[c]	Potential final dry weight of a single tiler without grain (g)	3.0
	MXGWT[c]	maximum kernel weight (100 = no effect)	55.0
	GRNO[c]	Kernels per stem weight at grain filling (kernels g^{-1} $stem^{-1}$)	25.0
	MXFIL[c]	Potential kernel growth rate (mg $kernel^{-1}$ d^{-1}): Values between 1.0 and 3.0	1.5
	SLAP1[c]	ratio of leaf area to mass at emergence (cm^2 g^{-1})	300.0
	SLAP2[c]	ratio of leaf area to mass at end of leaf growth (cm^2 g^{-1})	270.0
	TC1P1[b]	tiller number from emergence to terminal spikelet	2.5
Cropsim	P1[b]	Thermal time from emergence to double ridges (°C d)	350
	VREQ[b]	Vernalization required for max. development rate (VDays)	44
	P5[b]		50
	P8[b]	Thermal time from the onset of grain filling to maturity (°C d)	390
	PPS1[b]	Photoperiod sensitivity % drop-in rate	70
	PHINT[c]	Interval between successive leaf appearances (°C d)	86
	LA1S[c]	Area of standard first leaf (cm^2)	3.5
	LAFV[c]	Increase in potential area of leaves, vegetative phase (fractions per leaf)	2.0
	SHWTS[c]	Standard, non-stressed shoot dry weight, maturity (g)	4.0
	GWTS[c]	Standard grain size, optimum conditions, normal plant density (mg)	50
	G#WTS[c]	Standard grain number per unit canopy weight at anthesis (grain no. g^{-1})	14
	LAFR[c]	Increase in potential area of leaves, reproductive phase (fractions per leaf)	0.5

[a]AMC, automated model calibration.
[b]Phenology.
[c]Growth and yield.

selection threshold (Figure 2) that is based on the target variable scale and the mean of in-season observations. If, for example, the mean of all in-season observations of LAI equals 2.0, then the initial mathematical threshold based on LAI time-series observations is 0.6, where LAIDCriteria is equal to ObservedLAIDMean (2.0) times LAIDStep (0.3). In the case of tops weight, the mathematical threshold is 600 kg ha^{-1} if the mean of all in-season observations is 2,000 kg ha^{-1}. The example above shows only cultivar coefficient combinations resulting in LAI and tops weight

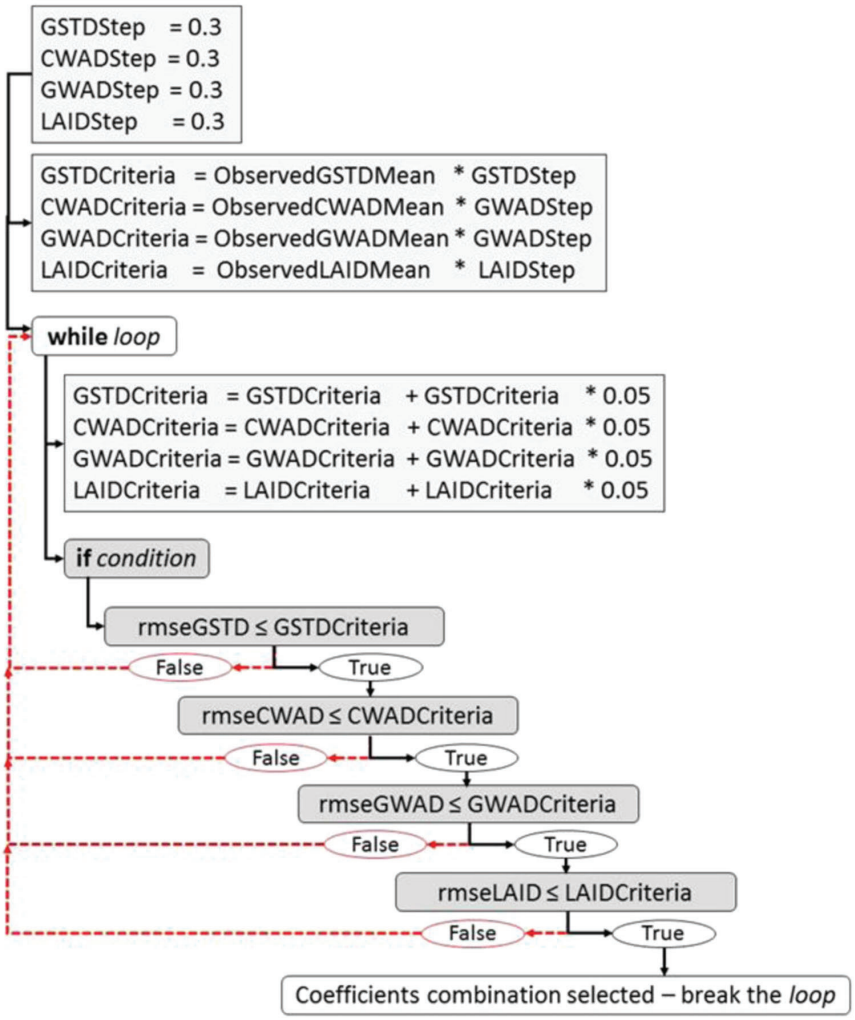

FIGURE 2 Simplified optimal combination selection criteria for GSTD (growth stage; phenological development), LAID (leaf area index), GWAD (grain weight dry matter), and CWAD (tops weight dry matter)

RMSE lower than 0.6 and 600 kg ha^{-1}, respectively. If none of the tested combinations provides satisfying RMSE values, the while loop will be restarted and LAIDCriteria and tops weight (CWADCriteria) are increased by 5% [e.g., LAIDCriteria = LAIDCriteria + 0.5(LAIDCriteria)], allowing combinations with higher RMSE to be considered as optimal. If the weight coefficient is set lower for some of the target variables, the selection criteria will favor those coefficient combinations with lower RMSE (Figure 2).

The while loop (flow controlling statement in programming languages executed repeatedly until breaking it) starts and runs as long as the if condition is not met and break introduced (Figure 2). The if condition was set in a way to ignore simulation extremes in which only one of the investigated target variables (e.g., LAID or CWAD) has a very low RMSE, while the other has a higher RMSE than the one set in the criteria. The optimal solution will be the one with minimum RMSEs (compromised solution to avoid overfitting of LAID or CWAD; Figure 2).

The calibration procedure was conducted on the 2016 and 2017 dataset using the developed calibrator. In order to avoid errors in the calibration between the different models, coefficients with similar effects on target variable simulation outputs were chosen (Table 3). Based on literature and manual evaluation, the most relevant coefficients for optimization of the phenological events and growth-related target variables (simultaneously across three crop models) were prioritized (Table 3) and implemented in the AMC calibration program (specific hardcoded solutions within this study), for further optimization.

TABLE 4 Example of the cultivar coefficients used for optimizing phenological wheat growth and dry matter growth in the CERES model

		Range reduction through global steps				
		1st			2nd	3rd
	Coefficients	Min	Max	[Inc][a]	Min/Max[b] [Inc]	Min/Max[Inc]
Phenology:	P1[c] (1)[d]	200	350	[50]	± 20 [20]	± 0
	P2(3)	250	350	[50]	± 0	± 20 [20]
	P3(4)	250	350	[50]	± 0	± 0
	P4(7)	250	350	[50]	± 0	± 0
	P1V(1)	15	45	[10]	± 5 [5]	± 2 [2]
	P1D(2)	60	140	[40]	± 20 [20]	± 10 [10]
	P5(3)	200	600	[200]	± 100	± 50 [50]
Growth:	G1(4)	30	30	0	± 10 [10]	± 2 [2]
	G2(5)	40	40	0	± 20 [10]	± 5 [5]
	G3(6)	200	200	0	± 100 [100]	± 50 [50]
	PHINT(7)	50	110	[20]	± 10 [5]	± 2 [2]

[a][Inc], increment steps.
[b]Min/Max, minimum and maximum coefficient range setup based on the agronomic criteria;
[c]See Table 3 for calibration coefficient definitions.
[d]Values in parentheses correspond to numbering in the respective files.

Cultivar coefficients related to plant phenology (flowering, physiological maturity, reproductive phase initialization, etc.) are optimized first (based on the RMSE selection criteria), as they are preconditions for correct simulation of yield and aboveground biomass accumulation rates. In the next step, traits like aboveground biomass accumulation rates, grain yield, and so forth are optimized as they depend on phenology (Table 4). Hence, during the optimization of phenology related cultivar coefficients, yield-related coefficients are nominally determined by using default values (theory based). This procedure can distort some of the growth defining mathematical functions if an assumption of stress-free conditions was incorrect (e.g., water or fertilizer stress).

The calibration procedure was conducted in different steps, prioritizing the optimization of phenological development in a first step (Table 4) and based on the selection criteria, optimum cultivar coefficients were estimated. In the second step, tops weight and grain yield were optimized (in second and third run underlined coefficient ranges are activated). As shown in Table 4, some coefficients were optimized throughout all optimization phases, as they had a simultaneous influence on both phenological and growth traits. Phenological events such as day of onset of flowering are commonly observed on a weekly basis (depending on percent of plants flowering in the field), and because of that small error was allowed in simulation of phenological events in order to accomplish better simulation of in-season aboveground biomass accumulation rates and grain yield.

The division of the calibration procedure in different optimization steps was carried out due to the impracticality of optimizing all eleven coefficients simultaneously with a huge amount of range combinations. The exhaustive gridding method is more systematic when compared to some random generation of cultivar coefficient combinations. However, the overall process is time consuming and therefore, not efficient. In order to reduce the number of model runs in this study, the method of range reduction was implemented. This method includes three-layered global steps (after every step in between optimization is conducted based on corresponding RMSE values) that reduce the number of combinations executed in the calibration procedure (Table 5; Phase 2 and 3). A simplified example of the range reduction method is shown in Table 5. Taking the example of the Phyllochron interval (PHINT) coefficient (Table 5), which was varied in the range of Min = 50, Max = 110 with incremental steps of 2, a total number of possible coefficient combinations was 31 (in that case, the model is executed 31 times). The range reduction method through three-layered global steps resulted in a total of 12 coefficient combinations (61% less model runs) with the same final coefficient value PHINT = 92 (Table 5).

2.4 | Statistical evaluation

The model assessment was conducted by comparing the simulated and observed growth stages, LAI, yield, tops

TABLE 5 Example of coefficient estimation using a range reduction method implemented as global three-layered steps

	Exhaustive gridding	Range reduction through global three-layered steps					
	1st 50–110 [2][a]	1st 50–110 [20][b]		2nd ± 10 [5]		3rd ± 2	
	50	50		80			
	52	70		85		88	
	…	90	→ 90	90	→ 90	90	
	92 → 92	110		95		92	→ 92
	…			100			
	108						
	110						
Number of combinations	31	4		5		3	
Total	31	(4 + 5 + 3) = 12					

[a]Phyllochron interval (PHINT), interval between successive leaf tip appearances.
[b]Values in brackets indicate increment steps.

weight, and N content for every model and every N treatment. For statistical evaluation, the root mean square error ($RMSE_m$; Equation 1), normalized root mean square error ($nRMSE_m$; Equation 2), and the index of agreement (d-$index_m$; Equation 3) (Willmott, 1982) of the respective model were used. The simulated values of the respective model are represented as S_{mi} and O_i is the observed values from the experiment. The $RMSE_m$ quantifies the amount of variation between simulated and measured values on a metric scale for the respective model. It keeps the units of the target parameter. For model under or over estimation or model comparison, the d-index was used. For a proper fit between simulated and observed data, the $RMSE_m$ should be close to 0, and the d-index should have a value of 1.0. The statistical evaluation was carried out for all N treatments, each year, and each model separately. Afterward, the $RMSE_{mean}$, $nRMSE_{mean}$, and d-$index_{mean}$ were calculated by weighing all simulated values as $0.\overline{33}$.

Root mean square error single model ($RMSE_m$):

$$RMSE_m = \left[\frac{1}{n}\sum_{i=1}^{n}(S_{mi} - O_i)^2\right]^{0.5} \quad (1)$$

Normalized root mean square error ($nRMSE_m$)

$$nRMSE_m = \frac{RMSE_m}{\bar{O}}\,100 \quad (2)$$

Index of agreement single model (d_m):

$$d_m = 1 - \left[\frac{\sum_{i=1}^{n}(S_{mi} - O_i)^2}{\sum_{i=1}^{n}\left(|S_{mi} - \bar{O}| + |O_i - \bar{O}|\right)^2}\right] \quad (3)$$

Root mean square error Multi-Model ($RMSE_{mean}$):

$$RMSE_{mean} = \left[\frac{1}{n}\sum_{i=1}^{n}\left(\frac{\sum_{m=1}^{3} S_{mi}}{3} - O_i\right)^2\right]^{0.5} \quad (4)$$

Normalized root mean square error of the mean ($nRMSE_{mean}$)

$$nRMSE_{mean} = \frac{RMSE_{mean}}{\bar{O}}\,100 \quad (5)$$

Model mean Index of agreement Multi-Model (d_{mean}):

$$d_{mean} = 1 - \left[\frac{\sum_{i=1}^{n}\left(\frac{\sum_{m=1}^{3} S_{mi}}{3} - O_i\right)^2}{\sum_{i=1}^{n}\left(\left|\frac{\sum_{m=1}^{3} S_{mi}}{3} - \bar{O}\right| + |O_i - \bar{O}|\right)^2}\right] \quad (6)$$

Models mean:

$$\text{Models mean} = \frac{S_{m1} + S_{m2} + S_{m2}}{3} \quad (7)$$

3 | RESULTS AND DISCUSSION

3.1 | Model calibration

The developed AMC makes the calibration of different models more standardized and enables the implementation of measured time-series data for cultivar parameter

TABLE 6 Statistical metrics of CERES, NWheat, and Cropsim for different plant parameters in the calibration dataset across all seven nitrogen treatments

Years	Variable		CERES	NWheat	Cropsim	Multi-Model mean
2016	Growth stage	nRMSE[a]	10.18	9.28	20.61	10.01
		d-index	.99	.99	.97	.99
2016	Tops weight	nRMSE	40.26	33.19	27.05	32.14
		d-index	.94	.96	.98	.96
2016	LAI	nRMSE	28.25	22.27	24.27	20.91
		d-index	.91	.96	.93	.95
2016	Grain weight	nRMSE	13.44	13.65	14.95	12.46
		d-index	.92	.95	.93	.98
2016	Vegetative nitrogen concentration %	nRMSE	15.70	28.01	23.73	18.01
		d-index	.96	.89	.87	.94
2017	Growth stage	nRMSE	12.26	13.46	15.53	11.91
		d-index	.99	.98	.98	.99
2017	Tops weight	nRMSE	19.77	20.02	28.29	23.48
		d-index	.97	.97	.94	.97
2017	LAI	nRMSE	22.82	28.64	33.07	25.89
		d-index	.93	.91	.84	.92
2017	Grain weight	nRMSE	10.83	19.13	14.23	13.87
		d-index	.84	.74	.81	.81
2017	Vegetative nitrogen concentration %	nRMSE	19.11	49.59	39.77	30.80
		d-index	.89	.58	.71	.78
	Overall mean	nRMSE	19.26	23.72	24.15	19.95
		d-index	.93	.89	.89	.93

[a]nRMSE, normalized root mean square error; LAI, leaf area index.

estimation. This ensures a user-independent calibration of all included models and gives a broader perspective for the scientific community. The calibration approach showed satisfying results across both years and for all seven N treatments.

The overall model mean (Table 6) for 2016 and 2017 of the calibration dataset showed a slightly higher d-index (.93) for CERES and similar values (.89) for NWheat and Cropsim. All models were able to predict the relevant phenological stages (i.e., anthesis and maturity) quite well. This finding was indicated by a high d-index for growth stage, varying between .97 and .99 for all models and years (Table 6).

Tops weight also showed a high d-index (over .94) across all models and N levels within the calibration dataset (in 2016 and 2017). Ahmed et al. (2016) considered an accurate simulation of tops weight as a sign for robust model calibration. They showed similar results for the d-index for CERES and APSIM-Wheat, which ranged between .89 and .98 in different spring wheat cultivars.

Plant parameters like LAI or vegetative N concentration were simulated with slightly lower statistical values across different models and years. The nRMSE for LAI in 2016 showed a similar range (22.27–28.25) for the three models, and performed slightly weaker in 2017 (nRMSE values of 22.82 to 33.07). Vegetative N revealed the same pattern and nRMSE ranged between 15.70 and 28.01 in 2016 and 19.11 and 49.49 in 2017. Grain weight was simulated at the same level in 2016. In 2016, nRMSE ranged between 13.44 and 14.95 and between 10.83 and 19.13 in 2017. The statistical values were comparable with the results of Asseng (2013) where the maximum nRMSE for LAI was reported as 35, for vegetative N content as 40, and for grain weight as 30.

Nevertheless, one reason for the differences between the years of the calibration datasets can be explained by different mineralization of residues of the previous crops. The Godwin method, which was used for organic matter decomposition in the models, has some limitations in mineralization. This has also been reported in the literature (Gijsman, Hoogenboom, Parton, & Kerridge, 2002). In 2016, the previous crop was winter barley while in 2017 it was oilseed rape. Several researchers mentioned that after oilseed rape, high amounts of N remain in the field due to the low N use efficiency and the low N harvest index (Hocking, Randall, & DeMarco, 1997; Schjoerring, Bock, Gammelvind, Jensen, & Mogensen, 1995). The

TABLE 7 Statistical metrics of CERES, NWheat, and Cropsim for different plant parameters in the evaluation dataset across all seven nitrogen treatments

Years	Variable		CERES	NWheat	Cropsim	Multi -Model mean
2015	Growth stage	nRMSE[a]	15.91	11.37	15.90	12.52
		d-index	.98	.99	.98	.99
2015	Tops weight	nRMSE	54.38	49.15	52.84	50.76
		d-index	.91	.93	.92	.93
2015	LAI	nRMSE	19.59	75.40	60.72	43.96
		d-index	.97	.81	.83	.91
2015	Grain weight	nRMSE	20.02	13.06	12.10	14.01
		d-index	.84	.96	.96	.94
2015	Vegetative N concentration %	nRMSE	35.83	31.65	36.31	23.65
		d-index	.78	.87	.77	.90
2018	Growth stage	nRMSE	8.86	17.16	10.27	9.70
		d-index	.99	.97	.99	.99
2018	Tops weight	nRMSE	50.59	21.17	50.04	36.05
		d-index	.72	.96	.73	.86
2018	LAI	nRMSE	45.75	33.82	47.22	29.40
		d-index	.50	.70	.32	.56
2018	Grain weight	nRMSE	46.62	20.58	43.44	24.33
		d-index	.34	.75	.39	.61
2018	Vegetative N concentration %	nRMSE	33.67	47.45	25.68	24.37
		d-index	.38	.34	.54	.44
	Overall mean	nRMSE	33.12	32.08	35.45	26.88
		d-index	.74	.83	.74	.81

[a]nRMSE, normalized root mean square error; LAI, leaf area index.

initial conditions for residues, N, and water were set up before model calibration, but it cannot be excluded that N mineralization from oilseed rape, in reality, differs from the model simulation. This assumption was supported by the overall slightly lower vegetative N simulation in 2017 across all models.

3.2 | Model evaluation

The evaluation dataset (2015 and 2018) showed slightly weaker statistical values for both years compared with the automated calibration dataset results. The overall mean d-index (Table 7) ranged between .74 (CERES and Cropsim) and .83 (NWheat).

Slightly weaker model performance in the evaluation datasets compared to the calibration datasets is widely reported in crop modeling literature. In several publications like Jing et al. (2017) or Attia et al. (2016), this effect was shown. The reason for the slight difference between calibration and validation is common. It occurs due to the fact that all datasets used for calibration include experimental errors, which can lead to a distortion of model calibration. The calibration procedure ideally is conducted with stress-free experimental observations (which are extremely difficult to accomplish). The models use solar radiation and daily temperatures in the simulation process that are active during the calibration procedure as well. Due to the nature of these model inputs (variation from year to year), some effects are considered in the optimization process of cultivar coefficients, even though ideally, that should not happen. (Boote et al., 2016; Kersebaum et al., 2015). Hence, an application to new independent datasets like what is done in the model evaluation can lead to weaker model performance.

In 2015, the d-index for growth stage varied between .98 and .99, between .91 and .93 for tops weight, between .81 and .97 for LAI, and between .84 and .96 for grain weight across all models. The d-index for vegetative N content in the same year was around .77 for CERES and Cropsim and at .87 for NWheat.

Within the 2018 dataset, the phenology parameter growth stage showed high d-index values over .97 across all models. However, the CERES and Cropsim models showed lower d-index values for tops weight (.72; .73), LAI (.50; .32), and grain weight (.34; .39) compared to NWheat.

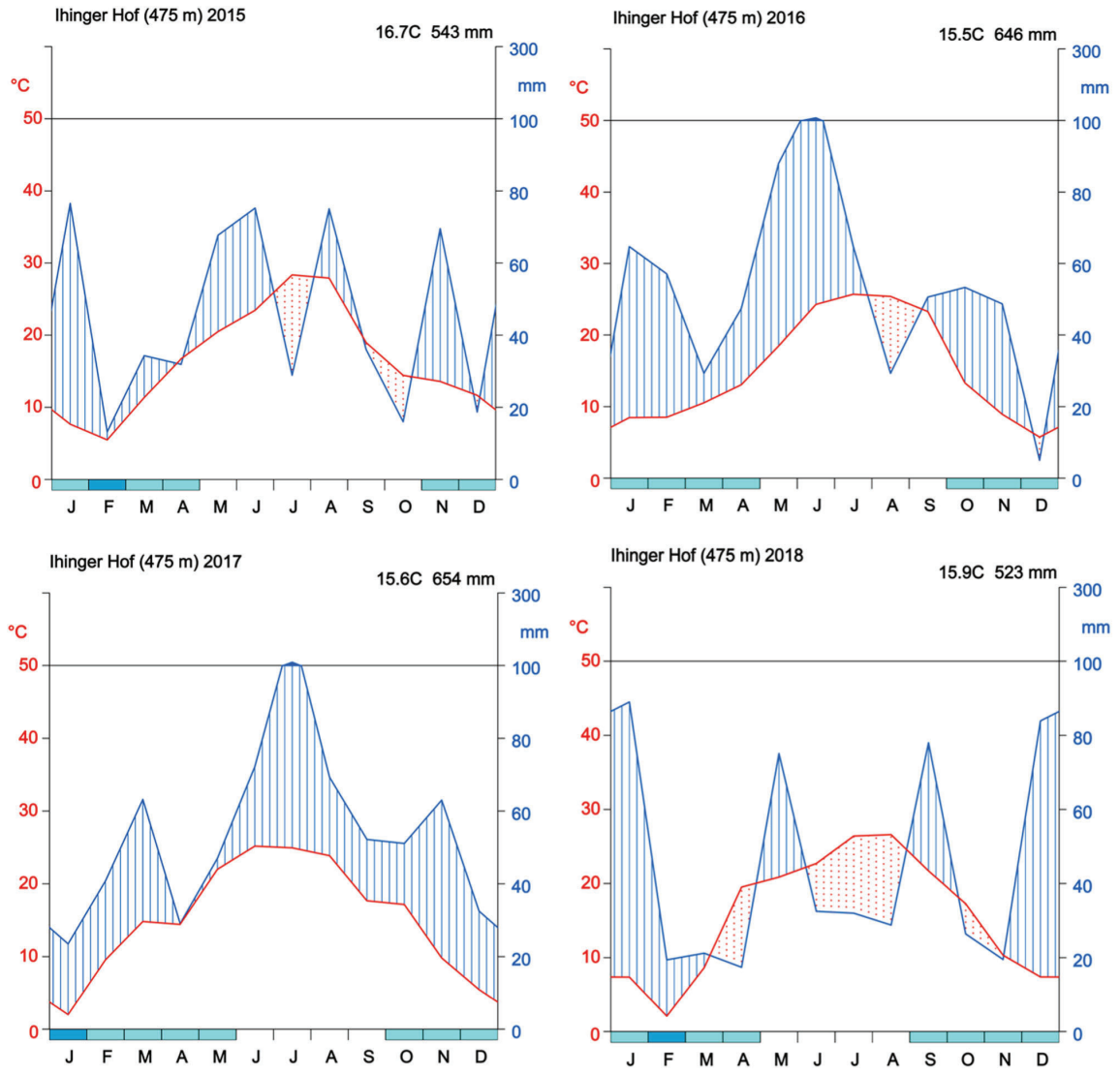

FIGURE 3 The Walter and Lieth climatic diagram for temperature (red line) and precipitation (blue line) series of Ihinger Hof for 2015–2018, including the annual mean temperature and mean precipitation. The horizontal line refers to the different months. The shades of blue on the horizontal line indicate the months where the absolute daily min temperatures are below 0 °C

NWheat showed higher d-indices for tops weight (.96), LAI (.70), and grain weight (.75). The reason for this model differences can be seen in the weather period in June and July 2018, where low rainfall occurred (Figure 3). This drought period did not happen in 2015, 2016, and 2017 (Figure 3). The reason for the higher modeling accuracy of NWheat in 2018 might be associated with different handling of evapotranspiration. CERES and Cropsim use the potential evapotranspiration, while NWheat uses the critical fraction approach (Kassie et al., 2016). This critical fraction approach was developed under Australian conditions and seems to be more suitable under drought conditions. In addition, Kassie et al. (2016) reported a slight overestimation of NWheat for grain weight under dry conditions which were also observed in the drier year of 2018.

3.2.1 | Multi modeling approach

Using an automated calibration method for a Multi Modeling approach, in all 4 yr, and across different N levels, the MM mean improved the results in comparison to the simulation results of the single models (Table 6; Table 7). Overall, the MM approach resulted in a higher d-index (.61–.99)

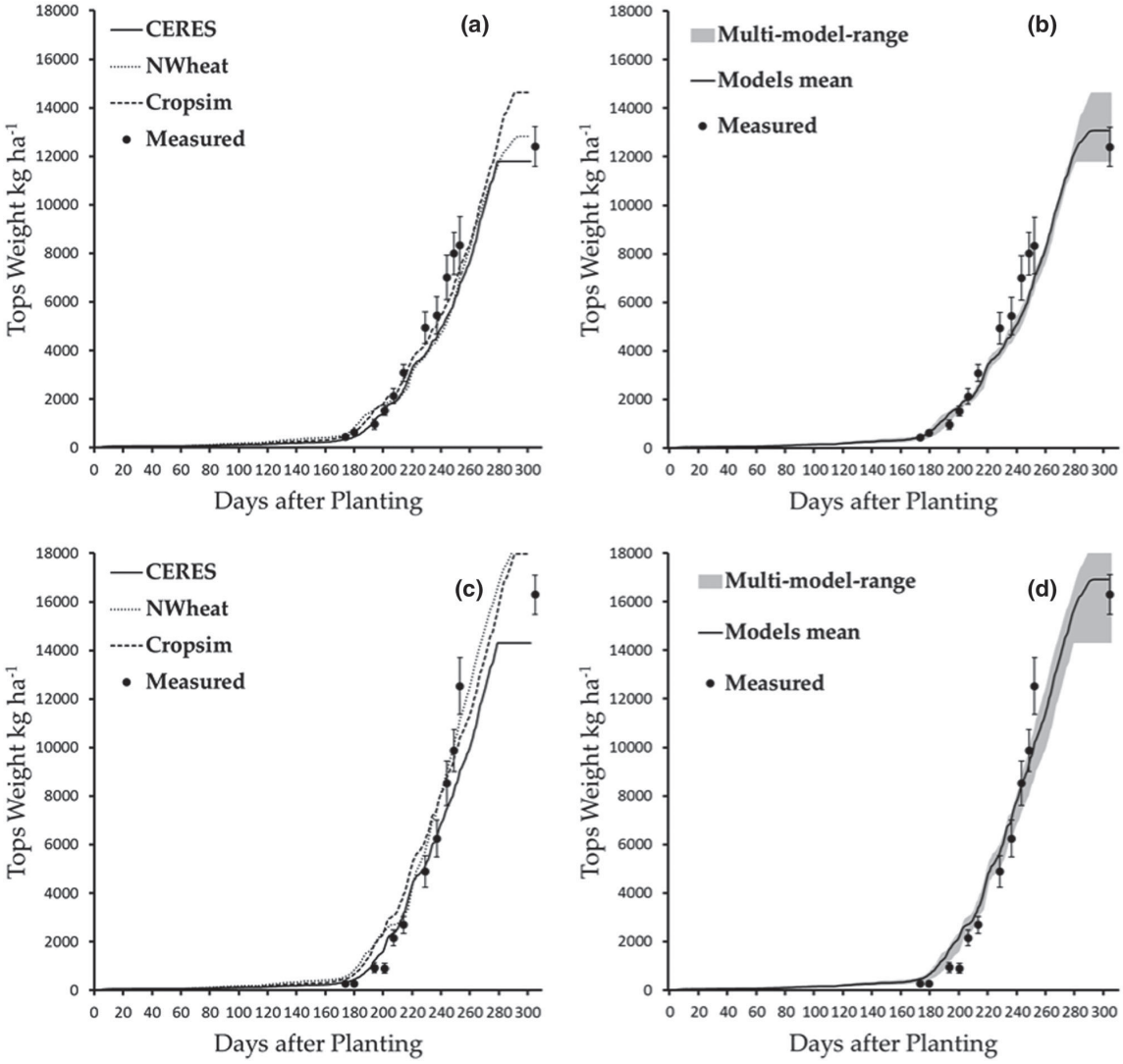

FIGURE 4 Simulation of tops weight of CERES, NWheat, and Cropsim and measured in 2016 (a–d). The simulated model range of the multi-model approach is represented by the grey area (b, d), including the overall model mean (b, d). Figures represent exemplarily the applied nitrogen amounts of 120 kg ha^{-1} N (a, b) and 240 kg ha^{-1} N (c, d). The error bars indicate the standard error

and was even higher than the values reported by Palosuo et al. (2011; .40–.74).

For 2015–2018, simulation of growth stage was very close to the observed values represented by a high d-index of .99. The d-index of the growth stages for the single model simulations was always over .97, nevertheless, the MM led to slight model improvement. The MM mean for tops weight showed the lowest d-index of .86 and the modeling accuracy was slightly improved in comparison to the single model approach (d-index CERES .72; NWheat .73). For 2015–2017, the d-index was always above .93 and indicated an accurate simulation.

Focusing on two different N application rates (120 kg ha^{-1} N and 240 kg ha^{-1} N) in 2016 Figure 4b, 4d) the model mean of all three models matched the measured values of the tops weight closely. All models showed almost no difference between 0 and 260 d after planting (DAP). After 260 DAP, NWheat and Cropsim performed similar at high N levels, and CERES and NWheat showed similar simulations for the 120 kg ha^{-1} N application

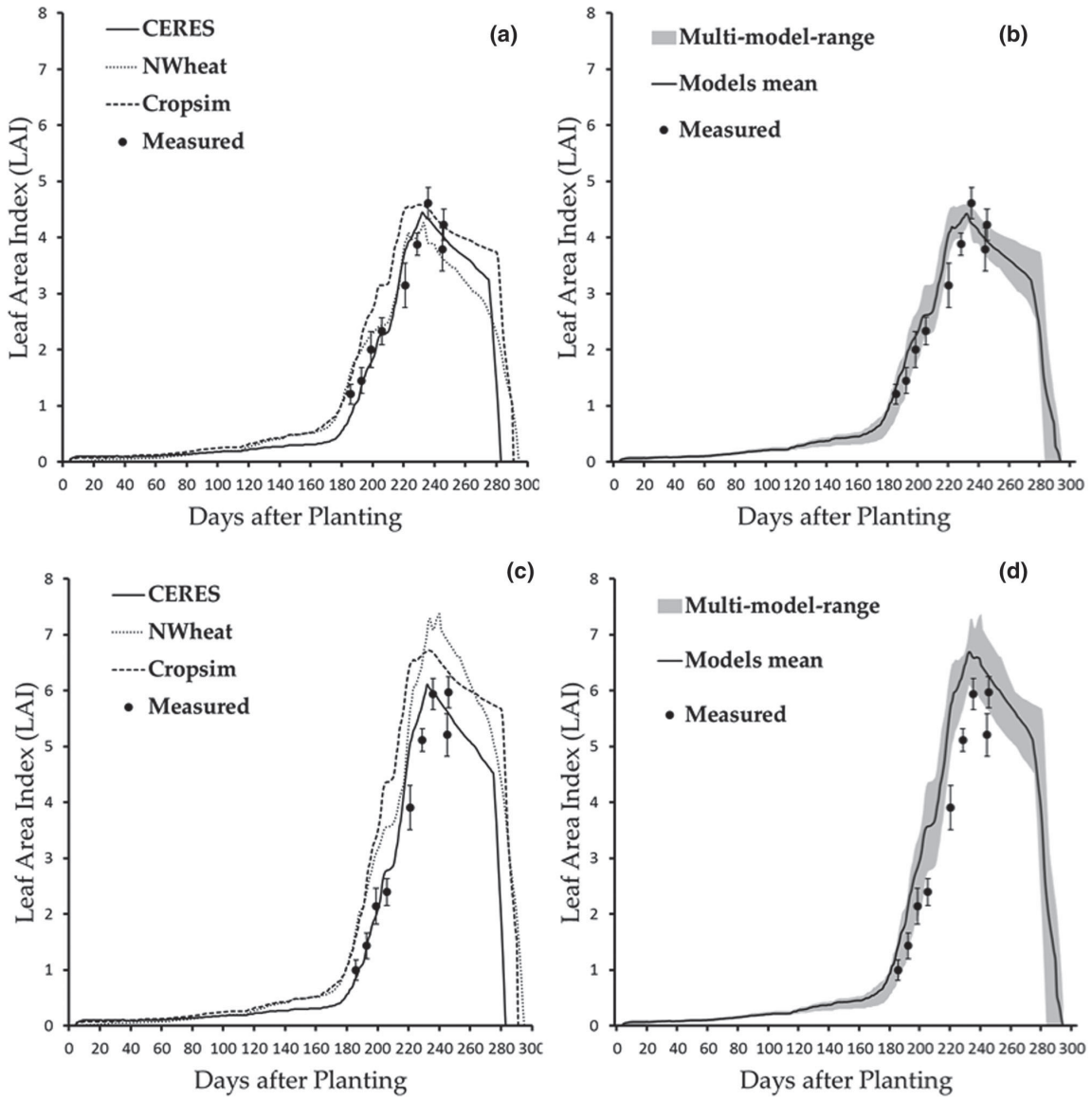

FIGURE 5 Simulation of leaf area index (LAI) of CERES, NWheat, and Cropsim and measured in 2016 (a–d). The simulated model range of the Multi-Model approach is represented by the grey area (b, d) including the overall model mean (b, d). Applications of 120 (a, b) and 240 kg ha^{-1} N (c, d) are shown. The error bars indicate the standard error

(Figure 4a, 4c). The results of this study were comparable with results gained from a performance test of NWheat at the location in the Netherlands (Kassie et al., 2016), where tops weight reached similar values at harvest for low N (14,500 kg ha^{-1}) and high N (18,000 kg ha^{-1}).

In general, the LAI was simulated slightly weaker compared to tops weight, but a high d-index was obtained for the MM mean which ranged between .91 (2015), .92 (2017), and .95 (2016). The d-index for the dry year in 2018 was around .56 and has to be considered in the context that Cropsim reached only a d-index of 0.32. Hence, MM mean increased the modeling accuracy substantially. Considering the LAI for 120 and 240 kg ha^{-1} N of the 2016 dataset, the difference between the models was higher compared to the simulation of tops weight (Figure 5a, 5c). All three models showed similar performance and reached the maximum LAI at almost the same date (230 DAP). The simulated maximum LAI and the measured maximum LAI were very close for the 120 kg ha^{-1} N treatment, but they showed a higher difference in the

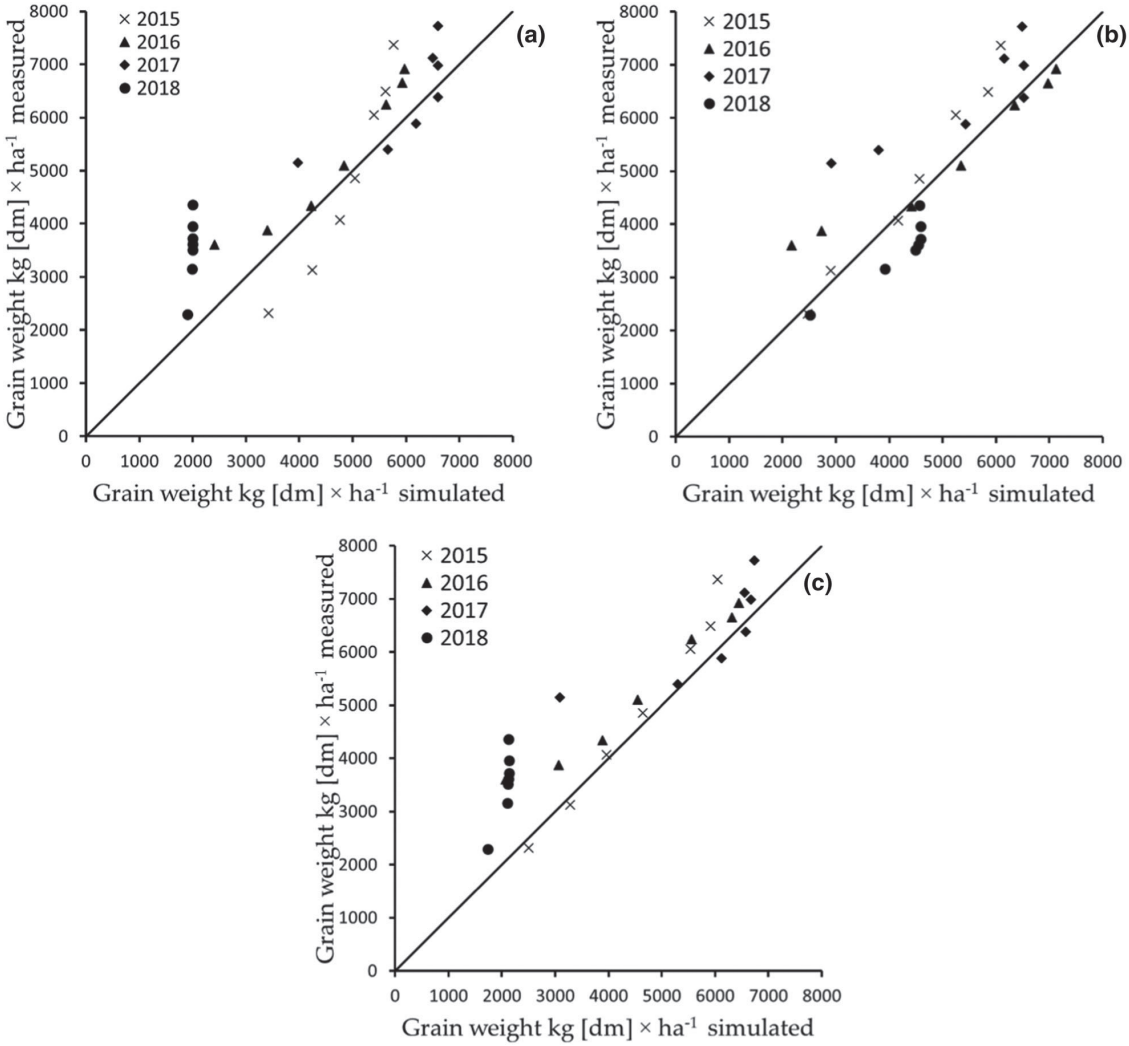

FIGURE 6 Grain weight simulation of CERES (a), N-Wheat (b), and Cropsim (c) compared with simulated values on the 1:1 line, including all seven nitrogen treatments and four simulated years (2016–2017 calibration; 2015–2018 evaluation). Dm, dry matter

240 kg ha^{-1} N treatment. The NWheat model in particular showed a stronger overestimation of LAI compared to CERES and Cropsim. Cropsim also had this tendency, especially in the period between 180 and 220 DAP, but NWheat overestimated the maximum LAI when compared to Cropsim. Kassie et al. (2016) reported the tendency of LAI overestimation in the NWheat model, but in this study, the overestimation was restricted to the high N (240 kg ha^{-1} N) level. This was also shown by the statistics, where a high d-index of .96 was reached for LAI (Table 6) across different N levels. Nevertheless, Asseng et al. (2004) also reported small effects on crop growth and yield if the simulated LAI is greater than 3. This difference had less influence on the yield formation process.

The MM mean for grain weight was quite accurate and reached a d-index over .81 (2017; Table 6). Remarkably, the d-index of the MM mean was higher that the single models almost every year. Especially in years where one model was weaker, another model was able to compensate this weakness: in 2015, CERES had a d-index of .84 and the MM mean reached a d-index of .94. Nevertheless, the NWheat model showed a high modeling accuracy for grain weight (Figure 6), whereas CERES and Cropsim tended to underestimate the grain weight. Especially in the dry year of 2018, CERES and Cropsim showed similar grain weight patterns and underestimated the yield. In the same year, NWheat performed differently and had a higher d-index of .75. As previously mentioned, the changes in

the model structure by replacing the crop water uptake routine (Kassie et al., 2016) during the migration process from CERES to NWheat resulted in lower evapotranspiration. Therefore, water might be preserved in the soil and could be used in later growing periods to increase grain yield in the different N fertilizer treatments. Figure 6 showed almost no yield response for CERES and Cropsim according to the different N treatments, which supports the assumption of less water availability in the soil during the generative phase. The simulated soil water content (data not shown) supported this water-preserving effect which could be observed in the simulation for the whole season in NWheat.

CERES and Cropsim still have similar equations for potential evapotranspiration calculation. Where CERES uses the Ritchie and Otter (1985) approach, Cropsim uses an adaption of the Priestly and Taylor (1972) function, which may explain the similar reaction. Errors could have also occurred in the soil profile based on values of soil texture or organic residues, but this influence seemed to be unlikely because all three models were using the same soil profile information as model inputs. Prediction of vegetative N in crop models is crucial (Pan et al., 2006) and resulted for the MM mean in a d-index of .78 (2017), .90 (2015), and .94 (2016), including N levels between 0 and 240 kg ha^{-1} N.

In the dry year of 2018, the dataset indicated a clearly lower d-index of .44. which is probably due to the interaction of the N balance in the model and the water balance (Kersebaum et al., 2015). Two different N application rates, 120 and 240 kg ha^{-1} N (Figure 7), were selected to demonstrate the strength of the MM approach. Comparing the simulated plant N content for 120 and 240 kg ha^{-1} N, similar peaks at certain days were observed. These peaks indicated an increase of N content that reflected the N application date. The CERES model showed slightly lower plant N contents in both treatments. Especially in spring around 140 DAP, a difference between simulated and observed N content was observed. Later in the season, after 180 DAP, the simulation fitted almost perfectly with the measured values. NWheat and Cropsim behaved slightly different, which resulted in an overall higher plant N content and a more accurate simulation between 140 and 170 DAP. After 220 DAP, the Cropsim model showed a different behavior. While simulated plant N contents were reduced in CERES and NWheat until harvest, the Cropsim model stayed at higher N contents. This was also observed in other years and seemed to be a model-specific anomaly. The model mean showed the highest d-index at .90 for all N treatments in 2015 (Table 6).

3.2.2 | Limitations of the automated calibration and the MM Approach

Using an MM approach does not always result in the best statistical fit for a single year or a single variable (Palosuo et al., 2011). For example, the CERES model showed the highest d-index of .97 for the LAI in 2015, while the MM mean indicated .91 (Table 7). This reduction in modeling accuracy of a single variable in a single year can be considered as a compromise while leading to an improvement of all variables across years. This fact was also suspected by Rötter et al. (2012) where several models across different seasons and sites performed better than one individual model.

However, there are several sources of simulation uncertainties in an MM approach caused by model structure, parameterization, and input data (Van Oijen & Ewert, 1999). Model structure and parameterization differed between the models used in this study. Hunt and Pararajasingham (1995) showed the model changes during the migration from CERES to Cropsim, and Kassie et al. (2016) showed the model changes in NWheat. These structural model changes are influencing the parameterization, which also affects the modeling results. Hence, even if strongly related models like CERES and Cropsim are used, they may lead to different results (Asseng, 2013).

The parameterization uncertainty is mainly performed within the DSSAT environment by calibration of coefficients. This error and the specific model user bias were minimized in this study due to the automatic selection process of the developed calibrator (with underlining assumption that in-season observations are error free, which is rarely the case). Nevertheless, when using an automatic calibrator, it might not be possible to control and optimize all cultivar coefficients simultaneously, especially if the dataset is not suitable for adjusting these coefficients, for example, if LAI is not reported, default values have to be used. This will increase the uncertainty, but it facilitates the simulation.

The third simulation uncertainty is represented by input data and can be considered to have less influence on the modeling results of this study. All three models are running within the DSSAT environment and are using the same input files for the weather, soil, and management. This can be seen as a strength of an MM approach if the MM approach is applied within the same modeling platform, such as DSSAT.

The superiority of the MM is clearly shown in 2018 for all variables except for the growth stage. Using the mean between the models seems to be a straightforward

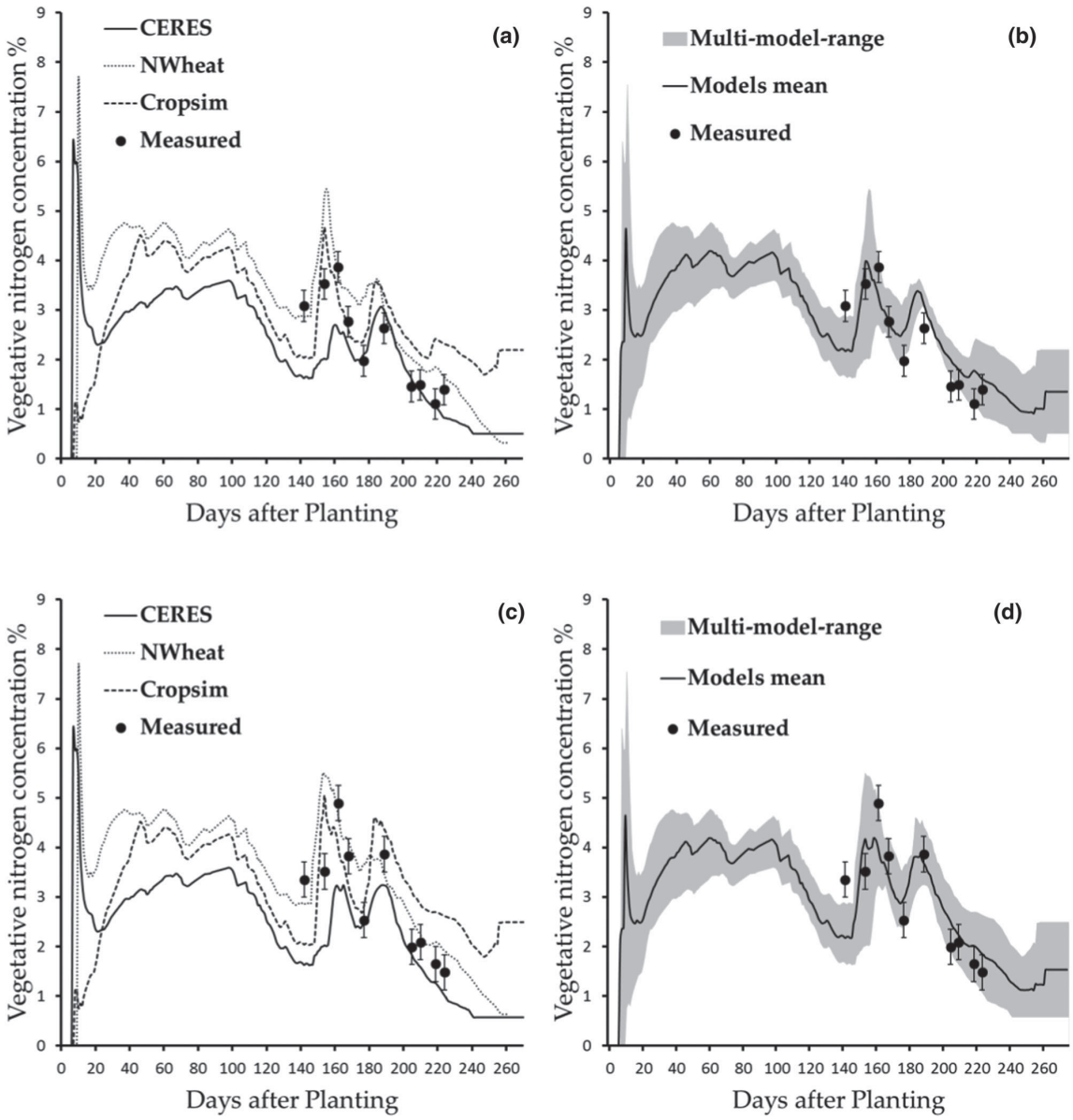

FIGURE 7 Simulation of vegetative nitrogen content (%) for CERES, NWheat, and Cropsim and measured in 2015 (a–d). The simulated model range of the multi-model approach is represented by the grey area (b, d) including the overall model mean (b, d). Applications of 120 (a, b) and 240 kg ha^{-1} N (c, d) are shown

procedure for MM applications. Other MM studies also evaluated the median of the different models (Maiorano et al., 2017; Martre et al., 2015), which is commonly used in climate modeling (Knutti, 2010). Using the median for the three models seems to be not useful. The median is defined in the order from the smallest to the largest value and the selection of the middle value. Using this procedure for three models will result in a selection of values simulated only by one model. Therefore, it seems more practical to use the mean by weighting each model as one third.

Changing the weighting factor as suggested by Tebaldi and Knutti (2007) can mitigate the effects of weaker model performance under severe conditions. This approach is used in meteorological modeling were models are weighed based on historical performance. Tebaldi and Knutti (2007) also mentioned the difficulty of quantifying the model

skills and derive the model weights accordingly. Conveying this method to crop models does not seem like an easy task because of the limited evaluation datasets (Palosuo et al., 2011). Palosuo et al. (2011) reported this issue for crop models, where reusing of the same datasets often occurs, and accurate simulations should be considered as questionable. Independent, long-term data are also sparse and often limited to historical weather data, which were used for modeling purposes (Andarzian, Hoogenboom, Bannayan, Shirali, & Andarzian, 2015). In conclusion, weighing different models is hard to carry out if datasets for model development and evaluation bias towards those data (Rötter et al., 2012).

3.3 | Future model application

The AMC combined with an MM approach worked very well in this study. However, the approach has to be evaluated in further studies under different climates and soil conditions. In addition, the effect of climate change should also be considered. Some researchers suggest increased drought periods (Witcombe, Hollington, Howarth, Reader, & Steele, 2008) and more heat stress events due to climate change (Semenov, 2007) in the future. At the moment, there is a lack in describing the implication of climate change sufficiently for a lot of the current models (Rötter et al., 2012). This can have a substantial effect on the estimation of climate change on wheat production (Lobell, Sibley, & Ivan Ortiz-Monasterio, 2012). Using MM approaches combined with AMC can help detect weaknesses in the models and give suggestions for model improvement (Liu et al., 2016).

It is also feasible to extend the AMC software to other MM approaches within the DSSAT shell for other crops. The current version of DSSAT includes CERES Maize (Jones & Kiriny, 1986) and CSM-IXIM (Lizaso et al., 2011), and the combination of both models seems to be suitable for an MM approach. In addition, AMC can also be used for single-model calibrations and offers the opportunity for broader use and more user-independent calibrations.

4 | CONCLUSIONS

This study showed that MM has the potential to increase modeling accuracy, especially when the structural difference between multiple models gets obvious in the simulation results. Nevertheless, the most challenging part of MM is the calibration procedure. Existing calibration procedures typically exclude time-series data and are only able to use one observation per season. This can lead to a manual user adjustment and is not user independent. Consequently, an AMC for the three wheat models within the DSSAT 4.7 environment was developed and enabled the use of time-series data to ensure a user-independent standardized calibration procedure for each model separately.

Overall, the simulations showed satisfying results for the calibration and the evaluation dataset. Especially in the dry year of 2018, the MM approach led to a better understanding of single model's weaknesses and increased the overall model accuracy. Hence, the MM approach, combined with AMC seems to be promising but has to be tested in further studies under different soil and climate conditions.

ACKNOWLEDGMENTS

Many thanks to the DSSAT group for providing model information. Especially to William D. Batchelor, Kenneth J. Boote, Senthold Asseng, Anthony L. Hunt, and Gerrit Hoogenboom.

FUNDING

This research was funded by the German Federal Environmental Foundation (DBU) (Project No. 33143/01)

CONFLICT OF INTEREST

The authors declare that they have no conflict of interest.

ORCID

Georg Röll https://orcid.org/0000-0001-7127-4293
Simone Graeff-Hönninger https://orcid.org/0000-0001-9996-961X

REFERENCES

Ahmed, M., Akram, M. N., Asim, M., Aslam, M., ul Hassan, F., Higgins, S., … Hoogenboom, G. (2016). Calibration and validation of APSIM-Wheat and CERES-Wheat for spring wheat under rainfed conditions: Models evaluation and application. *Computers and Electronics in Agriculture*, *123*, 384–401. https://doi.org/10.1016/j.compag.2016.03.015.

Andarzian, B. B., Hoogenboom, G., Bannayan, M., Shirali, M., & Andarzian, B. B. (2015). Determining optimum sowing date of wheat using CSM-CERES-Wheat model. *Journal of the Saudi Society of Agricultural Sciences*, *14*(2), 189–199. https://doi.org/10.1016/j.jssas.2014.04.004.

Asseng, S. (2013). Uncertainty in simulating wheat yields under climate change. *Nature Climate Change*, *3*(9), 627–632. https://doi.org/10.1038/ncliamte1916.

Asseng, S., Bar-Tal, A., Bowden, J. W., Keating, B. A., Van Herqaarden, A., Palta, J. A., … Probert, M. E. (2002). Simulation of grain protein content whit APSIM-Nwheat. *European Journal of Agronomy*, *16*, 25–42. https://doi.org/10.1016/S1161-0301(01)00116-2

Asseng, S., Jamieson, P. D., Kimball, B., Pinter, P., Sayre, K., Bowden, J. W., & Howden, S. M. (2004). Simulated wheat growth affected by rising temperature, increased water deficit and elevated atmospheric CO2. *Field Crops Research*, *85*(2–3), 85–102. https://doi.org/10.1016/S0378-4290(03)00154-0

Asseng, S., Keating, B. A., Fillery, I. R. P., Gregory, P. J., Bowden, J. W., Turner, N. C., … Abrecht, D. G. (1998). Performance of the APSIM-wheat model in Western Australia. *Field Crops Research*, *57*(2), 163–179. https://doi.org/10.1016/S0378-4290(97)00117-2

Asseng, S., Kheir, A. M. S., Kassie, B. T., Hoogenboom, G., Abdelaal, A. I. N., Haman, D. Z., & Ruane, A. C. (2018). Can Egypt become self-sufficient in wheat? *Environmental Research Letters*, *13*(9). https://doi.org/10.1088/1748-9326/aada50.

Attia, A., Rajan, N., Xue, Q., Nair, S., Ibrahim, A., & Hays, D. (2016). Application of DSSAT-CERES-Wheat model to simulate winter wheat response to irrigation management in the Texas High Plains. *Agricultural Water Management*, *165*, 50–60. https://doi.org/10.1016/j.agwat.2015.11.002

Bannayan, M., Crout, N. M. J., & Hoogenboom, G. (2003). Application of the CERES-Wheat model for within-season prediction of winter wheat yield in the United Kingdom. *Agronomy Journal*, *95*(1), 114–125. https://doi.org/10.2134/agronj2003.0114

Bannayan, M., & Hoogenboom, G. (2009). Using pattern recognition for estimating cultivar coefficients of a crop simulation model. *Field Crops Research*, *111*(3), 290–302. https://doi.org/10.1016/j.fcr.2009.01.007

Bassler, R., & Hoffmann, G. (1997). Bestimmung von mineralischen, (Nitrat-) Stickstoff in Bodenprofilen, Nmin-Labormethode. In *VDLUFA Methodenburch Band I* (4th ed., pp. A6.1.4.1.1–A6.1.4.1.20). Darmstadt, Germany: VDLUFA-Verlag.

Boote, K. J. (Ed.) (2019). *Advances in crop modelling for a sustainable agriculture*. London, UK: Burleigh Dodds Science Publishing. https://www.taylorfrancis.com/books/9780429266591.

Boote, K. J., Porter, C., Jones, J. W., Thorburn, P. J., Kersebaum, K. C., Hoogenboom, G., … Fleisher, D. (2016). Sentinel site data for crop model improvement—definition and characterization. *Improving Modeling Tools to Assess Climate Change Effects on Crop Response*, *7*, 125–158. https://doi.org/10.2134/advagricsystmodel7.2014.0019

Botterweg, P. (1995). The user's influence on model calibration results: An example of the model SOIL, independently calibrated by two users. *Ecological Modelling*, *81*(1–3), 71–81. https://doi.org/10.1016/0304-3800(94)00161-A

Brisson, N., Gary, C., Justes, E., Roche, R., Mary, B., Ripoche, D., … Sinoquet, H. (2003). An overview of the crop model Stics. *European Journal of Agronomy*, *18*, 309–332. https://doi.org/10.1016/S0223-5234(03)00100-4

Buddhaboon, C., Jintrawet, A., & Hoogenboom, G. (2018). Methodology to estimate rice genetic coefficients for the CSM-CERES-Rice model using GENCALC and GLUE genetic coefficient estimators. *Journal of Agricultural Science*, *156*(4), 482–492. https://doi.org/10.1017/S0021859618000527

Chipanshi, A. C., Ripley, E. A., & Lawford, R. G. (1999). Large-scale simulation of wheat yields in a semi-arid environment using a crop-growth model. *Agricultural Systems*, *59*(1), 57–66. https://doi.org/10.1016/S0308-521X(98)00082-1.

Confalonieri, R., Orlando, F., Paleari, L., Stella, T., Gilardelli, C., Movedi, E., … Acutis, M. (2016). Uncertainty in crop model predictions: What is the role of users? *Environmental Modelling & Software*, *81*, 165–173. https://doi.org/10.1016/j.envsoft.2016.04.009

Duan, Q., Sorooshian, S., & Gupta, V. (1992). Effective and efficient global optimization for conceptual rainfall-runoff models. *Water Resources Research*, *28*(4), 1015–1031. https://doi.org/10.1029/91WR02985

Eckhardt, K., Fohrer, N., & Frede, H. G. (2005). Automatic model calibration. *Hydrological Processes*, *19*(3), 651–658. https://doi.org/10.1002/hyp.5613

Gijsman, A. J., Hoogenboom, G., Parton, W. J., & Kerridge, P. C. (2002). Modifying DSSAT crop models for low-input agricultural systems using a soil organic matter-residue module from CENTURY. *Agronomy Journal*, *94*(3), 462–474. https://doi.org/10.2134/agronj2002.0462

Grenouillet, G., Buisson, L., Casajus, N., & Lek, S. (2011). Ensemble modelling of species distribution: The effects of geographical and environmental ranges. *Ecography (Cop.)*, *34*(1), 9–17. https://doi.org/10.1111/j.1600-0587.2010.06152.x

Grimm, S. S., Jones, J. W., Boote, K. J., & Hesketh, J. D. (1993). Parameter estimation for predicting flowering date of soybean cultivars. *Crop Science*, *33*(1), 137. https://doi.org/10.2135/cropsci1993.0011183X003300010025x

Hocking, P. J., Randall, P. J., & DeMarco, D. (1997). The response of dryland canola to nitrogen fertilizer: Partitioning and mobilization of dry matter and nitrogen, and nitrogen effects on yield components. *Field Crops Research*, *54*(2–3), 201–220. https://doi.org/10.1016/S0378-4290(97)00049-X

Hunt, L. A., & Pararajasingham, S. (1995). CROPSIM - WHEAT: A model describing the growth and development of wheat. *Canadian Journal of Plant Science*, 619–632. https://doi.org/10.4141/cjps95-107

Hunt, L. A., Pararajasingham, S., Jones, J. W., Hoogenboom, G., Imamura, D. T., & Ogoshi, R. M. (1993). GENCALC: Software to facilitate the use of crop models for analyzing field experiments. *Agronomy Journal*, *85*(5), 1090–1094. https://doi.org/10.2134/agronj1993.00021962008500050025x

Hunt, L. A., Reynolds, M. P., Sayre, K. D., Rajaram, S., White, J. W., & Yan, W. (2003). Crop modeling and the identification of stable coefficients that may reflect significant groups of genes. *Agronomy Journal*, *95*(1), 20–31. https://doi.org/10.2134/agronj2003.2000

Jamieson, P. D., Semenov, M. A., Brooking, I. R., & Francis, G. S. (1998). Sirius: a mechanistic model of wheat response to environmental variation. *European Journal of Agronomy*, *8*, 161–179. https://doi.org/10.1016/S1161-0301(98)00020-3

Jing, Q., Qian, B., Shang, J., Huffman, T., Liu, J., Pattey, E., … Wang, J. (2017). Assessing the options to improve regional wheat yield in eastern Canada using the csm–ceres–wheat model. *Agronomy Journal*, *109*(2), 510–523. https://doi.org/10.2134/agronj2016.06.0364

Jones, J. W., He, J., Boote, K. J., Wilkens, P., Porter, C. H., Hu, Z., … Ma, L. (2011). Estimating DSSAT Cropping System Cultivar-Specific Parameters Using Bayesian Techniques. *Advances in Agricultural Systems Modeling*, *2*, 365–393. https://doi.org/10.2134/advagricsystmodel2.c13

Jones, J. W., Hoogenboom, G., Porter, C. H., Boote, K. J., Batchelor, W. D., Hunt, L. A., … Ritchie, J. T. (2003). The DSSAT cropping system model. *European Journal of Agronomy*, *18*, 235–265. https://doi.org/10.1016/S1161-0301(02)00107-7

Jones, C. A., & Kiriny, R. (1986). *CERES-Maize: A Simulation Model of Maize Growth and Development*. College Station, TX: Texas A & M University Press.

Kassie, B. T., Asseng, S., Porter, C. H., & Royce, F. S. (2016). Performance of DSSAT-Nwheat across a wide range of current and future growing conditions. *European Journal of Agronomy*, *81*, 27–36. https://doi.org/10.1016/j.eja.2016.08.012

Keating, B. A., Carberry, P. S., Hammer, G. L., Probert, M. E., Robertson, M. J., Holzworth, D., … Smith, C. J. (2003). An overview of the crop model APSIM. *European Journal of Agronomy*, *18*, 309–332. https://doi.org/10.1016/S1161-0301(02)00108-9

Keating, B. A., McCown, R. L., & Cresswell, H. P. (1995). Paddock-scale models and catchment-scale problems: The role for APSIM in the Liverpool Plains. In *Proceedings of the International Congress on Modelling and Simulation* (Vol. 1, pp. 158–165). Canberra, Australia: Modelling and Simulation Society of Australia.

Kersebaum, K. C., Boote, K. J., Jorgenson, J. S., Nendel, C., Bindi, M., Frühauf, C., … Wegehenkel, M. (2015). Analysis and classification of data sets for calibration and validation of agro-ecosystem models. *Environmental Modelling & Software*, *72*, 402–417. https://doi.org/10.1016/j.envsoft.2015.05.009

Knutti, R. (2010). The end of model democracy? *Climatic Change*, *102*(3), 395–404. https://doi.org/10.1007/s10584-010-9800-2

Liu, B., Asseng, S., Liu, L., Tang, L., Cao, W., & Zhu, Y. (2016). Testing the responses of four wheat crop models to heat stress at anthesis and grain filling. *Global Change Biology*, *22*(5), 1890–1903. https://doi.org/10.1111/gcb.13212

Lizaso, J. I., Boote, K. J., Jones, J. W., Porter, C. H., Echarte, L., Westgate, M. E., & Sonohat, G. (2011). CSM-IXIM: A new maize simulation model for DSSAT version 4.5. *Agronomy Journal*, *103*(3), 766–779. https://doi.org/10.2134/agronj2010.0423

Lobell, D. B., Sibley, A., & Ivan Ortiz-Monasterio, J. (2012). Extreme heat effects on wheat senescence in India. *Nature Climate Change*, *2*(3), 186–189. https://doi.org/10.1038/nclimate1356

Maiorano, A., Martre, P., Asseng, S., Ewert, F., Müller, C., Rötter, R. P., … Zhu, Y. (2017). Crop model improvement reduces the uncertainty of the response to temperature of multi-model ensembles. *Field Crops Research*, *202*, 5–20. https://doi.org/10.1016/j.fcr.2016.05.001

Martre, P., Wallach, D., Asseng, S., Ewert, F., Jones, J. W., Rötter, R. P., … Wolf, J. (2015). Multimodel ensembles of wheat growth: Many models are better than one. *Global Change Biology*, *21*(2), 911–925. https://doi.org/10.1111/gcb.12768

Mavromatis, T., Boote, K. J., Jones, J. W., Irmak, A., Shinde, D., & Hoogenboom, G. (2001). Developing genetic coefficients for crop simulation models with data from crop performance trials. *Crop Science*, *41*(1), 40–51. https://doi.org/10.2135/cropsci2001.41140x

McMaster, G. S., White, J. W., Hunt, L. A., Jamieson, P. D., Dhillon, S. S., & Ortiz-Monasterio, J. I. (2008). Simulating the influence of vernalization, photoperiod and optimum temperature on wheat developmental rates. *Annals of Botany*, *102*(4), 561–569. https://doi.org/10.1093/aob/mcn115

Meinke, H., Hammer, G. L., van Keulen, H., Rabbinge, R., & Keating, B. A. (1997). Improving wheat simulation capabilities in Australia from a cropping systems perspective: Water and nitrogen effects on spring wheat in a semi-arid environment. *Developments in Crop Science*, *25*(C), 99–112. https://doi.org/10.1016/S0378-519X(97)80012-8

Palosuo, T., Kersebaum, K. C., Angulo, C., Hlavinka, P., Moriondo, M., Olesen, J. E., … Rötter, R. (2011). Simulation of winter wheat yield and its variability in different climates of Europe: A comparison of eight crop growth models. *European Journal of Agronomy*, *35*(3), 103–114. https://doi.org/10.1016/j.eja.2011.05.001

Pan, J., Zhu, Y., Jiang, D., Dai, T., Li, Y., & Cao, W. (2006). Modeling plant nitrogen uptake and grain nitrogen accumulation in wheat. *Field Crops Research*, *97*(2–3), 322–336. https://doi.org/10.1016/j.fcr.2005.11.006

Priestley, C. H. B., & Taylor, R. J. (1972). On the assessment of surface heat flux and evaporation using large-scale parameters. *Monthly Weather Review*, *100*(2), 81–92. https://doi.org/10.1175/1520-0493(1972)100⟨0081:oTaosh⟩2.3.co;2

Ritchie, J. T. (1991). Wheat phasic development. In Hanks, J., & Ritchie, J. T. (Eds.), *Modeling plant and soil systems* (pp. 31–54). Madison, WI: ASA-CSSA-SSSA.

Ritchie, J. T., & Otter, S. (1985). Description and performance of CERES-Wheat: A user-oriented wheat yield model. *USDA-ARS*, *38*(July), 159–175.

Ritchie, J. T. T., Singh, U., Godwin, D. C. C., & Bowen, W. T. T. (1998). Cereal growth, development and yield. *Understanding Options for Agricultural Production*, *7*, 79–98. https://doi.org/10.1007/978-94-017-3624-4

Röll, G., Batchelor, W., Castro, A., Simón, M., & Graeff-Hönninger, S. (2019). Development and evaluation of a leaf disease damage extension in Cropsim–CERES Wheat. *Agronomy*, *9*(3), 120. https://doi.org/10.3390/agronomy9030120

Rötter, R. P., Palosuo, T., Kersebaum, K. C., Angulo, C., Bindi, M., Ewert, F., … Trnka, M. (2012). Simulation of spring barley yield in different climatic zones of Northern and Central Europe: A comparison of nine crop models. *Field Crops Research*, *133*, 23–36. https://doi.org/10.1016/j.fcr.2012.03.016

Sardinia, S., Dettori, M., Cesaraccio, C., Motroni, A., Spano, D., & Duce, P. (2011). Field crops research using CERES–Wheat to simulate durum wheat production and phenology in. *Field Crops Research*, *120*(1), 179–188. https://doi.org/10.1016/j.fcr.2010.09.008

Savin, R., Satorre, E. H., Hall, A. J., & Slafer, G. A. (1995). Assessing strategies for wheat cropping in the monsoonal climate of the Pampas using the CERES-Wheat simulation model. *Field Crops Research*, *42*(2–3), 81–91. https://doi.org/10.1016/0378-4290(95)00029-P

Schjoerring, J. K., Bock, J. G. H., Gammelvind, L., Jensen, C. R., & Mogensen, V. O. (1995). Nitrogen incorporation and remobilization in different shoot components of field-grown winter oilseed rape (*Brassica napus* L.) as affected by rate of nitrogen application and irrigation. *Plant and Soil*, *177*(2), 255–264. https://doi.org/10.1007/BF00010132

Semenov, M. A. (2007). Development of high-resolution UKCIP02-based climate change scenarios in the UK. *Agricultural and Forest Meteorology*, *144*(1–2), 127–138. https://doi.org/10.1016/j.agrformet.2007.02.003

Singh, A. K., Tripathy, R., & Chopra, U. K. (2008). Evaluation of CERES-Wheat and CropSyst models for water-nitrogen interactions in wheat crop. *Agricultural Water Management*, *95*(7), 776–786. https://doi.org/10.1016/j.agwat.2008.02.006

Stapper, A. (1984). *SIMTAG: A simulation model of wheat genotypes. Model documentation*. Aleppo, Syria: International Center for Agricultural Research in the Dry Areas.

Stöckle, C. O., Donatelli, M., & Nelson, R. (2003). CropSyst, a cropping systems simulation model. *European Journal of Agronomy*, *18*, 289–307. https://doi.org/10.1016/S1161-0301(02)00109-0

Tebaldi, C., & Knutti, R. (2007). The use of the multi-model ensemble in probabilistic climate projections. *Philosophical Transactions of the Royal Society A: Mathematical, Physical and Engineering Sciences*, *365*(1857), 2053–2075. https://doi.org/10.1098/rsta.2007.2076

Thorp, K. R., Hunsaker, D. J., French, A. N., White, J. W., & Clarke, T. R. (2010). Evaluation of the CSM–CROPSIM–CERES–Wheat Model as a Tool for Crop Water Management. *Transactions of the ASABE*, *53*(2006), 1–17. https://doi.org/10.13031/2013.29505

Tubiello, F. N., Rosenzweig, C., Kimball, B. A., Pinter, P. J., Wall, G. W., Hunsaker, D. J., … Garcia, R. L. (1999). Testing CERES–Wheat with free-air carbon dioxide Enrichment (FACE) experiment data: CO2 and water interactions. *Agronomy Journal*, *91*(2), 247. https://doi.org/10.2134/agronj1999.00021962009100020012x

Van Oijen, M., & Ewert, F. (1999). The effects of climatic variation in Europe on the yield response of spring wheat cv. Minaret to elevated CO2 and O3: An analysis of open-top chamber experiments by means of two crop growth simulation models. *European Journal of Agronomy*, *10*(3–4), 249–264. https://doi.org/10.1016/S1161-0301(99)00014-3

Willmott, C. J. (1982). Some comments on the evaluation of model performance. *Journal of Applied Physics*, *36*(2), 3009–1313. Retrieved from http://link.aip.org/link/?JAPIAU/36/3014/1

Witcombe, J. R., Hollington, P. A., Howarth, C. J., Reader, S., & Steele, K. A. (2008). Breeding for abiotic stresses for sustainable agriculture. *Philosophical Transactions of the Royal Society B*, *363*, 703–716. https://doi.org/10.1098/rstb.2007.2179

Yan, M., Cao, W., Luo, W., & Jiang, H. (2000). A mechanistic model of phasic and phenological development of wheat. I. Assumption and description of the model. *The Journal of Applied Ecology*, *11*(3), 355–359. Retrieved from http://europepmc.org/abstract/MED/11767631

Yang, J. M., Yang, J. Y., Liu, S., & Hoogenboom, G. (2014). An evaluation of the statistical methods for testing the performance of crop models with observed data. *Agricultural Systems*, *127*, 81–89. https://doi.org/10.1016/j.agsy.2014.01.008

Zadoks, J. C., Chang, T. T., & Konzak, C. F. (1974). A decimal code for the growth stages of cereals. *Weed Research*, *14*(6), 415–421. https://doi.org/10.1111/j.1365-3180.1974.tb01084.x

How to cite this article: Röll G, Memic E, Graeff-Hönninger S. Implementation of an automatic time-series calibration method for the DSSAT wheat models to enhance multi-model approaches. *Agronomy Journal*. 2020;1–22. https://doi.org/10.1002/agj2.20328

6 General discussion

The main goal of this thesis is to develop an N application strategy that can account for different types of in-field variabilities by combining spectral sensors and crop models. The combination should lead to better adaptation of applied N and, thus, reduce the potentially involved environmental side effects. In the last few decades different sensor techniques and crop models were developed to adjust the N application and were tested separately [132, 151].

A combination of both techniques has the potential to reduce simulation and measurement uncertainty and to increase N application accuracy. The main advantage of crop models exists in the simulation of yield in response to various parameters (genetic, environment, management) while different N application scenarios can be simulated [132].

Crop models are mainly used in the scientific community and require a skill set for setting up and calibrating every single step in the model properly [147]. Profound knowledge about the location and management is also necessary.

While crop models simulate plant growth and development based on genetics, environment and management conditions, spectral sensors only rely on the output of reflectance or spectral indices. These sensors lack crop-growth information [152] and thus can result in under- or over-fertilization [153]. Spectral sensors focus mainly on the photoactive biochemical pigments such as carotenoids, xanthophyll, and chlorophyll [154]. Chlorophyll is most important for photosynthesis, and there is a strong relationship between N content in green vegetation because of which it exhibits a sensitive surrogate for plant N deficiency detection [154].

Commercial products for adjusting N applications via spectral sensors were developed and are available to agriculture today [155]. These sensors can be either active or passive and take different wavelength ranges into account to obtain the N content of a plant [156]. Combining both crop modeling and sensor techniques in a decision support system might lead to more reliable N prescriptions over a wide range of environmental conditions [157, 158].

6.1 Validity of Sensor Data for Nitrogen and Determination of Other Plant Stresses

The use of existing spectral indices showed that the differentiation between leaf layers or positions on the leaf could be considered as less important for plant N content estimation via remote sensing technique [159]. Nevertheless, the ground cover, mainly influenced by LAI and biomass, also has substantial effects on spectral reflectance [160–162]. This is especially the case in the early vegetative growth stages, where the soil is more dominant (i.e., LAI < 1.5) [163]. Different soil properties such as moisture, organic N content, and color influence the reflectance characteristics [164].

Therefore, commercial sensors are not normally used in the early period, because an accurate N fertilizer adjustment is hard to perform in early vegetative growth stages [165–167]. Nevertheless, not using sensors in this period results in a significant drawback in N application because the early growth stages are essential for yield determination [168]. A system that can overcome this issue would enable a more appropriate N management, especially on spatial

heterogeneity that can occur within a field. The first attempts at addressing this issue were made by developing spectral indices, such as OSAVI or TOSAVI, that could reduce soil influence [164, 169]. Further attempts were carried out by Eitel et al. [168] where a green scanning laser exhibited superiority in N content determination in early growth stages compared to current spectral sensors. Laser scanners are costly and require a considerable amount of time for spatial mapping [170] which makes it less feasible for agricultural on-farm use. A more promising approach was used by Hamuda et al. [171], where differentiation between soil and plant was made by using an image analyzing technique that classified an image into non-plant and plant pixels. This technique was used for RGB images; but it is also feasible to be applied to hyperspectral images where spectral information from plant pixels can be used, and information for soil pixels are eliminated from the image.

Besides the spectral properties of soils, further soil conditions, for example soil moisture, can also indirectly impact the spectral reflectance of crops [172]. This is the case if plant stress occurs due to water shortage or water excess in the soil. Stress symptoms detected via remote sensing are the result of changing cell compounds and also the plant architecture. This can lead to misinterpretation of the plant N content in an N prescription technique system that relies only on sensor data [115].

Further plant stresses resulting in a distortion of remote sensing signals can occur under plant disease infection [173]. While root diseases may influence the reflectance indirectly due to wilting or change in plant pigment content (chlorophyll, carotenoid, anthocyanin), leaf diseases can be detected via remote sensing directly [174]. Between the onset of leaf disease and the fungus fruit formation, a change in the spectral reflectance was reported [175–177].

The four major destruction steps by a disease pathogen can be classified as

1. Destruction of pigment systems
2. Lesions or fructification structures due to infection
3. Reduction of biomass and decrease of LAI and
4. Plant wilting/ early senescence.

These steps heavily depend on the control by fungicides and on the fungus type [174, 178] and may lead to uncertainties in disease detection [161, 179]. An additional issue in measuring the spectral reflectance is reported by several researchers where a change in specific wavelengths over time occurs during disease development. In other words, specific wavelengths proven to be right for disease detection in early development stages of disease symptoms tend to fail at later development stages [177].

Nevertheless, further challenges face the detection of diseases via remote sensing techniques. For example, disease development normally starts at the bottom of the plant and rises to the top. This can lead to detection difficulties because of the overlapping of leaves and the non-uniform distribution of the lesions or pustules across the plant [180–183].

The detection of plant disease seems to be more complex than the determination of plant N. While having a high spectral resolution for plant N determination, the spatial resolution has to be even higher for disease detection [184] because disease infection often occurs in patches [185].

Several researchers have developed techniques on how the disease can be monitored in different ways ranging from synthetic aperture radar, fluorescence, thermal systems, and visible as well as near-infrared spectral system [174, 186]. The concept of using different sensors and fusing together the information obtained from them to generate a comprehensive picture of the disease infection was introduced by Bauriegel and Herppich [187].

This approach has the potential to perform the following tasks:

1. Detecting disease infection
2. Differentiation of different diseases and
3. Estimation of disease severity

Detection of disease and estimation of disease severity are essential for using the sensor data in crop growth models in order to develop an N prescription. Plants under disease infection reduce the attainable yield on a specific location due to injury and damage sustained by them, which causes biotic stress [188, 189]. This requires adjustment of N application strategies in terms of amount and timing [189]. In addition, several studies showed that an increase in N application also increases disease severity [190, 191] which has to be considered in the N application strategy. While a lack of N supply in a given field is mainly soil-borne, plant diseases are more variable in terms of spore spread and further disease development depending on favorable weather conditions [192]. This makes the development of an N application strategy under disease infection even harder.

Including different disease types in the model-based N prescription makes differentiation is desirable. It can be assumed, however, that if the effects on the plant are similar, no clear differentiation is mandatory. This is the case, for example, if we consider stripe rust (*Puccinia striiformis f. sp. tritici*) and leaf rust (*Puccinia triticina*) in wheat which have a similar effect on the plant [193].

Having different effects on the plant, like leaf rust and septoria tritici (*Zymoseptoria tritici D.),* makes it necessary to introduce differentiation and it must be done separately in the model. The disease subroutine has been developed generically and it considers disease as a reduction of photosynthetic leaf area and destruction of leaf mass [194].

The effect of the fungus on the surrounding leaf tissue, depending on the fungus, can also be accounted for by the model. This is represented in the developed model extension for CERES Wheat as a surrounding leaf tissue factor and similar to the β-value approach reported by Bastiaans [195]. If no effect on the surrounding tissue occurs, the factor is kept at 1. If the effect on the surrounding tissue is present, the factor is > than 1 [194].

In order to integrate disease infection in an N fertilizer application strategy, it is important that the disease or stress symptoms occur during typical N application dates. That means if drought stress occurs at grain filling or disease infection at flowering, for example, due to Fusarium head blight (*Fusarium graminearum*), it has an effect on yield parameters but the N application cannot be changed anymore.

6.2 Integration of Sensor Measured Nitrogen Content and Other Stress Symptoms into Crop Models

The integration of measured N content or other stress symptoms into crop models can be accomplished by modifying an existing model input data file used in in-season crop measurements. Within the DSSAT environment [120], the File-T represents a tailor-made solution to makes sensor data available to the models. The File-T is normally used in storing measured time-series values of different plant parameters like such as LAI, aboveground biomass, or yield to make it available for statistical and graphical model evaluation [120]. Using this file enables the integration of sensor measured time-series plant information. After initializing the File-T, the plant information is available for comparing with simulated measured data. Measured data would then be included to adjust the model state variables. In general, three different ways (Recalibration, Updating, and Forcing) of adjusting the model parameters were reported by Delécolle et al. [196].

Forcing the model to adjust the model simulation according to sensor data (Figure 3) can be performed by replacing the state variable with the observed value. This method requires a fixed time step, which is normally daily or weekly, depending on the model. If the observations are less frequent than the model time step, an interpolation technique has to be used [197].

The recalibration method (Figure 3) is based on the recalibration of the model assuming that the model is insufficiently calibrated or the input files include errors. If a difference between simulated values and the value collected by the sensor occurs, the model undergoes a model rerun to minimize the gap between simulated and measured values. This procedure seems to be very promising for introducing N content values generated from sensors in the model. Plant N mainly depends on the availability of N in the soil (crop-soil dynamics) which is mainly affected by carbon stored in the soil. Estimation of soil carbon and the mineralization can be a challenging task. In order to obtain this missing information, the recalibration of the soil conditions seems to be helpful to meet the values observed by remote sensing techniques.

The model updating technique (Figure 3) involves the updating of model state variables, every time an observation is made [198]. In contrast to the forcing method, the state variable is only updated on the day of observation and not during the whole simulation process. The theory behind this method is that adjustment of state variables at a certain day will also improve the simulation accuracy for following days [134]. Every procedure has its own advantages and disadvantages. It is feasible to use different methods for different stress symptoms.

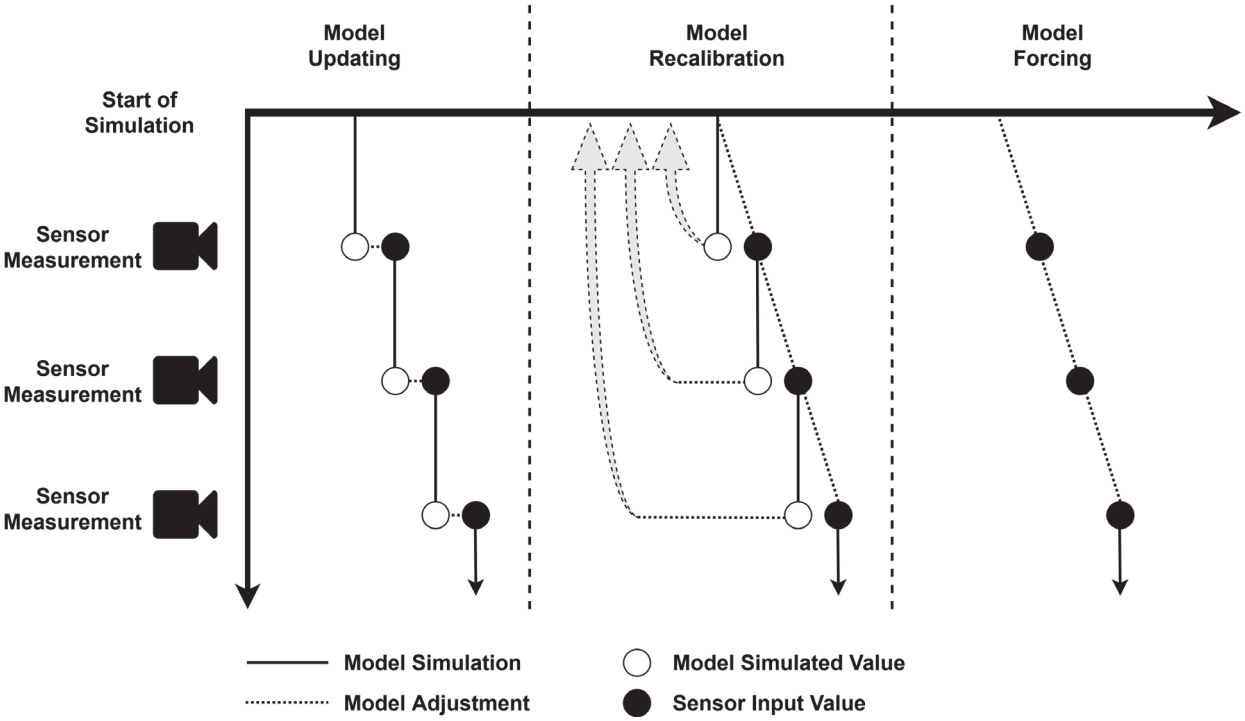

Figure 3: Scheme for different methods of model adjustment by using sensor measurements (based on the concept of Delécolle et al.).

Delécolle et al. [196] did not identify the "best" calibration method, but they assumed it to be also dependent on the crop model. By integrating sensor data into crop models, both techniques are no error-free systems that can lead to misinterpretation [199]. Forcing the model eliminates information on target state variable. The calibration and updating method in contrast still contains model information [134]. Nouvellon et al. [200] suggested representative crop model adjustments by using model recalibration. Nevertheless, the major drawback of model recalibration is the requirement of immense computation time depending on the calibration parameter [134]. By limiting this effect, it is feasible not to restrict the model adjustments to one specific adjustment procedure.

A combination of different model adjustments methods can be applied to specific crop parameters that have been collected by remote sensing techniques. This is the case for example for plant N content and for disease infection where different ways of adjustments can be applied. While plant N content is calculated from the beginning of the simulation and, later on is strongly

dependent on soil conditions, leaf disease infection can occur spontaneously under favorable conditions.

Adjusting the N content in the model due to model recalibration is the most suitable procedure, because plant N content is strongly dependent on soil conditions such as mineralization of organic matter or soil moisture. This can cause several uncertainties in model simulation ranging from incorrect soil organic matter to soil texture or to incorrect setup of initial conditions. A model recalibration is necessary to adjust these uncertainties in order to reach greater modeling efficiency.

In case of model adjustments for leaf diseases, a different approach seems to be more suitable, because disease infection occurs based on the inoculum spread in a field and weather conditions. The disease routine developed for CSM-CERES Wheat uses a combination of forcing and updating procedures [194]. The disease infection detected by a remote sensing application enters the model as a percentage disease infection. According to the type of leaf disease, the incubation time is used to set up the onset of disease in the interpolation subroutine by updating the disease infection in order to calculate the daily percentage of disease damage. The absolute disease damage is then calculated based on the simulated leaf area, forcing the leaf area to reduce by the calculated disease damage. The results show the ability of the model to account for the leaf disease *Septoria tritici* in wheat and keep the model information.

Suppressing model information seems feasible for conditions such as drought stress. Normally, drought stress is based on the water holding capacity of the soil which is closely related to soil texture and organic content. This part should be covered by the recalibration of the initial conditions and the adjustment of soil parameters in the model N content. If the model is unable to detect the drought stress, another adjustment pathway can be constructed within the DSSAT models.

Daily photosynthesis, growth of new tissues and leaf area expansion can be modified by a water stress index ranging between 0 and 1, where 0 represents no drought stress and 1 high drought stress [124,201]. By forcing this factor, drought stress can be applied to the model. This method seems reasonable only if the drought stress is clearly identified. As mentioned above, the detection of several stress symptoms at once is not a simple task. They overlap (correlate) and lead to misinterpretation.

In order to address this issue, a crosscheck routine can be applied between the model and the sensor system. If the sensor system delivers the information, it can be crosschecked with values delivered from the model simulation. If the difference between the sensor and the model is above a certain threshold, the sensor value can be rejected and excluded from the model adjustment. This is also possible if a model simulation output is set in a certain range. The model can then be directly adjusted.

6.3 Multi-Model (MM) Integration Approach

A Multi-Model (MM) approach can be accomplished by using more than one model to increase modeling accuracy over a broad range of environmental conditions [202]. When using various models, variation in the simulation output due to differences in the key processes of the model (e.g. leaf area and development, light utilization, crop phenology or soil moisture dynamics) can occur [145, 203]. In an MM approach, modeling errors from one model can be compensated by another model. When combining remote sensing data and MM as a decision support system for N application, the complexity of the system greatly increases. Especially the initial calibration and later the model adjustment procedure require an immense effort. The automatic calibration procedure that has been developed, seems able to overcome this obstacle [204]. The calibrator can be used for accurate initial calibration of all genetic variables of the models based on historical datasets. Furthermore, the recalibration of soil conditions based on sensor measurements can be performed by the same calibration approach. Instead of calibrating genetic variables, the calibration procedure optimizes soil conditions.

Assembling an MM approach in a N application system seems to be a promising step in the simulation of adverse weather conditions [205]. Due to climate changes, there are reports about various weather extremes ranging from changes in rainfall patterns to high temperatures in critical developmental stages [206, 207]. As a result, the yield variability will increase, especially on a spatial scale [208], which requires a better adjustment of the N fertilization [209]. Rötter et al. [203] reported a lack of crop models in describing climate change effects adequately. In an MM approach, this obstacle can be overcome resulting in higher modeling accuracy which will finally increase N prescription accuracy.

The use of MM approach for N application needs further testing and development. Uncertainties exist on how many crop models have to be used in an MM assemble. Numbers for scientific purposes range between three [210] and thirty-two [211] different crop models. While the use of thirty-two crop models seems to be an impossible endeavor in terms of setting up the necessary calibration files to derive N application prescriptions, the use of three models within the same simulation environment seems more promising.

Currently, no disease information can be used in the other wheat models included in the DSSAT environment, because the developed disease subroutine works only for the CERES-Wheat model. The disease subroutine has also to be migrated to NWheat and CropSim Wheat in order to insure a full functionality of a MM N application system.

Once that is accomplished, further extension to other crops such as maize (CERES and IXIM) rye and barley is also feasible under the same concept described in Röll et al. [204]. Various researchers have already adjusted the wheat model for barley and rye [203,212], thus facilitating its straightforward incorporation into the decision support system for N application.

6.4 Nitrogen Application Prescription System (NAPS)

In this thesis, a holistic concept has been developed that combines MM and remote sensing techniques to adjust the amount of N applied and reduce the environmental side effects. Basic requirements (Figure 4) are the genetic coefficients for MM calibration based on a long-term dataset. The developed calibration procedure [204] is suitable for the task.

As soon as the genetic coefficients are determined, the initial MM setup for a given field location can be performed. Essential information about the management (sowing date, sowing density, etc.), the predominant soil information, and the weather information for each given day have to be provided.

The core of the NAPS consists of five main steps that are repeatedly performed at each N application date (Figure 4):

A. Assessment of the current plant status via remote sensing
B. Incorporation of sensor data by model adjustment
C. Using weather forecast and running weather generator
D. Running different N application scenarios and
E. Evaluation based on economical and ecological criteria to derive the prescription of N application in accordance with environmental conditions

The assessment of the current plant status can be accomplished via tractor-mounted, drone-mounted, or satellite imaging techniques. If the technique is not able to differentiate between plant stress types, for example if N content is influenced by drought stress, the model can be used to validate the sensor values. When the model is detecting drought stress, the sensor values can be rejected and the NAPS can be run without them.

If the sensor values are valid, the model can be adjusted through recalibration, forcing or updating. After that process, the weather file has to be extended by the following ten days of the weather forecast and further weather data has to be generated until the expected harvest date. Different programs such as WGEN [213] and SIMMETEO [214] were developed within the DSSAT environment to produce weather scenarios based on a stochastic approach. A minimum recorded dataset of thirty years is required to reduce weather generation uncertainties [215]. A primary concern for using weather generators is inadequate representation of the statistical properties of the observed weather series [216]. This can lead to simulation accuracy between 28% and 60% [217] which shows difficulty with weather generation for several weeks or even months.

Nevertheless, if N application is split into different application timings as it is followed in the case of cereals (wheat, rye, barley), the closer the N application timing gets to the harvest date, the more is the real measured weather data available. Hence, if for example drought stress occurred several days after the first N application, which was not predicted, the N application would not be accurate because the model did not expect drought stress. During the calculation for second application, the drought stress is available to the model based on the measured weather and the second application can be further adjusted by considering the N application of the first date.

While running the model for different N application scenarios, the NAPS requires information about the number of N applications and the approximate timing of these applications. This information can be either fixed to growth stages or estimated by N application dates from

historical records. The amount of N can be varied between different application timings. Two different scenarios are feasible: First, the amount of N will be fixed based on the yield potential. The model can now simulate the maximum yield based on the fixed applied N. The second strategy is to use the model to evaluate the leaching potential based on different N application rates. This strategy can also be coupled with an upper limit on maximum applied N to fulfill the environmental standards, which seems to be the preferred strategy to meet the requirement of the nitrogen directive.

Further selection criteria can be included such as the price of the crop, the cost of N, and the governmental compensation payment for N reduction in fragile groundwater protection zones. The goal is the selection of N application strategies that reconcile cost-efficient crop production with the reduction of the environmental impact of crop production. The basic concept of choosing the best combination between the cost of N, price of the harvested crop, and compensation payment has already been successfully tested by Link et al. [218] for model-based N application prescriptions on a site-specific scale.

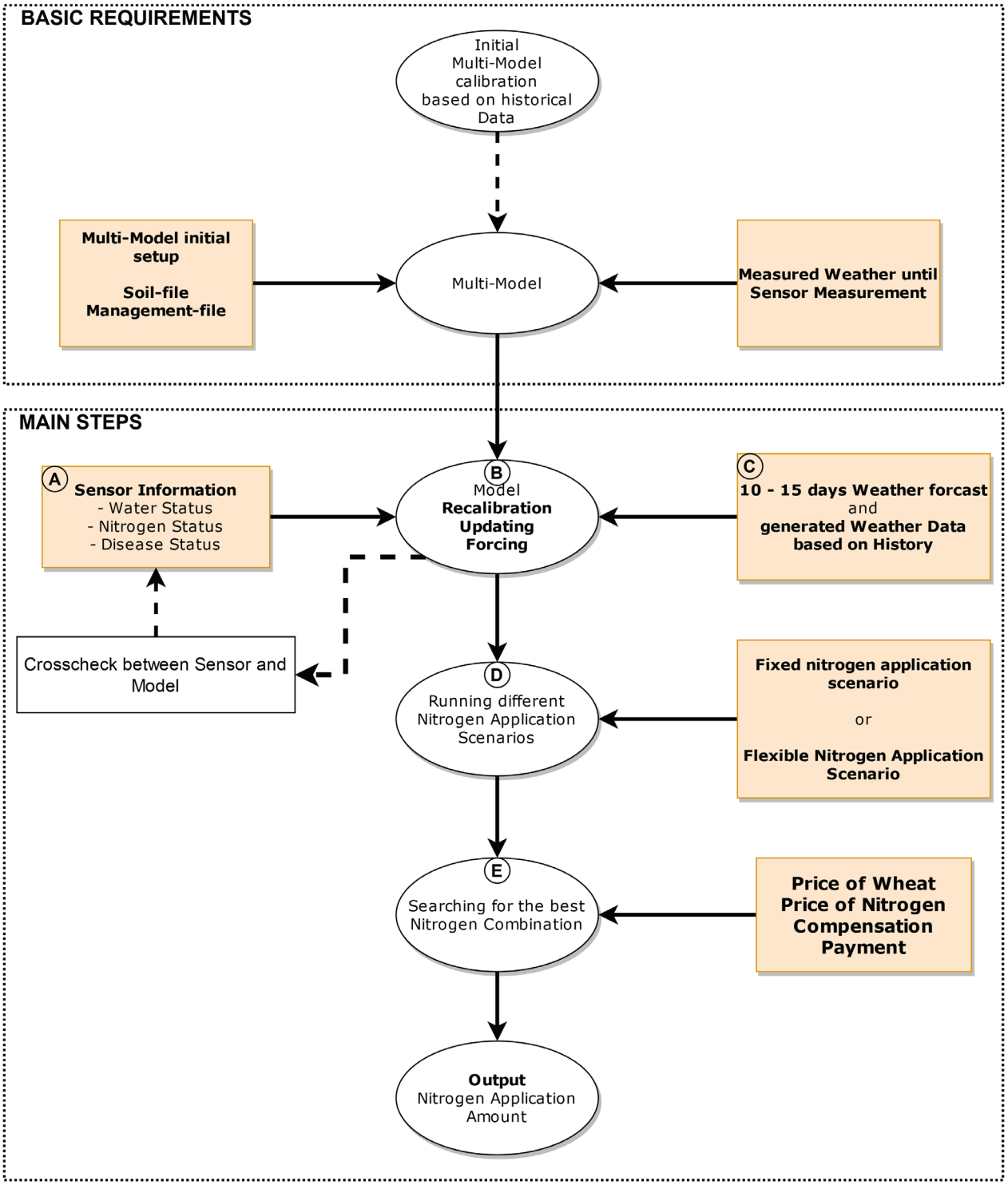

Figure 4: Flowchart for the Nitrogen Application Prescription System (NAPS) combining multi-modelling and remote sensing.

6.4.1 Applying NAPS Concept on a Spatial Scale

In order to account for different soil conditions in a given field, the NAPS concept has to be applied on a spatial scale. After several decades of development, sensor systems are available for PF to apply the right amount of inputs based on spatial variability types within a field [83]. Recent studies showed that PF did not always improve the profitability of site-specific management compared to a conventional system for wheat [219]. The profitability of existing sensor-based N application systems ranges between -30$ ha^{-1} and 70$ ha^{-1} depending on crop, sensor, and location [220]. Diverse site-specific N fertilization studies also show low profitability, due to high investment costs which result in low economic return [221, 222]. The profitability is also highly influenced by the variability of the crop response to fertilizer application on a spatial scale [223, 224]. A weakness of the existing sensors is that they estimate the N demand based on sensor readings [225] and exclude or neglect N supply from soil very often [220].

Also, further site-specific approaches based on combined yield monitoring can not represent a proper picture for N application. Gandorfer and Meyer-Aurich [222] reported differences in site-specific production functions that had different slopes and show different yield responses to the fertilizer input.

The NAPS concept has the ability to overcome this issue by accounting for soil N supply based on the calculation of future mineralization in the soil module that accounts for future weather scenarios. In addition, the NAPS concept can be applied for site-specific N application by using the APOLLO concept for simulation of spatial yield variability within a field [132]. The key part of APOLLO consists of DSSAT crop models, where crop growth and development is simulated on a site-specific scale. Due to the spatial field variability influenced by interactions between different factors, including soil physical properties, rooting depth, water stress, or nutrients, the APOLLO software adjusts the soil parameters within the input file to account for soil-borne variability based on crop yield.

The implementation of the APOLLO soil parameter adjustment theory in the NAPS concept for MM site-specific soil calibration exhibits a solution for proper initial soil parameter adjustment on a spatial scale. The calibration is performed on a rectangular grid which represents the typical management size (site-specific spraying, fertilizer application) [132, 226]. Within those grid cells, homogeneous soil and weather conditions are assumed. After soil calibration, the NAPS concept can be applied on a grid-based scale by using grid-based sensor data for site-specific N prescriptions.

The NAPS system applied on the spatial scale makes the use of historic yield monitoring data, that are rarely used by farmers [68, 91] but functional for site-specific model calibration. Furthermore, the integration of site-specific sensor data into the model can quantify biotic and abiotic factors in a given field and can control the N fertilizer adjustment. This is a strong advantage of this concept, because several researchers have reported that more than 50% of the yield difference in a given field is caused by biotic and abiotic factors that are usually not quantified [96, 97].

6.4.2 Possible Challenges and Uncertainties in the NAPS

Besides varying N application on the spatial scale, the variation of timing has also to be considered. While common N recommendations for cereals promote a split N application, normally in three to four quantities [227, 228], some researchers also recommend only one application [229]. Splitting N applications is normally performed to avoid lodging, to prevent N losses [230, 231] and to insure high crude protein contents, especially for baking wheat [211, 232].

Müller et al. [233] reported that the total amount of N applied was more important for yield and grain quality than split N applications. By applying only one N application on a site-specific scale, the NAPS concept can also be used to determine the total N amount. A single N application in the spring prevents the possibility of further seasonal N adjustments, as the weather conditions for the next three to four months until harvest are unknown. Furthermore, applying all N at once might increase the risk of NO_3^- loss, especially on sandy and shallow silty soils [234]. On these soil types the NAPS concept seems suitable for adjusting the N timing in order to reduce N losses. While using the NAPS concept in split N applications, the sensors data can deliver information about stress conditions during the vegetation period and the weather uncertainty can be limited to only one month, which might help to lower the overall N loss and diminish the environmental side effects.

Researchers using different sensors for plant stress parameters (plant N determination, disease detection, etc.), must bear in mind the sensors should ideally work on the same grid-based resolution. This is the case if satellite data are used to at least the same grid resolution of the NAPS. It has to be pointed out that the data assimilation via sensors and models can lead to different assumptions and misleading N application strategies. Dorigo et al. [134] also described the challenge: Should the assumptions rely on the sensor or the model? A crosscheck can mitigate this effect between model and sensor data by setting up ranges for plausibility (Figure 4).

Computing the data for an online setup can be a bottleneck for the NAPS. The collection and processing of plant data via remote sensors take some time depending on the hardware as well as software, and therefore, it limits the forward speed for fertilizer application. Currently, forward speed for N application up to 3.3 m s^{-1} is common [235]. Noh et al. [236] used a multi-spectral sensor for variable N application for corn and reported an online approach that was able to operate at 0.5 m s^{-1}. This speed limitation makes an online setup for a farmer tough [237, 238].

A solution for this issue can be an offline system, where sensor data is collected and processed in the NAPS independent of the N application. The drawback of offline solutions is that they have to be performed separately, which results in an additional run on the field using a tractor-mounted sensor. This will increase the operation cost of the NAPS. In addition, calibrating the NAPS based on long-year management, weather and yield data can be a huge challenge for an ordinary farmer. A promising solution seems to be to outsource the NAPS calibration, the sensor data integration, and N prescription to provide application maps for the farmer. N application maps can only be valid if sensor measurement dates are close to the application date. This is very challenging especially if weather conditions are changing fast and the farmer is unable to apply the prescribed N in time due to wet field conditions. Furthermore, a weather generator may fail in certain years while predicting future weather scenarios. Especially, the use of historical data, dating as far back

as thirty years, for instance, is questionable for future weather scenarios, because climate change effects can increase simulation and N prescription uncertainties.

Besides, a ready-to-use-product for farmers will not be accepted by the customers if the system fails in the first one or two years due to uncertainties. Higher prescription uncertainties can also occur in areas, where poor weather records are available and no long time yield record exists.

Finally, the NAPS concept must be tested under practical farming conditions on heterogeneous soils to evaluate its potential for increasing N use efficiency and lowering the environmental side effects.

6.5 Outlook and Further Development

The presented NAPS concept has to be tested for different soil types, crops, and diseases. Different soil types affect plant growth and development as they have different soil textures, cation exchange capacities and organic biomass. These factors can vary spatially within a given field. The APOLLO approach uses site specific soil texture and adjusts different growth limitation factors such as drainage, hydraulic conductivity or root distribution. Normally, this soil texture data are collected through expensive soil texture surveys. The use of further sensor technologies like soil electrical conductivity measurements (EC_a) [239, 240] seems to be a useful technique for spatial soil data collection. Heil and Schmidhalter [241] described a method to characterize soil texture (sand, silt, clay) via EC_a measurement on a site-specific scale. Zanella et al. [153] generated soil texture information via electrical EC_a measurement in combination with soil reference samples in a regression kriging analysis. Deriving soil information from EC_a values, exhibits an inexpensive and rapid method for soil texture and has the potential to reduce site-specific soil uncertainties. Finally, it will increase the N prescription accuracy of the NAPS.

The current NAPS concept was developed for wheat. Nevertheless the DSSAT environment incorporates 42 crop growth models [126] while sharing common routines written in Fortran [242]. This makes the use of a disease routine and the developed model calibrator available for a broad range of crops. The maize models for example originate from the CERES model and are closely related to the wheat model, which also makes an MM arrangement suitable.

The developed disease routine could be a further coupling point for the integration of disease infection models on the NAPS concept. It seems feasible to couple a disease progress model such as Septo3D [243], that simulates the extent of damage in future based on the generation of future weather for the disease routine [194]. Coupling disease progress models also provides farmers with opportunities for fungicide spraying recommendations especially if future weather scenarios produced by the NAPS weather generator are used.

For providing final N prescription maps additional trials have to be set up for validation of the N leaching routine. Especially the model`s sensitivity on heterogeneous soils within a field has to be tested. It is an essential cornerstone within the NAPS concept to make sure the leaching routine works properly over a broad range of environments. It ensures an environmentally friendly N application. He et al. [244] successfully tested the DSSAT model for potential N leaching in spring wheat and maize on two different locations in Canada.

Finally, the NAPS concept shows a geat potential for managing different kind of in-field variability by combining sensor data and crop models to obtain an environmentally friendly and cost-efficient N prescription strategy that is geared toward a sustainable agricultural production.

7 Summary

Today, agricultural production accounts up to 35% of global greenhouse gas emissions, threatens land degradation and freshwater due to excessive land use and over-fertilization. Especially the US, China, Northern India, and Western Europe have to deal with excessive nutrient applications. Mainly, the excessive use of nitrogen (N) fertilizer increased the release of greenhouse gases such as CO_2 during production and N_2O released from soils after application. It also causes eutrophication in surface and groundwater due to runoff and leaching. These problems were realized by national governments and Bills for protecting the environment were introduced by China and the USA.

The European Union is also facing problems of escaping N in the environment. In the last thirty years, various directives were issued in order to mitigate these side effects, but none of them improved the environmental conditions significantly. Germany, which had to face the issue of nitrate pollution of groundwater, passed recently new regulations for further nitrogen reduction in nitrogen application to avoid an accusation of the European Court of Justice of violating the Nitrates Directive, which could have ended up in a €850,000 fine per day. Agriculture is at a crossroads and new strategies for environmentally friendly crop production have to be developed in order to enhance crop production without harming the environment.

A solution for more cost-effective and less environment affecting crop production could be Precision Farming (PF). PF is the management of different farm inputs by applying the right management practice at the right time and at the right location. One key point is to adjust N application to temporal and spatial variations that occur in a field.

Different sensor technologies were developed to account for field variabilities. The applications range from soil conductivity measurements, to cameras, and to spectral sensors. In order to adjust the N fertilization application, spectral sensors are mainly used. In general, spectral sensors are non-contact sensors and are based on electromagnetic reflectance between 300 and 2500 nm. The reflectance of vegetation is mainly determined by a low reflectance in the visible spectrum (400 – 700 nm) and a high reflectance in the near-infrared (700 – 1000 nm) region. This characteristic allows the detection of the N status of plants. While chlorophyll content shows a strong correlation with N availability, it can also be affected by disease infection, drought stress, or other nutrient deficiencies. These circumstances can lead to errors in N prescriptions.

Whereas sensor technologies are helpful to measure actual N content in a plant, crop models may help to predict the N demand. Process-based plant growth models were developed in the last thirty years to analyze yield gaps and for decision support. They simulate growth and development of plants based on weather and management conditions. The major drawback of these models is their intensive calibration procedure and the different complexities of the model structure which even experienced users struggle with. Even more challenging for users is the combination of different model structures in an MM approach where simulation accuracy can be further increased.

Nevertheless, an MM approach cannot overcome the obstacle of a lack of information on existing heterogeneity (abiotic and biotic stresses) within a field. Ignoring these factors can lead to inaccurate decision making, which is not appropriate for on-farm usage. Some researchers realized this issue and suggested an approach of using remote sensing techniques for periodically updating specific model state-variables to account for variabilities in the field. This might help increase the overall modeling accuracy.

Coupling of spectral sensors and crop modeling techniques requires reliable and accurate data acquisition for plant N content in terms of using it as a "nitrogen prescription system." There is a gap of knowledge on plant N determination via remote sensing techniques, especially if the differentiation between leaf and positions on different leaves is necessary. Only if these measured values are valid, does an adjustment of the crop model seems to be useful.

Furthermore, model adjustments are required due to leaf disease infection in order to simulate the yield accurately. In general, leaf diseases lower the potential yield by modifying the photosynthetic leaf area or by "stealing" the assimilates. Lowering the yield potential goes hand in hand with an adjustment of the N application rates. The current DSSAT Wheat crop models are unable to account for any disease infection. This limits the applicability of "nitrogen prescription" only to scenarios without disease infections

The crucial question in this thesis was: How can remote sensing data and crop models be used to derive an N fertilizer strategy that is capable of lowering the environmental side effects of N fertilizer application? Within this context, specific objectives were raised:

(i) To test the influence of different leaves and positions on the leaf on the reflectance of wheat plants cultivated under different N levels and under drought stress;
(ii) to incorporate leaf disease damage into a DSSAT Wheat model to enable the simulation of the impact of leaf disease on yield;
(iii) to evaluate an automatic calibration procedure in a multi-model approach for winter wheat to increase modeling accuracy and eliminate the subjectivity factor in model calibration; and
(iv) to use a multi-model approach to improve the overall modeling accuracy.

To address the first objective (i), two hydroponic greenhouse trials were carried out (Publication I). In the first experiment, the N fertilizer amount and growth stage for the determination of N content was varied, while the second experiment focused on a secondary induction of N deficiency due to drought stress. For each plant, reflectance measurements were taken from three leaves (L1, L2, L3) and at three positions on the leaf (P1, P2, P3). In addition, the N content (%) of the whole plant was determined by chemical lab analysis. It varied between 0.75% and 4.88%. Reflectance spectrometer measurements (400–1650 nm) were used to calculate 16 vegetation indices for each combination of leaf and position. N content (%) was predicted by using each vegetation index for each leaf and each position. A Significantly lower mean residual error variance (MREV) was found for leaves L1 and L3 and for measurement position on P3 in the N trial, but the difference in MREV between the leaves was very low and therefore considered as irrelevant. The drought stress trial also led to no significant differences in MREV between leaves

and positions. Neither the position on the leaf nor the leaf number had an impact on the accuracy of plant N determination via spectral reflectance measurements, whereas measurements taken at the canopy level seemed to be a valid approach.

Other stress symptoms such as drought or disease infection seem necessary to differentiate between different leaves. Leaf disease starts typically at the bottom of the plant and rises to the top. There are also reports that the spectral reflectance changes over-time during the disease development, which makes it hard to detect unless differentiation between different leaves occurs.

To integrate sensor information in crop growth models, models state variables have to be updated. The second publication aims to incorporate leaf disease ratings in the DSSAT Wheat model to account for leaf diseases. A model extension was developed by adding a disease damage module to the existing wheat model. The module simulated the impact of daily damage on photosynthesis and leaf area index (LAI). The approach was tested on a two-year dataset from Argentina with different wheat cultivars and different inoculum levels of septoria tritici blotch (STB). The accuracy of the simulated yield and LAI was improved. The root mean squared error (RMSE) values for yield (1144 kg ha^{-1}) and LAI (1.19 m^2 m^{-2}) were reduced by half (499 kg ha^{-1}) for yield and LAI (0.69 m^2 m^{-2}). In addition, a sensitivity analysis of different disease progress curves on LAI and yield was performed by using a dataset from Germany. The sensitivity analysis demonstrated the ability of the model to reduce yield accurately in an exponential relationship with increasing infection levels (0–70%). The extended model is suitable for site-specific simulations, coupled with for example, available remote sensing data on STB infection.

In addition, modeling accuracy might be further improved by using an MM approach, which has the ability to enhance the modeling accuracy significantly, especially under extreme weather conditions. The DSSAT 4.7 environment includes three wheat models that are sharing the same input structure and are tailor-made for an MM approach. Assembling more models increases the complexity of the simulation and the involved calibration procedure especially if the user is unfamiliar with the models.

In order to avoid these possibilities, an automated calibration program was evaluated in Publication III. The publication aimed at the optimization of cultivar coefficients based on RMSE of time series data while using an automated calibrator tool. Furthermore, the potential of MM approaches for decision support in the future should be highlighted. Model calibration was performed on a four year wheat N fertilizer trial (0 – 240 kg ha^{-1} N) in southwest Germany. The evaluation mean showed satisfying results for the calibration (d-Index 0.93) and evaluation dataset (d-Index 0.81). In the fourth objective (iv), different years were compared in the MM approach which led to an improved modeling accuracy in most cases. Especially, in the drought season 2018, the MM approach revealed higher modeling accuracy for yield (d-Index 0.61) in contrast to a single simulation of CERES (d-Index 0.34) and Cropsim (d-Index 0.39). This demonstrated the advantage of an MM approach as different modeling structures could compensate for errors that might occur in single modeling approaches.

Based on the combination of an MM approach and the incorporation of sensor data, an outline of a Nitrogen Application Prescription System (NAPS) was developed. This system enables model adjustments for a different kind of plant information generated by a sensor. It offers model

adjustment, model recalibration and model forcing approaches. Plant N and drought stress should be integrated into the model via model recalibration for the soil parameters, while the disease integration uses a combination of model updating and model forcing.

The initial NAPS setup requires long term recorded data (yield, weather, and soil) to insure proper MM calibration. After calibration, information on the current growing conditions is required (weather, management information) until the N application date. Afterward, the NAPS incorporates sensor information and generates weather data for running future N application scenarios. The selection of the proper amount of N is determined by economic and ecological criteria. The implementation for regulations of groundwater protection zones can also be integrated into the selection process for the right amount of nitrogen. Furthermore, while the NAPS concept accounts for differences in in-field variabilities and delivers site-specific N prescriptions, it has to be applied on a geospatial scale by changing soil parameters spatially.

A significant drawback of the NAPS concept is its complex setup procedure that requires specialized knowledge which is not the domain of an ordinary farmer. In addition, the enormous computing time required by an online N application system can limit the vehicle speed. Switching to an offline approach can resolve this issue.

Overall, the NAPS concept has the potential to adjust N application more economically and ecologically by using current sensor data, historical yield records, and future weather predictions to derive a more precise N application strategy. Finally, this concept exhibits the potential for reconciling the issue of economic agricultural production with keeping the environment out of harm`s way.

8 Zusammenfassung

Die landwirtschaftliche Produktion ist heute für 35% aller weltweiten Treibhausgasemissionen verantwortlich und bedroht Boden- und Trinkwasserqualität in Folge von übermäßiger Landnutzung und Überdüngung. Besonders in den USA, China, Nordindien und Westeuropa werden die Folgen von Überdüngung deutlich. Der erhöhte Einsatz von stickstoffhaltigen Düngemitteln führt bereits bei der Produktion zu einer Zunahme von Treibhausgasen (CO_2). Auch die Ausbringung von N auf landwirtschaftliche Nutzflächen trägt zur Treibhausgasbildung bei (N_2O). Die Auswaschung von N führt weiterhin zu einer Eutrophierung von oberirdischen Gewässern und dem Grundwasser. Weltweit wurden diese Probleme von Regierungen erkannt und Gesetze zum Schutz der Umwelt erlassen.

Hohe Stickstoffeinträge in die Umwelt stellen ebenfalls in der Europäischen Union ein ernsthaftes Problem dar. In den letzten dreißig Jahren wurden deshalb diverse Richtlinien und Maßnahmenpakete verabschiedet, um die ökologischen Konsequenzen eines überhöhten Stickstoffeintrags zu vermindern. Keine der Maßnahmen zeigte jedoch bisher eine deutliche Verbesserung dieses Problems. In Deutschland steht insbesondere die Nitratverunreinigung des Grundwassers im Fokus. So wurde die Düngeverordnung in der Bundesrepublik im Mai 2020 weiter verschärft um einer Anklage des Europäischen Gerichtshofs zu entgehen. Als Geldstrafe standen bis zu 850.000 € pro Tag im Raum. Die Landwirtschaft befindet sich an einem Scheideweg. Es müssen dringend neue Strategien für eine umweltfreundliche Pflanzenproduktion entwickelt werden, um die Umweltauswirkungen der landwirtschaftlichen Pflanzenproduktion zu minimieren.

Eine Lösung für eine kosteneffektivere und weniger umweltbelastende Pflanzenproduktion stellt Precision Farming (PF) dar. Die zentrale Aufgabe von PF ist die Anwendung verschiedener landwirtschaftlicher Betriebsmittel zur richtigen Zeit und am richtigen Ort.

Einer der Hauptaspekte von PF ist die Anpassung der N-Ausbringung an die zeitliche und räumliche Variabilität innerhalb eines Schlags. Unterschiedliche Sensortechnologien ermöglichen es, die Feldvariabilitäten zu berücksichtigen: Die Technologien reichen von Bodenleitfähigkeitsmessungen über Kameras bis hin zur Spektralsensortechnik. Zur Anpassung der N-Düngung werden hauptsächlich Spektralsensoren eingesetzt. Im Allgemeinen sind Spektralsensoren berührungslose Sensoren und basieren auf dem Prinzip der elektromagnetischen Reflexion zwischen den Wellenlängen 300 nm und 2500 nm. Die Reflexion der Vegetation wird hauptsächlich durch ein niedriges Reflexionsvermögen im sichtbaren Spektrum (400 - 700 nm) und ein hohes Reflexionsvermögen im nahen Infrarotbereich (700 - 1000 nm), charakterisiert. Diese Eigenschaft ermöglicht die Bestimmung der N Konzentration bei Pflanzen. Zwar korreliert der Chlorophyllgehalt eng mit der N Konzentration, jedoch kann der Chlorophyllgehalt auch durch Krankheit-, Trockenstress oder andere Nährstoffdefizite beeinflusst werden. Das gleichzeitige Auftreten verschiedener Stressfaktoren kann daher zu falschen N Empfehlungen führen. Während Sensortechnologien hilfreich sind, um die

tatsächliche N-Konzentration in einer Pflanze zu messen, können Pflanzenmodelle genutzt werden, um den N-Bedarf zu berechnen.

In den letzten dreißig Jahren wurden prozessorientierte Pflanzenwachstumsmodelle zur Analyse von Mindererträgen und zur Entscheidungshilfe entwickelt. Sie simulieren das Wachstum und die Entwicklung von Pflanzen auf der Grundlage von Wetter- und Managementbedingungen. Der Hauptnachteil dieser Modelle ist das intensive Kalibrierungsverfahren und die unterschiedliche Komplexität der Modelle, die selbst erfahrenen Anwendern Schwierigkeiten bereitet. Eine noch größere Herausforderung für Anwender ist die Kombination verschiedener Modelle in einem so genannten Multi-Model-Ansatz, durch den die Simulationsgenauigkeit weiter erhöht werden kann.

Trotz der höheren Simulationsgenauigkeit können heterogene Bedingungen innerhalb des Schlags (abiotische und biotische Faktoren) nicht vom MM Ansatz berücksichtigt werden. Eine daraus resultierende Unsicherheit in der Entscheidungsfindung limitiert die Nutzung des MM auf dem landwirtschaftlichen Betrieb. Einige Forscher entwickelten deshalb einen Ansatz, der Daten aus Fernerkundungssensoren zur regelmäßigen Aktualisierung spezifischer Modellvariablen verwendet, um variable Feldbedingungen zu berücksichtigen. So kann die allgemeine Modellierungsgenauigkeit erhöht werden. Die Kopplung von Spektralsensoren und Pflanzenmodellierung als „Decision-Support-System“ für die Ausbringung von N erfordert eine zuverlässige und genaue Datenerfassung der N-Konzentration der Pflanze. Ob eine Unterscheidung zwischen Blattetagen und Blattposition bei der N-Bestimmung mittels Sensor notwendig ist, ist bisher unklar. Eine Anpassung des Pflanzenwachstumsmodells ist nur dann sinnvoll, wenn diese Frage geklärt ist und etwaige Messungen so als valide betrachtet werden können.

Zur präzisen Simulation des Ertrags sind weitere Modellanpassungen für zusätzliche Stressfaktoren wie Blattkrankheiten erforderlich. Blattkrankheiten, vermindern den potentiellen Ertrag durch die Reduktion der fotosynthetisch aktiven Blattfläche und/oder durch den Entzug von Assimilaten. In der aktuellen DSSAT Versionen sind die Weizenpflanzenmodelle nicht in der Lage solche Infektionen zu berücksichtigen. Dies beschränkt die Verwendung der Modelle auf eine "Stickstoffempfehlung" bei „gesunden“ Szenarien.

In dieser Arbeit wurde eruiert, ob mit Hilfe von Sensordaten und Pflanzenwachstumsmodellen eine N-Düngemittelstrategie abgeleitet werden kann, die in der Lage ist die ökologischen Belastung durch Düngung zu verringern. Dies umfasst die Evaluation folgender Fragestellungen:

(i) Welchen Einfluss haben verschiedener Blattetagen und -positionen auf die Reflexion von Weizenpflanzen, die bei unterschiedlicher N-Ernährung und Trockenstress kultiviert wurden?

(ii) Wie können Blattkrankheiten in das DSSAT-Weizenmodell integriert werden, damit die Auswirkungen der Blattkrankheit auf den Ertrag simuliert werden können?

(iii) Kann die Modellierungsgenauigkeit durch ein automatisches Kalibrierungsverfahren in einem Multi-Modell-Ansatz in Winterweizen erhöht und der Subjektivitätsfaktor der Modellkalibrierung eliminiert werden?

(iv) Wird die Gesamtmodelliergenauigkeit durch die Verwendung eines Multi-Modell-Ansatzes Verbessert?

Um die erste Fragestellung (i) zu evaluieren, wurden zwei hydroponische Gewächshausversuche durchgeführt (Publikation I). Im ersten Versuch wurden die N-Düngermenge und die Wachstumsstadium für die Bestimmung der N-Konzentration variiert, während sich der zweite Versuch auf eine sekundäre Induktion von N-Mangel aufgrund von Trockenstress konzentrierte. Für jede Pflanze wurden Sensormessungen an drei Blättern (Blattetagen: L1, L2, L3) und an drei Positionen auf dem Blatt (P1, P2, P3) durchgeführt. Darüber hinaus wurde die N-Konzentration (%) der gesamten Pflanze durch chemische Laboranalysen bestimmt. Er schwankte zwischen 0,75 % und 4,88 %. Mit Hilfe von Spektrometermessungen (400-1650 nm) wurden 16 Vegetationsindizes für jede Kombination von Blattetage und Position errechnet. Die N-Konzentration (%) wurde unter Verwendung jedes Vegetationsindexes für jede Blattetage und jede Position vorhergesagt. Für die Blätter L1 und L3 sowie für die Messposition auf P3 wurde im N-Versuch eine signifikant niedrigere mittlere Restfehlervarianz (MREV) gezeigt. Insgesamt wurde ein minimaler Unterschied der MREV zwischen den Blättern registriert, der jedoch nicht relevant war. Der Trockenstressversuch führte auch zu keinen signifikanten Unterschieden in der MREV zwischen den Blattetagen und Positionen. Weder die Position auf dem Blatt noch die Blattetage hatten einen Einfluss auf die Genauigkeit der Bestimmung der N-Konzentration der Pflanze durch spektrale Reflexionsmessungen. Daher sind Messungen auf Bestandsebene ausreichend.

Falls jedoch weitere Stressfaktoren wie Trockenheit oder Krankheitsbefall auftreten, kann nicht ausgeschlossen werden, dass eine Differenzierung zwischen verschiedenen Blattetagen notwendig ist. Die Blattkrankheit beginnt typischerweise an den älteren Blattetagen der Pflanze und steigt nach oben. Es gibt auch Berichte, dass sich die spektrale Reflexion im Laufe der Krankheitsentwicklung verändert, was eine Detektion erschwert, falls nicht zwischen den Blattetagen unterschieden wird.

Eine Integration von Sensorinformationen in Pflanzenwachstumsmodellen erfordert die Anpassung von Modellvariablen. In der nächsten Fragestellung (ii) (Publikation II) wurde untersucht, wie Blatterkrankungen in ein DSSAT-Weizenmodell integriert werden können, um so die Auswirkungen von Blatterkrankungen auf den Ertrag zu simulieren. Eine Modellerweiterung wurde entwickelt, indem das bestehende DSSAT Weizenmodell um ein Krankheitsmodul erweitert wurde. Das Modul simuliert die Auswirkungen des Krankheitsbefalls auf die Photosynthese und den Blattflächenindex auf einer täglichen Basis. Der Ansatz wurde anhand eines zweijährigen Datensatzes aus Argentinien mit verschiedenen Weizensorten und unterschiedlichen Inokulumniveaus von Septoria tritici-Blotch (STB) getestet. Die Genauigkeit des simulierten Ertrags und des Blattflächenindex (LAI) wurde verbessert. Die Werte der mittleren quadratischen Wurzel (RMSE) für Ertrag (1144 kg ha^{-1}) und LAI (1,19 m^2 m^{-2}) wurden um die Hälfte (499 kg ha^{-1}) für Ertrag und LAI (0,69 m^2 m^{-2}) reduziert. Darüber hinaus wurde eine Sensitivitätsanalyse mit verschiedenen Krankheitsfortschrittskurven für den Blattflächenindex und den Ertrag mit Hilfe eines Datensatzes aus Deutschland durchgeführt. Die Sensitivitätsanalyse zeigte die Möglichkeit des Modells, den Ertrag in einer exponentiellen

Beziehung mit zunehmendem Infektionsgrad (0-70%) genau zu reduzieren. Das erweiterte Modell stellt somit eine Möglichkeit dar, STB-Infektionen standortspezifisch in Verbindung mit verfügbaren Sensordaten zu simulieren.

Darüber hinaus könnte die Modellierungsgenauigkeit durch die Verwendung eines MM-Ansatzes weiter verbessert werden. Die Modellierungsgenauigkeit wird so insbesondere bei extremen Wetterbedingungen erhöht. Die DSSAT 4.7-Version umfasst drei Weizenmodelle, welche die gleichen Inputsfiles verwenden und somit geeignet für einen MM-Ansatz sind. Die gleichzeitige Verwendung mehrerer Modelle erhöht die Komplexität der Simulation und des damit verbundenen Kalibrierungsverfahrens, insbesondere wenn der Benutzer nicht mit allen Modellen vertraut ist.

Um dieses Problem zu lösen, wurde in Publikation III ein automatisiertes Kalibrierungsprogramm entwickelt und getestet. Die dritte Fragestellung (iii) untersuchte, ob objektive Kalibrierungsergebnisse gewährleitet werden könnten, wenn die „cultivar coefficients" im Modell auf der Basis des RMSE von time-seris Daten optimiert wurden. Darüber hinaus sollte das Potenzial für MM-Ansätze zur Entscheidungsunterstützung verwendet werden. Die Modellkalibrierung wurde an einem vierjährigen N-Weizendüngeversuch (0 - 240 kgN ha^{-1}) in Südwestdeutschland durchgeführt. Es zeigten sich zufriedenstellende Ergebnisse für die Kalibrierung (d-Index 0,93) und den Evaluierungsdatensatz (d-Index 0,81).

Schließlich (iv) wurde zusätzlich in Publikation III der MM-Ansatz verschiedener Jahre miteinander verglichen. In den meisten Fällen verbesserte sich die Modellierungsgenauigkeit durch die Verwendung mehrerer Modelle. Insbesondere in der Trockenperiode 2018 zeigte der MM-Ansatz eine höhere Modellierungsgenauigkeit für den Ertrag (d-Index 0,61) im Gegensatz zu einer einzelnen Simulation von CERES (d-Index 0,34) und Cropsim (d-Index 0,39). Dies untermauert den Vorteil eines MM-Ansatzes. Durch die Kombination unterschiedlicher Modelle werden Simulationsunsicherheiten kompensiert.

Basierend auf der Kombination eines MM-Ansatzes und der Einbeziehung von Sensordaten wurde ein „Nitrogen Application Prescription System" (NAPS) entwickelt. Dieses System ermöglicht Modellanpassungen für unterschiedliche vom Sensor generierte Pflanzeninformationen. Die Anpassungen können durch „model adjustment", „model recalibration" und „model forcing" erfolgen. Pflanzen-N-Konzentration und Trockenstress sollten über den Ansatz der „model recalibration" durch die Anpassung der Bodenparameter in das Modell integriert werden, während die Krankheitsintegration eine Kombination aus „model adjustment" und „model forcing" erfordert.

Eine Voraussetzung für das NAPS-Konzept ist das Vorhandensein von Langzeit-Daten (Ertrag, Klima- und Bodenbedingungen), um eine korrekte MM-Kalibrierung zu gewährleisten. Nach der Kalibrierung werden die Bedingungen der aktuellen Wachstumssaison (Wetter, Managementinformationen) bis zum Düngetermin benötigt. Anschließend berechnet das NAPS basierend auf Fernerkundungsinformationen und simulierten Wetterbedingungen verschiedene Düngeszenarien. Ökonomische und ökologische Kriterien bestimmen die richtige Düngemenge. Auflagen zu Grundwasserschutzzonen können ebenfalls in den Auswahlprozess für die N Düngung integriert werden. Darüber hinaus muss das NAPS-Konzept auf räumlicher Ebene

arbeiten, indem es die Bodenparameter berücksichtigt. So kann unter Beachtung der Feldvariabilität eine standortspezifische N-Ausbringung gewährleistet werden. Ein wesentlicher Nachteil der Anwendung des NAPS-Konzepts ist das komplexe Setup, welches Spezialwissen erfordert und für einen normalen Landwirt kaum realisierbar ist. Zudem kann die enorme Rechenzeit des Online-N-Applikationssystems die Fahrzeuggeschwindigkeit einschränken. Der Wechsel zu einem Offline-Ansatz.

Zusammenfassend zeigt sich, dass NAPS das Potential besitzt, die Düngung an ökonomische und ökologische Faktoren anzupassen, indem es aktuelle Sensordaten, historische Ertragsaufzeichnungen und zukünftige Wettervorhersagen zur Ermittlung einer präziseren N-Ausbringung nutzt. Das Konzept schafft so die Möglichkeit, die nachteiligen Auswirkungen einer Überdüngung zu begrenzen, so dass eine umweltfreundlichere landwirtschaftliche Produktion gewährleistet wird.

9 References

1. Hoeppner, J. M.; Hughes, L. Climate readiness of recovery plans for threatened Australian species. *Conserv. Biol.* **2019**, *33*, 534–542, doi:10.1111/cobi.13270.
2. Fujimori, S.; Su, X.; Liu, J.-Y.; Hasegawa, T.; Takahashi, K.; Masui, T.; Takimi, M. Erratum to: Implication of Paris Agreement in the context of long-term climate mitigation goals. *Springerplus* **2017**, *5*, 2118, doi:10.1186/s40064-017-3787-3.
3. Erisman, J. W.; Sutton, M. A.; Galloway, J.; Klimont, Z.; Winiwarter, W. How a century of ammonia synthesis changed the world. *Nat. Geosci.* **2008**, *1*, 636–639, doi:10.1038/ngeo325.
4. Jackson, R. B.; Le Quéré, C.; Andrew, R. M.; Canadell, J. G.; Korsbakken, J. I.; Liu, Z.; Peters, G. P.; Zheng, B. Global energy growth is outpacing decarbonization. *Environ. Res. Lett.* **2018**, *13*, 120401, doi:10.1088/1748-9326/aaf303.
5. Sanford, T.; Frumhoff, P. C.; Luers, A.; Gulledge, J. The climate policy narrative for a dangerously warming world. *Nat. Clim. Chang.* **2014**, *4*, 164–166, doi:10.1038/nclimate2148.
6. Mora, C.; Spirandelli, D.; Franklin, E. C.; Lynham, J.; Kantar, M. B.; Miles, W.; Smith, C. Z.; Freel, K.; Moy, J.; Louis, L. V.; Barba, E. W.; Bettinger, K.; Frazier, A. G.; Colburn IX, J. F.; Hanasaki, N.; Hawkins, E.; Hirabayashi, Y.; Knorr, W.; Little, C. M.; Emanuel, K.; Sheffield, J.; Patz, J. A.; Hunter, C. L. Broad threat to humanity from cumulative climate hazards intensified by greenhouse gas emissions. *Nat. Clim. Chang.* **2018**, *8*, 1062–1071, doi:10.1038/s41558-018-0315-6.
7. Urban, M. C. Accelerating extinction risk from climate change. *Science (80-.).* **2015**, *348*, 571–573, doi:10.1126/science.aaa4984.
8. Kang, L.; Ma, L.; Liu, Y. Loss evaluation of farmland caused by sea level rise and storm surge in the Pearl River Delta region under global climate change. *Dili Xuebao/Acta Geogr. Sin.* **2015**, *70*, 1375–1389, doi:10.11821/dlxb201509002.
9. Olesen, J. E.; Trnka, M.; Kersebaum, K. C.; Skjelvåg, A. O.; Seguin, B.; Peltonen-Sainio, P.; Rossi, F.; Kozyra, J.; Micale, F. Impacts and adaptation of European crop production systems to climate change. *Eur. J. Agron.* **2011**, *34*, 96–112, doi:10.1016/j.eja.2010.11.003.
10. Cheeseman, J. *Food Security in the Face of Salinity, Drought, Climate Change, and Population Growth*; Elsevier Inc., 2016; ISBN 9780128018545.
11. Ganie, S. A.; Lone, A.; Haq, S. Impact of Climate Change on Plant Diseases. **2016**, doi:2327-3364.
12. Deutsch, C. A.; Tewksbury, J. J.; Tigchelaar, M.; Battisti, D. S.; Merrill, S. C.; Huey, R. B.; Naylor, R. L. Increase in crop losses to insect pests in a warming climate. *Science (80-.).* **2018**, *361*, 916–919, doi:10.1126/science.aat3466.
13. United Nations. World Population Prospects 2019: Highlights (ST/ESA/SER.A/423). *Dep. Econ. Soc. Aff. Popul. Div.* **2019**.
14. Pardey, P. G.; Beddow, J. M.; Hurley, T. M.; Beatty, T. K. M.; Eidman, V. R. A Bounds Analysis of World Food Futures: Global Agriculture Through to 2050. *Aust. J. Agric. Resour. Econ.* **2014**, *58*, 571–589, doi:10.1111/1467-8489.12072.
15. Tilman, D.; Clark, M. Global diets link environmental sustainability and human health. *Nature* **2014**, *515*, 518–522, doi:10.1038/nature13959.
16. Ramankutty, N.; Mehrabi, Z.; Waha, K.; Jarvis, L.; Kremen, C.; Herrero, M.; Rieseberg, L.

H. Trends in Global Agricultural Land Use: Implications for Environmental Health and Food Security. *Annu. Rev. Plant Biol.* **2018**, *69*, doi:10.1146/annurev-arplant-042817-040256.

17. Vijay, V.; Reid, C. D.; Finer, M.; Jenkins, C. N.; Pimm, S. L. Deforestation risks posed by oil palm expansion in the Peruvian Amazon. *Environ. Res. Lett.* **2018**, *13*, 114010, doi:10.1088/1748-9326/aae540.
18. Fehlenberg, V.; Baumann, M.; Gasparri, N. I.; Piquer-Rodriguez, M.; Gavier-Pizarro, G.; Kuemmerle, T. The role of soybean production as an underlying driver of deforestation in the South American Chaco. *Glob. Environ. Chang.* **2017**, *45*, 24–34, doi:10.1016/j.gloenvcha.2017.05.001.
19. Volante, J. N.; Mosciaro, M. J.; Gavier-Pizarro, G. I.; Paruelo, J. M. Agricultural expansion in the Semiarid Chaco: Poorly selective contagious advance. *Land use policy* **2016**, *55*, 154–165, doi:10.1016/j.landusepol.2016.03.025.
20. Jenkins, C. N.; Pimm, S. L.; Joppa, L. N. Global patterns of terrestrial vertebrate diversity and conservation. *Proc. Natl. Acad. Sci.* **2013**, *110*, E2602–E2610, doi:10.1073/pnas.1302251110.
21. Joppa, L. N.; Visconti, P.; Jenkins, C. N.; Pimm, S. L. Achieving the Convention on Biological Diversity's Goals for Plant Conservation. *Science (80-.).* **2013**, *341*, 1100–1103, doi:10.1126/science.1241706.
22. Carlson, K. M.; Curran, L. M.; Asner, G. P.; Pittman, A. M.; Trigg, S. N.; Marion Adeney, J. Carbon emissions from forest conversion by Kalimantan oil palm plantations. *Nat. Clim. Chang.* **2012**, *3*, 283.
23. Levy, M. A.; Redo, D.; Bonilla-moheno, M. Deforestation and reforestation of latin america and the caribbean. **2013**, *45*, 262–271.
24. Rose, S. K.; Kriegler, E.; Bibas, R.; Calvin, K.; Popp, A.; van Vuuren, D. P.; Weyant, J. Bioenergy in energy transformation and climate management. *Clim. Change* **2014**, *123*, 477–493, doi:10.1007/s10584-013-0965-3.
25. Popp, A.; Humpenöder, F.; Weindl, I.; Bodirsky, B. L.; Bonsch, M.; Lotze-Campen, H.; Müller, C.; Biewald, A.; Rolinski, S.; Stevanovic, M.; Dietrich, J. P. Land-use protection for climate change mitigation. *Nat. Clim. Chang.* **2014**, *4*, 1095.
26. Fuss, S.; Canadell, J. G.; Peters, G. P.; Tavoni, M.; Andrew, R. M.; Ciais, P.; Jackson, R. B.; Jones, C. D.; Kraxner, F.; Nakicenovic, N.; Le Quéré, C.; Raupach, M. R.; Sharifi, A.; Smith, P.; Yamagata, Y. Betting on negative emissions. *Nat. Clim. Chang.* **2014**, *4*, 850.
27. Foley, J. A.; Ramankutty, N.; Brauman, K. A.; Cassidy, E. S.; Gerber, J. S.; Johnston, M.; Mueller, N. D.; O'Connell, C.; Ray, D. K.; West, P. C.; Balzer, C.; Bennett, E. M.; Carpenter, S. R.; Hill, J.; Monfreda, C.; Polasky, S.; Rockström, J.; Sheehan, J.; Siebert, S.; Tilman, D.; Zaks, D. P. M. Solutions for a cultivated planet. *Nature* **2011**, *478*, 337–342, doi:10.1038/nature10452.
28. Borrelli, P.; Lugato, E.; Montanarella, L.; Panagos, P. A New Assessment of Soil Loss Due to Wind Erosion in European Agricultural Soils Using a Quantitative Spatially Distributed Modelling Approach. *L. Degrad. Dev.* **2017**, *28*, 335–344, doi:10.1002/ldr.2588.
29. Foley, J. A.; DeFries, R.; Asner, G. P.; Barford, C.; Bonan, G.; Carpenter, S. R.; Chapin, F. S.; Coe, M. T.; Daily, G. C.; Gibbs, H. K.; Helkowski, J. H.; Holloway, T.; Howard, E. A.; Kucharik, C. J.; Monfreda, C.; Patz, J. A.; Prentice, I. C.; Ramankutty, N.; Snyder, P. K. Global consequences of land use. *Science (80-.).* **2005**, *309*, 570–574,

doi:10.1126/science.1111772.

30. Zhu, Q.; Liu, X.; Hao, T.; Zeng, M.; Shen, J.; Zhang, F.; de Vries, W. Cropland acidification increases risk of yield losses and food insecurity in China. *Environ. Pollut.* **2019**, 113145, doi:10.1016/j.envpol.2019.113145.
31. Vitousek, P. M.; Naylor, R.; Crews, T.; David, M. B.; Drinkwater, L. E.; Holland, E.; Johnes, P. J.; Katzenberger, J.; Martinelli, L. A.; Matson, P. A.; Nziguheba, G.; Ojima, D.; Palm, C. A.; Robertson, G. P.; Sanchez, P. A.; Townsend, A. R.; Zhang, F. S. Nutrient imbalances in agricultural development. *Science (80-.).* **2009**, *324*, 1519–1520, doi:10.1126/science.1170261.
32. Matson, P. A.; Parton, W. J.; Powe, A. G.; Swift, M. J. Agricultural Intensification and Ecosystem Properties. *Science (80-.).* **1997**, *277*, 504–509, doi:10.1126/science.277.5325.504.
33. Tilman, D.; Fargione, J.; Wolff, B.; D'Antonio, C.; Dobson, A.; Howarth, R.; Schindler, D.; Schlesinger, W. H.; Simberloff, D.; Swackhamer, D. Forecasting agriculturally driven global environmental change. *Science (80-.).* **2001**, *292*, 281–284, doi:10.1126/science.1057544.
34. Rosegrant, M. W.; Cline, S. A. Global Food Security: Challenges and Policies. *Science (80-.).* **2003**, *302*, 1917–1919, doi:10.1126/science.1092958.
35. Grassini, P.; Eskridge, K. M.; Cassman, K. G. Distinguishing between yield advances and yield plateaus in historical crop production trends. *Nat. Commun.* **2013**, *4*, doi:10.1038/ncomms3918.
36. Evenson, R. E.; Gollin, D. Assessing the impact of the Green Revolution, 1960 to 2000. *Science (80-.).* **2003**, *300*, 758–762, doi:10.1126/science.1078710.
37. Wik, M.; Pingali, P.; Broca, S. Global agricultural performance: past trends and future prospects. *World Bank Washingt. DC* **2008**, 44.
38. Gervois, S.; Ciais, P.; de Noblet-Ducoudré, N.; Brisson, N.; Vuichard, N.; Viovy, N. Carbon and water balance of European croplands throughout the 20th century. *Global Biogeochem. Cycles* **2008**, *22*, 1–13, doi:10.1029/2007GB003018.
39. Pingali, P. L. Green revolution: Impacts, limits, andthe path ahead. *Proc. Natl. Acad. Sci. U. S. A.* **2012**, *109*, 12302–12308, doi:10.1073/pnas.0912953109.
40. Cassman, K. G. Ecological intensification of cereal production systems: Yield potential, soil quality, and precision agriculture. *Proc. Natl. Acad. Sci. U. S. A.* **1999**, *96*, 5952–5959, doi:10.1073/pnas.96.11.5952.
41. Finger, R. Evidence of slowing yield growth - The example of Swiss cereal yields. *Food Policy* **2010**, *35*, 175–182, doi:10.1016/j.foodpol.2009.11.004.
42. Peltonen-Sainio, P.; Jauhiainen, L.; Laurila, I. P. Cereal yield trends in northern European conditions: Changes in yield potential and its realisation. *F. Crop. Res.* **2009**, *110*, 85–90, doi:10.1016/j.fcr.2008.07.007.
43. Brisson, N.; Gate, P.; Gouache, D.; Charmet, G.; Oury, F. X.; Huard, F. Why are wheat yields stagnating in Europe? A comprehensive data analysis for France. *F. Crop. Res.* **2010**, *119*, 201–212, doi:10.1016/j.fcr.2010.07.012.
44. Lin, M.; Huybers, P. Reckoning wheat yield trends. *Environ. Res. Lett.* **2012**, *7*, doi:10.1088/1748-9326/7/2/024016.
45. Calderini, D. F.; Slafer, G. A. Changes in yield and yield stability in wheat during the 20th century. *F. Crop. Res.* **1998**, *57*, 335–347, doi:10.1016/S0378-4290(98)00080-X.
46. Pimentel, D. Pesticides and Pest Control. In *Integrated Pest Management: Innovation-Development Process*; Springer Netherlands: Dordrecht, 2009; pp. 83–87.

47. Slemr, F.; Seiler, W. Field measurements of NO and NO2 emissions from fertilized and unfertilized soils. *J. Atmos. Chem.* **1984**, *2*, 1–24, doi:10.1007/BF00127260.
48. Kroeze, C.; Mosier, A.; Bouwman, L. Closing the global N 2 O budget: A retrospective analysis 1500-1994. *Global Biogeochem. Cycles* **1999**, *13*, 1–8, doi:10.1029/1998GB900020.
49. Ma, B. L.; Wu, T. Y.; Tremblay, N.; Deen, W.; Morrison, M. J.; Mclaughlin, N. B.; Gregorich, E. G.; Stewart, G. Nitrous oxide fluxes from corn fields: On-farm assessment of the amount and timing of nitrogen fertilizer. *Glob. Chang. Biol.* **2010**, *16*, 156–170, doi:10.1111/j.1365-2486.2009.01932.x.
50. Cui, Z.; Zhang, F.; Chen, X.; Dou, Z.; Li, J. In-season nitrogen management strategy for winter wheat: Maximizing yields, minimizing environmental impact in an over-fertilization context. *F. Crop. Res.* **2010**, *116*, 140–146, doi:10.1016/j.fcr.2009.12.004.
51. Cui, Z.; Chen, X.; Miao, Y.; Zhang, F.; Sun, Q.; Schroder, J.; Zhang, H.; Li, J.; Shi, L.; Xu, J.; Ye, Y.; Liu, C.; Yang, Z.; Zhang, Q.; Huang, S.; Bao, D. On-Farm Evaluation of the Improved Soil N–based Nitrogen Management for Summer Maize in North China Plain. *Agron. J.* **2008**, *100*, 517, doi:10.2134/agronj2007.0194.
52. Xu, R. T.; Pan, S. F.; Chen, J.; Chen, G. S.; Yang, J.; Dangal, S. R. S.; Shepard, J. P.; Tian, H. Q. Half-Century Ammonia Emissions From Agricultural Systems in Southern Asia: Magnitude, Spatiotemporal Patterns, and Implications for Human Health. *GeoHealth* **2018**, *2*, 40–53, doi:10.1002/2017gh000098.
53. Ju, X.-T.; Xing, G.-X.; Chen, X.-P.; Zhang, S.-L.; Zhang, L.-J.; Liu, X.-J.; Cui, Z.-L.; Yin, B.; Christie, P.; Zhu, Z.-L.; Zhang, F.-S. Reducing environmental risk by improving N management in intensive Chinese agricultural systems. *Proc. Natl. Acad. Sci.* **2009**, *106*, 3041–3046, doi:10.1073/pnas.0813417106.
54. Waters Coastal Clean. Understanding and Reducing the Effects of Nutrient Pollution. *Comm. Causes Manag. Coast. Eutrophication, Ocean. Stud. Board Water Sci. Technol. Board, Comm. Geosci. Environ. Resour. Natl. Res. Counc.* **2000**, 10.
55. Mississippi River *Action plan for reducing, mitigating, and controlling hypoxia in the Northern Gulf of Mexico*; Office of Wetlands, Oceans, and Watersheds, US Environmental Protection Agency, 2001;
56. Plan Gulf Hypoxia Action For reducing, mitigating, and controlling hypoxia in the northern Gulf of Mexico and improving water quality in the Mississippi River Basin. *Mississippi River/Gulf Mex. Watershed Nutr. Task Force, Washington, DC* **2008**.
57. Bricker, S. B.; Longstaff, B.; Dennison, W.; Jones, A.; Boicourt, K.; Wicks, C.; Woerner, J. Effects of nutrient enrichment in the nation's estuaries: A decade of change. *Harmful Algae* **2008**, *8*, 21–32, doi:10.1016/j.hal.2008.08.028.
58. EU, E. C. Directive 2000/60/EC of the European Parliament and of the Council of 23 October 2000 establishing a framework for Community action in the field of water policy. *Off. J. Eur. Union* **2000**, *327*, 193.
59. EU, E. C. Council Directive 91/676/EEC of 12 December 1991 concerning the protection of waters against pollution caused by nitrates from agricultural sources. *Off. J. Eur. Union* **1991**, *375*, 12.
60. Musacchio, A.; Re, V.; Mas-Pla, J.; Sacchi, E. EU Nitrates Directive, from theory to practice: Environmental effectiveness and influence of regional governance on its performance. *Ambio* **2019**, doi:10.1007/s13280-019-01197-8.

61. EU Commision Report from the Commission to the Council and the European Parliament on the Implementation of Council Directive 91/676/EEC Concerning the Protection of Waters against pollution caused by Nitrates from Agricultural Sources based on member state reports fo. **2013**.
62. Iefremova, B. I.; Lomakina, I.; Obiiukh, N. Groundwater Protection as an Essential Component of Water Management in the European Union in the Light of Modern Integration Processes : Legal Aspects of the Problem. **2019**, 354–368, doi:10.14207/ejsd.2019.v8n3p354.
63. Kuhn, T. The revision of the German Fertiliser Ordinance in 2017. **2017**, 25, doi:10.22004/ag.econ.262054.
64. Kuhn, T.; Schäfer, D.; Holm-Müller, K.; Britz, W. On-farm compliance costs with the EU-Nitrates Directive: A modelling approach for specialized livestock production in northwest Germany. *Agric. Syst.* **2019**, *173*, 233–243, doi:10.1016/j.agsy.2019.02.017.
65. Schaub, S. Salient to Whom ? The Positioning of German Political Parties on Agricultural Pollutants in Water Bodies. **2019**, 1–19, doi:10.3390/w11112278.
66. Euractiv. Germany may have to pay €850,000 per day for exceeding EU nitrate levels. Euractiv [Online], Jul 26, 2019. Available online: https://www.euractiv.com/section/agriculture-food/news/germany-may-have- to-pay-e850000-per-day-for-exceeding-eu-nitrate-levels/ (accessed on Nov 8, 2019).
67. Helbing, D. Societal, economic, ethical and legal challenges of the digital revolution: From big data to deep learning, artificial intelligence, and manipulative technologies. *Towar. Digit. Enlight. Essays Dark Light Sides Digit. Revolut.* **2018**, 47–72, doi:10.1007/978-3-319-90869-4_6.
68. Rotz, S.; Duncan, E.; Small, M.; Botschner, J.; Dara, R.; Mosby, I.; Reed, M.; Fraser, E. D. G. The Politics of Digital Agricultural Technologies: A Preliminary Review. *Sociol. Ruralis* **2019**, *59*, 203–229, doi:10.1111/soru.12233.
69. Rose, D. C.; Chilvers, J. Agriculture 4.0: Broadening Responsible Innovation in an Era of Smart Farming. *Front. Sustain. Food Syst.* **2018**, *2*, 1–7, doi:10.3389/fsufs.2018.00087.
70. Franks, J. R. Sustainable intensification: A UK perspective. *Food Policy* **2014**, *47*, 71–80, doi:10.1016/j.foodpol.2014.04.007.
71. Shibusawa, S.; Anom, W. S. I. M.; Sato, H.; Sasao, A.; Hirako, S.; Otomo, A.; Blackmore, S. On-line real-time soil spectrophotometer. In; Robert, P. C., Rust, R. H., Larson, W. E., Eds.; American Society of Agronomy: Madison, USA, 2000; pp. 1–13.
72. Lottes, P.; Khanna, R.; Pfeifer, J.; Siegwart, R.; Stachniss, C. UAV-based crop and weed classification for smart farming. In *2017 IEEE International Conference on Robotics and Automation (ICRA)*; IEEE, 2017; pp. 3024–3031.
73. López, I. D.; Corrales, J. C. A Smart Farming Approach in Automatic Detection of Favorable Conditions for Planting and Crop Production in the Upper Basin of Cauca River. In; 2018; pp. 223–233.
74. Thompson, A. L.; Thorp, K. R.; Conley, M. M.; Elshikha, D. M.; French, A. N.; Andrade-sanchez, P.; Pauli, D. Comparing Nadir and Multi-Angle View Sensor Technologies for Measuring in-Field Plant Height of Upland Cotton. **2019**, doi:10.3390/rs11060700.
75. Crookston, R. K. A top 10 list of developments and issue impacting crop management and ecology during the past 50 years. *Crop Sci.* **2006**, *46*, 2253–2262,

doi:10.2135/cropsci2005.11.0416gas.

76. Tsouvalis, J.; Seymour, S.; Watkins, C. Exploring Knowledge-Cultures: Precision Farming, Yield Mapping, and the Expert–Farmer Interface. *Environ. Plan. A Econ. Sp.* **2000**, *32*, 909–924, doi:10.1068/a32138.
77. Saeys, W.; Deblander, J.; Ramon, H.; Anthonis, J. High-performance flow control for site-specific application of liquid manure. *Biosyst. Eng.* **2008**, *99*, 22–34, doi:10.1016/j.biosystemseng.2007.09.009.
78. Hargreaves, P. R.; Peets, S.; Chamen, W. C. T.; White, D. R.; Misiewicz, P. A.; Godwin, R. J. Potential for Controlled Traffic Farming (CTF) in Grass Silage Production: Agronomics, system design and economics. *Adv. Anim. Biosci.* **2017**, *8*, 776–781, doi:10.1017/S2040470017000747.
79. Zhang, N.; Wang, M.; Wang, N. Precision agriculture—a worldwide overview. *Comput. Electron. Agric.* **2002**, *36*, 113–132, doi:10.1016/S0168-1699(02)00096-0.
80. Mulla, D. J. Twenty five years of remote sensing in precision agriculture: Key advances and remaining knowledge gaps. *Biosyst. Eng.* **2013**, *114*, 358–371, doi:10.1016/j.biosystemseng.2012.08.009.
81. Mulla, D. J.; Gowda, P.; Koskinen, W. C.; Khakural, B. R.; Johnson, G.; Robert, P. C. Modeling the Effect of Precision Agriculture: Pesticide Losses to Surface Waters. In; 2002; pp. 304–317.
82. Stafford, J. V. Implementing precision agriculture in the 21st century. *J. Agric. Eng. Res.* **2000**, *76*, 267–275, doi:10.1006/jaer.2000.0577.
83. Miao, Y.; Mulla, D. J.; Batchelor, W. D.; Paz, J. O.; Robert, P. C.; Wiebers, M. Evaluating management zone optimal nitrogen rates with a crop growth model. *Agron. J.* **2006**, *98*, 545–553, doi:10.2134/agronj2005.0153.
84. Dammer, K. H.; Thöle, H.; Volk, T.; Hau, B. Variable-rate fungicide spraying in real time by combining a plant cover sensor and a decision support system. *Precis. Agric.* **2009**, *10*, 431–442, doi:10.1007/s11119-008-9088-7.
85. Sökefeld, M. *Precision Crop Protection - the Challenge and Use of Heterogeneity*; Oerke, E.-C., Gerhards, R., Menz, G., Sikora, R. A., Eds.; Springer Netherlands: Dordrecht, 2010; ISBN 978-90-481-9276-2.
86. Grisso, R.; Alley, M.; Holshouser, D.; Thomason, W. Precision Farming Tools : Variable-Rate Application. **2011**, 1–16.
87. J. P. Fulton; C. J. Sobolik; S. A. Shearer; S. F. Higgins; T. F. Burks Grain Yield Monitor Flow Sensor Accuracy for Simulated Varying Field Slopes. *Appl. Eng. Agric.* **2009**, *25*, 15–21, doi:10.13031/2013.25425.
88. Grisso, R.; Alley, M.; Holshouser, D.; Thomason, W. Precision Farming Tools : Soil electrical conductivity. **2005**.
89. Stadler, A.; Rudolph, S.; Kupisch, M.; Langensiepen, M.; van der Kruk, J.; Ewert, F. Quantifying the effects of soil variability on crop growth using apparent soil electrical conductivity measurements. *Eur. J. Agron.* **2015**, *64*, 8–20, doi:10.1016/j.eja.2014.12.004.
90. Robert, P. C. Precision agriculture: a challenge for crop nutrition management. In *Progress in Plant Nutrition: Plenary Lectures of the XIV International Plant Nutrition Colloquium*; Springer Netherlands: Dordrecht, 2002; pp. 143–149.
91. Lindblom, J.; Lundström, C.; Ljung, M.; Jonsson, A. Promoting sustainable intensification

in precision agriculture: review of decision support systems development and strategies. *Precis. Agric.* **2017**, *18*, 309–331, doi:10.1007/s11119-016-9491-4.

92. Sadler, E. J.; Bauer, P. J.; Busscher, W. J. Site-Specific Analysis of a Droughted Corn Crop. *Agron. J.* **2000**, *92*, 395, doi:10.2134/agronj2000.923395x.
93. Machado, S.; Bynum, E. D.; Archer, T. L.; Bordovsky, J.; Rosenow, D. T.; Peterson, C.; Bronson, K.; Nesmith, D. M.; Lascano, R. J.; Wilson, L. T.; Segarra, E. Spatial and temporal variability of sorghum grain yield: Influence of soil, water, pests, and diseases relationships. *Precis. Agric.* **2002**, *3*, 389–406, doi:10.1023/A:1021597023005.
94. Braum, S. M.; Hinds, P.; Malzer, G. L.; Bell, J.; Mulla, D.; Robert, P. C. Terrain Attributes and Soil Nitrogen: Spatial Effects on Corn Yield Responses to Nitrogen Fertilization for a Northern, Glaciated Landscape. **1999**, 195–202, doi:10.2134/1999.precisionagproc4.c17.
95. Duncan, E. An Exploration of how the Relationship between Farmers and Retailers influences Precision Agriculture Adoption. **2018**.
96. Huggins, D. R.; Alderfer, R. D. Yield Variability Within a Long-Term Corn Management Study: Implications for Precision Farming. *ASA-CSSA-SSSA* **1995**, 417–426, doi:10.2134/1995.site-specificmanagement.c28.
97. Clarke, J.; Froment, M. A.; Stafford, J.; Lark, M. An Investigation into the Relationship Between Yield Maps, Soil Variation and Crop Development in the UK. In; 1996.
98. Cohen, Y.; Alchanatis, V.; Meron, M.; Saranga, Y.; Tsipris, J. Estimation of leaf water potential by thermal imagery and spatial analysis. *J. Exp. Bot.* **2005**, *56*, 1843–1852, doi:10.1093/jxb/eri174.
99. Linke, R.; Richter, K.; Haumann, J.; Schneider, W.; Weihs, P. Occurrence of repeated drought events: Can repetitive stress situations and recovery from drought be traced with lead reflectance? *Period. Biol.* **2008**, *110*, 219–229.
100. DeBacker, S.; Kempeneers, P.; Debruyn, W.; Scheunders, P. A Band Selection Technique for Spectral Classification. *IEEE Geosci. Remote Sens. Lett.* **2005**, *2*, 319–323, doi:10.1109/LGRS.2005.848511.
101. Pinter, Jr., P. J.; Hatfield, J. L.; Schepers, J. S.; Barnes, E. M.; Moran, M. S.; Daughtry, C. S. T.; Upchurch, D. R. Remote Sensing for Crop Management. *Photogramm. Eng. Remote Sens.* **2003**, *69*, 647–664, doi:10.14358/PERS.69.6.647.
102. Blackburn, G. A. Hyperspectral remote sensing of plant pigments. *J. Exp. Bot.* **2007**, *58*, 855–867, doi:10.1093/jxb/erl123.
103. Ayala-silva, T.; Beyl, C. A. Changes in spectral reflectance of wheat leaves in response to specific macronutrient deficiency. *Adv. Sp. Res.* **2005**, *35*, 305–317, doi:10.1016/j.asr.2004.09.008.
104. Zhao, D.; Reddy, K. R.; Kakani, V. G.; Reddy, V. R. Nitrogen deficiency effects on plant growth, leaf photosynthesis, and hyperspectral reflectance properties of sorghum. *Eur. J. Agron.* **2005**, *22*, 391–403, doi:10.1016/j.eja.2004.06.005.
105. Adams, M. L.; Philpot, W. D.; Norvell, W. A. Yellowness index: An application of spectral second derivatives to estimate chlorosis of leaves in stressed vegetation. *Int. J. Remote Sens.* **1999**, *20*, 3663–3675, doi:10.1080/014311699211264.
106. Serrano, L.; Filella, I.; Pen, J. Remote Sensing of Biomass and Yield of Winter Wheat under Different Nitrogen Supplies. **2000**, 723–731.
107. Sripada, R. P.; Schmidt, J. P.; Dellinger, A. E.; Beegle, D. B. Evaluating multiple indices from

a canopy reflectance sensor to estimate corn N requirements. *Agron. J.* **2008**, *100*, 1553–1561, doi:10.2134/agronj2008.0017.

108. Selige, T.; Böhner, J.; Schmidhalter, U. High resolution topsoil mapping using hyperspectral image and field data in multivariate regression modeling procedures. *Geoderma* **2006**, *136*, 235–244, doi:10.1016/j.geoderma.2006.03.050.
109. Link, A.; Reusch, S. Implementation of site-specific nitrogen application—status and development of the YARA N-Sensor. *NJF Semin.* **2006**, *390*.
110. Muñoz-Huerta, R. F.; Guevara-Gonzalez, R. G.; Contreras-Medina, L. M.; Torres-Pacheco, I.; Prado-Olivarez, J.; Ocampo-Velazquez, R. V A Review of Methods for Sensing the Nitrogen Status in Plants: Advantages, Disadvantages and Recent Advances. *Sensors* **2013**, *13*, 10823–10843, doi:10.3390/s130810823.
111. Zillmann, E.; Graeff, S.; Link, J.; Batchelor, W. D.; Claupein, W. Assessment of cereal nitrogen requirements derived by optical on-the-go sensors on heterogeneous soils. *Agron. J.* **2006**, *98*, 682–690, doi:10.2134/agronj2005.0253.
112. Berntsen, J.; Thomsen, A.; Schelde, K.; Hansen, O. M.; Knudsen, L.; Broge, N.; Hougaard, H.; Hørfarter, R. Algorithms for sensor-based redistribution of nitrogen fertilizer in winter wheat. *Precis. Agric.* **2006**, *7*, 65–83, doi:10.1007/s11119-006-9000-2.
113. J∅rgensen, R. N.; Hansen, P. M.; Bro, R. Exploratory study of winter wheat reflectance during vegetative growth using three-mode component analysis. *Int. J. Remote Sens.* **2006**, *27*, 919–937, doi:10.1080/01431160500117683.
114. Bao, Y.; Xu, K.; Min, J.; Xu, J. Estimating wheat shoot nitrogen content at vegetative stage from in situ hyperspectral measurements. *Crop Sci.* **2013**, *53*, 2063–2071, doi:10.2135/cropsci2013.01.0012.
115. Atta, B. M.; Saleem, M.; Ali, H.; Arshad, H. M. I.; Ahmed, M. Chlorophyll as a biomarker for early disease diagnosis. *Laser Phys.* **2018**, *28*, 65607, doi:10.1088/1555-6611/aab94f.
116. Meher; Shivakrishna, P.; Ashok Reddy, K.; Manohar Rao, D. Effect of PEG-6000 imposed drought stress on RNA content, relative water content (RWC), and chlorophyll content in peanut leaves and roots. *Saudi J. Biol. Sci.* **2018**, *25*, 285–289, doi:10.1016/j.sjbs.2017.04.008.
117. Holzworth, D. P.; Snow, V.; Janssen, S.; Athanasiadis, I. N.; Donatelli, M.; Hoogenboom, G.; White, J. W.; Thorburn, P. Agricultural production systems modelling and software: Current status and future prospects. *Environ. Model. Softw.* **2015**, *72*, 276–286, doi:10.1016/j.envsoft.2014.12.013.
118. Graves, A. R.; Hess, T.; Matthews, R. B.; Stephens, W.; Middleton, T. Crop Simulation Models as Tools in Computer Laboratory and Classroom-Based Education. *J. Nat. Resour. Life Sci. Educ.* **2002**, *31*, 48–54.
119. Martín, M. M. S.; Olesen, J. E.; Porter, J. R. A genotype, environment and management (GxExM) analysis of adaptation in winter wheat to climate change in Denmark. *Agric. For. Meteorol.* **2014**, *187*, 1–13, doi:10.1016/j.agrformet.2013.11.009.
120. Jones, J. W.; Hoogenboom, G.; Porter, C. H.; Boote, K. J.; Batchelor, W. D.; Hunt, L. A.; Wilkens, P. W.; Singh, U.; Gijsman, A. J.; Ritchie, J. T. The Dssat Cropping System Model. *Eur. J. Agron.* **2003**, *18*, 235–265.
121. Gao, L.; Jin, Z.; Huang, Y.; Zhang, L. Rice clock model—a computer model to simulate rice development. *Agric. For. Meteorol.* **1992**, *60*, 1–16, doi:10.1016/0168-1923(92)90071-B.
122. Mavromatis, T.; Boote, K. J.; Jones, J. W.; Irmak, A.; Shinde, D.; Hoogenboom, G.

Developing genetic coefficients for crop simulation models with data from crop performance trials. *Crop Sci.* **2001**, *41*, 40–51, doi:10.2135/cropsci2001.41140x.

123. Ahmed, M.; Akram, M. N.; Asim, M.; Aslam, M.; Hassan, F. ul; Higgins, S.; Stöckle, C. O.; Hoogenboom, G. Calibration and validation of APSIM-Wheat and CERES-Wheat for spring wheat under rainfed conditions: Models evaluation and application. *Comput. Electron. Agric.* **2016**, *123*, 384–401, doi:10.1016/j.compag.2016.03.015.
124. Singh, A. K.; Tripathy, R.; Chopra, U. K. Evaluation of CERES-Wheat and CropSyst models for water-nitrogen interactions in wheat crop. *Agric. Water Manag.* **2008**, *95*, 776–786, doi:10.1016/j.agwat.2008.02.006.
125. Hoogenboom, G.; Porter, C. H.; Shelia, V.; Boote, K. J.; Singh, U.; White, J. W.; Hunt, L. A.; Ogoshi, R.; Lizaso, J. I.; Koo, J. Decision Support System for Agrotechnology Transfer (DSSAT) Version 4.7 Available online: www.DSSAT.net.
126. Ritchie, J. T. Wheat Phasic Development. In *Modeling plant and soil systems.*; 1991; pp. 31–54.
127. He, J.; Dukes, M. D.; Hochmuth, G. J.; Jones, J. W.; Graham, W. D. Identifying irrigation and nitrogen best management practices for sweet corn production on sandy soils using CERES-Maize model. *Agric. Water Manag.* **2012**, *109*, 61–70, doi:10.1016/j.agwat.2012.02.007.
128. Kadiyala, M. D. M.; Jones, J. W.; Mylavarapu, R. S.; Li, Y. C.; Reddy, M. D. Identifying irrigation and nitrogen best management practices for aerobic rice–maize cropping system for semi-arid tropics using CERES-rice and maize models. *Agric. Water Manag.* **2015**, *149*, 23–32, doi:10.1016/j.agwat.2014.10.019.
129. Bannayan, M.; Crout, N. M. J.; Hoogenboom, G. Application of the CERES-Wheat model for within-season prediction of winter wheat yield in the United Kingdom. *Agron. J.* **2003**, *95*, 114–125, doi:10.2134/agronj2003.0114.
130. Attia, A.; Rajan, N.; Xue, Q.; Nair, S.; Ibrahim, A.; Hays, D. Application of DSSAT-CERES-Wheat model to simulate winter wheat response to irrigation management in the Texas High Plains. *Agric. Water Manag.* **2016**, *165*, 50–60, doi:10.1016/j.agwat.2015.11.002.
131. Zhang, D.; Wang, H.; Li, D.; Li, H.; Ju, H.; Li, R.; Batchelor, W. D.; Li, Y. DSSAT-CERES-Wheat model to optimize plant density and nitrogen best management practices. *Nutr. Cycl. Agroecosystems* **2019**, *114*, 19–32, doi:10.1007/s10705-019-09984-1.
132. Thorp, K. R.; DeJonge, K. C.; Kaleita, A. L.; Batchelor, W. D.; Paz, J. O. Methodology for the use of DSSAT models for precision agriculture decision support. *Comput. Electron. Agric.* **2008**, *64*, 276–285, doi:10.1016/j.compag.2008.05.022.
133. Inoue, Y. Synergy of remote sensing and modeling for estimating ecophysiological processes in plant production. *Plant Prod. Sci.* **2003**, *6*, 3–16, doi:10.1626/pps.6.3.
134. Dorigo, W. A.; Zurita-Milla, R.; de Wit, A. J. W.; Brazile, J.; Singh, R.; Schaepman, M. E. A review on reflective remote sensing and data assimilation techniques for enhanced agroecosystem modeling. *Int. J. Appl. Earth Obs. Geoinf.* **2007**, *9*, 165–193, doi:10.1016/j.jag.2006.05.003.
135. Thorp, K. R.; Hunsaker, D. J.; French, A. N. Assimilating leaf area index estimates from remote sensing into the simulations of a cropping systems model. **2010**, *53*, 251–262.
136. de Wit, A. J. W. Application of a genetic algorithm for crop model steering using NOAA-AVHRR data. In *Remote Sensing for Earth Science, Ocean, and Sea Ice Applications*; Cecchi, G., Engman, E. T., Zilioli, E., Eds.; 1999; Vol. 3868, p. 167.
137. Quaife, T.; Lewis, P.; De Kauwe, M.; Williams, M.; Law, B. E.; Disney, M.; Bowyer, P.

Assimilating canopy reflectance data into an ecosystem model with an Ensemble Kalman Filter. *Remote Sens. Environ.* **2008**, *112*, 1347–1364, doi:10.1016/j.rse.2007.05.020.

138. Atzberger, C.; Jarmer, T.; Schlerf, M.; Kotz, B.; Werner, W. Retrieval of wheat bio-physical attributes from hyperspectral data and SAILH+ PROSPECT radiative transfer model. *3rd EARSeL Work. Imaging Spectrosc.* **2003**, 473–482.
139. Atzberger, C. Object-based retrieval of biophysical canopy variables using artificial neural nets and radiative transfer models. *Remote Sens. Environ.* **2004**, *93*, 53–67, doi:10.1016/j.rse.2004.06.016.
140. Baret, F.; Guyot, G. Potentials and limits of vegetation indices for LAI and APAR assessment. *Remote Sens. Environ.* **1991**, *35*, 161–173, doi:10.1016/0034-4257(91)90009-U.
141. Hansen, P. M. M.; Schjoerring, J. K. K. Reflectance measurement of canopy biomass and nitrogen status in wheat crops using normalized difference vegetation indices and partial least squares regression. *Remote Sens. Environ.* **2003**, *86*, 542–553, doi:10.1016/S0034-4257(03)00131-7.
142. M. S. Seidl; W. D. Batchelor; J. O. Paz INTEGRATING REMOTELY SENSED IMAGES WITH A SOYBEAN MODEL TO IMPROVE SPATIAL YIELD SIMULATION. *Trans. ASAE* **2004**, *47*, 2081–2090, doi:10.13031/2013.17793.
143. Dente, L.; Satalino, G.; Mattia, F.; Rinaldi, M. Assimilation of leaf area index derived from ASAR and MERIS data into CERES-Wheat model to map wheat yield. *Remote Sens. Environ.* **2008**, *112*, 1395–1407, doi:10.1016/j.rse.2007.05.023.
144. Wallach, D.; Palosuo, T.; Thorburn, P.; Seidel, S. J.; Gourdain, E.; Asseng, S.; Basso, B.; Buis, S.; Crout, N.; Dibari, C.; Dumont, B.; Ferrise, R.; Gaiser, T.; Garcia, C.; Gayler, S.; Ghahramani, A.; Hochman, Z.; Hoek, S.; Horan, H.; Hoogenboom, G.; Huang, M.; Jabloun, M.; Jing, Q.; Justes, E.; Kersebaum, K. C.; Klosterhalfen, A.; Launay, M.; Luo, Q.; Maestrini, B.; Moriondo, M.; Zadeh, H. N.; Olesen, J. E.; Poyda, A.; Priesack, E.; Pullens, J. W. M.; Qian, B.; Schütze, N.; Shelia, V.; Souissi, A.; Specka, X.; Srivastava, A. K.; Stella, T.; Streck, T.; Trombi, G.; Wallor, E.; Wang, J.; Weber, T. K. D.; Weihermüller, L.; Wit, A. de; Wöhling, T.; Xiao, L.; Zhao, C.; Zhu, Y. How well do crop models predict phenology, with emphasis on the effect of calibration? *bioRxiv* **2019**, 708578, doi:10.1101/708578.
145. Palosuo, T.; Kersebaum, K. C.; Angulo, C.; Hlavinka, P.; Moriondo, M.; Olesen, J. E.; Patil, R. H.; Ruget, F.; Rumbaur, C.; Takáč, J.; Trnka, M.; Bindi, M.; Çaldağ, B.; Ewert, F.; Ferrise, R.; Mirschel, W.; Şaylan, L.; Šiška, B.; Rötter, R. Simulation of winter wheat yield and its variability in different climates of Europe: A comparison of eight crop growth models. *Eur. J. Agron.* **2011**, *35*, 103–114, doi:10.1016/j.eja.2011.05.001.
146. Maiorano, A.; Martre, P.; Asseng, S.; Ewert, F.; Müller, C.; Rötter, R. P.; Ruane, A. C.; Semenov, M. A.; Wallach, D.; Wang, E.; Alderman, P. D.; Kassie, B. T.; Biernath, C.; Basso, B.; Cammarano, D.; Challinor, A. J.; Doltra, J.; Dumont, B.; Rezaei, E. E.; Gayler, S.; Kersebaum, K. C.; Kimball, B. A.; Koehler, A. K.; Liu, B.; O'Leary, G. J.; Olesen, J. E.; Ottman, M. J.; Priesack, E.; Reynolds, M.; Stratonovitch, P.; Streck, T.; Thorburn, P. J.; Waha, K.; Wall, G. W.; White, J. W.; Zhao, Z.; Zhu, Y. Crop model improvement reduces the uncertainty of the response to temperature of multi-model ensembles. *F. Crop. Res.* **2017**, *202*, 5–20, doi:10.1016/j.fcr.2016.05.001.
147. Botterweg, P. The user's influence on model calibration results: an example of the model SOIL, independently calibrated by two users. *Ecol. Modell.* **1995**, *81*, 71–81, doi:10.1016/0304-

3800(94)00161-A.
148. Odilbekov, F.; Armoniené, R.; Henriksson, T.; Chawade, A. Proximal phenotyping and machine learning methods to identify septoria tritici blotch disease symptoms in wheat. *Front. Plant Sci.* **2018**, *9*, 1–11, doi:10.3389/fpls.2018.00685.
149. Waggoner, P. E.; Berger, R. D. Defoliation, Disease, and Growth. *Phytopathology* **1987**, *77*, 1495–1497.
150. Uehara, G.; Tsuji, G. Y. The IBSNAT project. *Syst. approaches Agric. Dev.* **1993**, 505–513, doi:10.1007/978-94-011-2842-1_31.
151. Basso, B.; Fiorentino, C.; Cammarano, D. Variable rate nitrogen fertilizer response in wheat using remote sensing. *Precis. Agric.* **2016**, *17*, 168–182, doi:10.1007/s11119-015-9414-9.
152. Ni, J.; Zhang, J.; Wu, R.; Pang, F.; Zhu, Y. Development of an Apparatus for Crop-Growth Monitoring and Diagnosis. *Sensors* **2018**, *18*, 3129, doi:10.3390/s18093129.
153. Zanella, V.; Ortiz, B. V.; Thorp, K. R.; Morari, F.; Mosca, G.; Hoogenboom, G. Combining crop sensing and simulation modeling to assess within-field corn nitrogen stress. *Wageningen Acad. Publ.* **2015**, 391–398, doi:10.7202/1016404ar.
154. Baret, F.; Fourty, T. Radiometric Estimates of Nitrogen Status of Leaves and Canopies. *Diagnosis Nitrogen Status Crop.* **1997**, 201–227, doi:10.1007/978-3-642-60684-7_12.
155. Kusnierek, K.; Korsaeth, A. Simultaneous identification of spring wheat nitrogen and water status using visible and near infrared spectra and Powered Partial Least Squares Regression. *Comput. Electron. Agric.* **2015**, *117*, 200–213, doi:10.1016/j.compag.2015.08.001.
156. Antille, D. L.; Lobsey, C. R.; McCarthy, C. L.; Thomasson, J. A.; Baillie, C. P. A review of the state of the art in agricultural automation. Part IV: Sensor-based nitrogen management technologies. In *2018 Detroit, Michigan July 29 - August 1, 2018*; American Society of Agricultural and Biological Engineers: St. Joseph, MI, 2018.
157. Seidl, M. S.; Paz, J. O.; Batchelor, W. D. Integrating remotely sensed images to improve spatial crop model calibration. In; American Society of Agricultural Engineers: St Joseph, USA, 2000; pp. 1–17.
158. Launay, M.; Guerif, M. Assimilating remote sensing data into a crop model to improve predictive performance for spatial applications. *Agric. Ecosyst. Environ.* **2005**, *111*, 321–339, doi:10.1016/j.agee.2005.06.005.
159. Röll, G.; Hartung, J.; Graeff-Hönninger, S. Determination of plant nitrogen content in wheat plants via spectral reflectance measurements: Impact of leaf number and leaf position. *Remote Sens.* **2019**, *11*, doi:10.3390/rs11232794.
160. Adelabu, S.; Mutanga, O.; Adam, E. Evaluating the impact of red-edge band from Rapideye image for classifying insect defoliation levels. *ISPRS J. Photogramm. Remote Sens.* **2014**, *95*, 34–41, doi:10.1016/j.isprsjprs.2014.05.013.
161. Eklundh, L.; Johansson, T.; Solberg, S. Mapping insect defoliation in Scots pine with MODIS time-series data. *Remote Sens. Environ.* **2009**, *113*, 1566–1573, doi:10.1016/j.rse.2009.03.008.
162. Hillnhütter, C.; Mahlein, A.-K.; Sikora, R. A.; Oerke, E.-C. Remote sensing to detect plant stress induced by Heterodera schachtii and Rhizoctonia solani in sugar beet fields. *F. Crop. Res.* **2011**, *122*, 70–77, doi:10.1016/j.fcr.2011.02.007.
163. Eitel, J. U. H.; Long, D. S.; Gessler, P. E.; Hunt, E. R.; Brown, D. J. Sensitivity of Ground-Based Remote Sensing Estimates of Wheat Chlorophyll Content to Variation in Soil Reflectance. *Soil Sci. Soc. Am. J.* **2009**, *73*, 1715–1723, doi:10.2136/sssaj2008.0288.

164. Rondeaux, G.; Steven, M.; Baret, F. Optimization of soil-adjusted vegetation indices. *Remote Sens. Environ.* **1996**, *55*, 95–107, doi:10.1016/0034-4257(95)00186-7.
165. Li, F.; Miao, Y.; Hennig, S. D.; Gnyp, M. L.; Chen, X.; Jia, L.; Bareth, G. Evaluating hyperspectral vegetation indices for estimating nitrogen concentration of winter wheat at different growth stages. *Precis. Agric.* **2010**, *11*, 335–357, doi:10.1007/s11119-010-9165-6.
166. Li, L.; Nielsen, D. C.; Yu, Q.; Ma, L.; Ahuja, L. R. Evaluating the Crop Water Stress Index and its correlation with latent heat and CO2 fluxes over winter wheat and maize in the North China plain. *Agric. Water Manag.* **2010**, *97*, 1146–1155, doi:10.1016/j.agwat.2008.09.015.
167. Thoren, D.; Schmidhalter, U. Nitrogen status and biomass determination of oilseed rape by laser-induced chlorophyll fluorescence. *Eur. J. Agron.* **2009**, *30*, 238–242, doi:10.1016/j.eja.2008.12.001.
168. Eitel, J. U. H.; Vierling, L. A.; Long, D. S.; Hunt, E. R. Early season remote sensing of wheat nitrogen status using a green scanning laser. *Agric. For. Meteorol.* **2011**, *151*, 1338–1345, doi:10.1016/j.agrformet.2011.05.015.
169. J. A. Thomasson; R. Sui; M. S. Cox; A. Al-Rajehy Soil reflectande sensing for determining soil properties in precision agriculture. *Trans. ASAE* **2001**, *44*, 1445, doi:10.13031/2013.7002.
170. Chen, M.; Yang, S.; Yi, X.; Wu, D. Real-time 3D mapping using a 2D laser scanner and IMU-aided visual SLAM. *2017 IEEE Int. Conf. Real-Time Comput. Robot. RCAR 2017* **2018**, *2017-July*, 297–302, doi:10.1109/RCAR.2017.8311877.
171. Hamuda, E.; Glavin, M.; Jones, E. A survey of image processing techniques for plant extraction and segmentation in the field. *Comput. Electron. Agric.* **2016**, *125*, 184–199, doi:10.1016/j.compag.2016.04.024.
172. Flowers, M.; Weisz, R.; Heiniger, R. Remote sensing of winter wheat tiller density for early nitrogen application decisions. *Agron. J.* **2001**, *93*, 783–789, doi:10.2134/agronj2001.934783x.
173. Devadas, R.; Lamb, D. W.; Backhouse, D.; Simpfendorfer, S. Sequential application of hyperspectral indices for delineation of stripe rust infection and nitrogen deficiency in wheat. *Precis. Agric.* **2015**, *16*, 477–491, doi:10.1007/s11119-015-9390-0.
174. Zhang, J.; Huang, Y.; Pu, R.; Gonzalez-Moreno, P.; Yuan, L.; Wu, K.; Huang, W. Monitoring plant diseases and pests through remote sensing technology: A review. *Comput. Electron. Agric.* **2019**, *165*, 104943, doi:10.1016/j.compag.2019.104943.
175. Shi, Y.; Huang, W.; González-Moreno, P.; Luke, B.; Dong, Y.; Zheng, Q.; Ma, H.; Liu, L. Wavelet-Based Rust Spectral Feature Set (WRSFs): A Novel Spectral Feature Set Based on Continuous Wavelet Transformation for Tracking Progressive Host–Pathogen Interaction of Yellow Rust on Wheat. *Remote Sens.* **2018**, *10*, 525, doi:10.3390/rs10040525.
176. Huang, W.; Lamb, D. W.; Niu, Z.; Zhang, Y.; Liu, L.; Wang, J. Identification of yellow rust in wheat using in-situ spectral reflectance measurements and airborne hyperspectral imaging. *Precis. Agric.* **2007**, *8*, 187–197, doi:10.1007/s11119-007-9038-9.
177. Zhang, J.-C.; Pu, R.; Wang, J.; Huang, W.; Yuan, L.; Luo, J. Detecting powdery mildew of winter wheat using leaf level hyperspectral measurements. *Comput. Electron. Agric.* **2012**, *85*, 13–23, doi:10.1016/j.compag.2012.03.006.
178. Xu, H. R.; Ying, Y. B.; Fu, X. P.; Zhu, S. P. Near-infrared Spectroscopy in detecting Leaf Miner Damage on Tomato Leaf. *Biosyst. Eng.* **2007**, *96*, 447–454, doi:10.1016/j.biosystemseng.2007.01.008.

179. Zhang, J.; Yuan, L.; Pu, R.; Loraamm, R. W.; Yang, G.; Wang, J. Comparison between wavelet spectral features and conventional spectral features in detecting yellow rust for winter wheat. *Comput. Electron. Agric.* **2014**, *100*, 79–87, doi:10.1016/j.compag.2013.11.001.
180. Gladders, P.; Paveley, N. D.; Barrie, I. A.; Hardwick, N. V; Hims, M. J.; Langton, S.; TaylorAYLOR, M. C. Agronomic and meteorological factors affecting the severity of leaf blotch caused by Mycosphaerella graminicola in commercial wheat crops in England. *Ann. Appl. Biol.* **2001**, *138*, 301–311, doi:10.1111/j.1744-7348.2001.tb00115.x.
181. Palmer, C.-L.; Skinner, W. Mycosphaerella graminicola: latent infection, crop devastation and genomics. *Mol. Plant Pathol.* **2002**, *3*, 63–70, doi:10.1046/j.1464-6722.2002.00100.x.
182. Royle, D. J.; Shaw, M. W.; Cook, R. J. Patterns of development of Septoria nodorum and S. tritici in some winter wheat crops in Western Europe, 1981-83. *Plant Pathol.* **1986**, *35*, 466–476, doi:10.1111/j.1365-3059.1986.tb02044.x.
183. Cao, X.; Luo, Y.; Zhou, Y.; Duan, X.; Cheng, D. Detection of powdery mildew in two winter wheat cultivars using canopy hyperspectral reflectance. *Crop Prot.* **2013**, *45*, 124–131, doi:10.1016/j.cropro.2012.12.002.
184. Mahlein, A.-K.; Kuska, M. T.; Thomas, S.; Bohnenkamp, D.; Alisaac, E.; Behmann, J.; Wahabzada, M.; Kersting, K. Plant disease detection by hyperspectral imaging: from the lab to the field. *Adv. Anim. Biosci.* **2017**, *8*, 238–243, doi:10.1017/S2040470017001248.
185. Yuan, L.; Pu, R.; Zhang, J.; Wang, J.; Yang, H. Using high spatial resolution satellite imagery for mapping powdery mildew at a regional scale. *Precis. Agric.* **2016**, *17*, 332–348, doi:10.1007/s11119-015-9421-x.
186. Khanal, S.; Fulton, J.; Shearer, S. An overview of current and potential applications of thermal remote sensing in precision agriculture. *Comput. Electron. Agric.* **2017**, *139*, 22–32, doi:10.1016/j.compag.2017.05.001.
187. Bauriegel, E.; Herppich, W. Hyperspectral and Chlorophyll Fluorescence Imaging for Early Detection of Plant Diseases, with Special Reference to Fusarium spec. Infections on Wheat. *Agriculture* **2014**, *4*, 32–57, doi:10.3390/agriculture4010032.
188. Teng, P. S.; Johnson, K. B. Analysis of Epidemiological Components in Yield Loss Assessment. In *Experimental Techniques in Plant Disease Epidemiology*; Springer Berlin Heidelberg: Berlin, Heidelberg, 1988; pp. 179–189.
189. Nutter, F. W.; Teng, P. S.; Royer, M. H. Terms and Concepts for Yield, Crop Loss, and Disease Thresholds. *Plant Pathol. Microbiol. Publ.* **1993**, *63*, 211–215, doi:10.1094/PD-77-211.
190. Ash, G.; Brown, J. Effect of Nitrogen Nutrition of the Host on the Epidemiology of Puccinia Striiformis F.sp. Tritici and Crop Yield in Wheat. *Australas. Plant Pathol.* **1991**, *20*, 108, doi:10.1071/APP9910108.
191. Devadas, R.; Simpfendorfer, S.; Backhouse, D.; Lamb, D. W. Effect of stripe rust on the yield response of wheat to nitrogen. *Crop J.* **2014**, *2*, 201–206, doi:10.1016/j.cj.2014.05.002.
192. Shah, D. A.; Paul, P. A.; De Wolf, E. D.; Madden, L. V. Predicting plant disease epidemics from functionally represented weather series. *Philos. Trans. R. Soc. B Biol. Sci.* **2019**, *374*, doi:10.1098/rstb.2018.0273.
193. McintINTOSH, R. A. Close genetic linkage of genes conferring adult-plant resistance to leaf rust and stripe rust in wheat. *Plant Pathol.* **2007**, *41*, 523–527, doi:10.1111/j.1365-3059.1992.tb02450.x.
194. Röll, G.; Batchelor, W.; Castro, A.; Simón, M.; Graeff-Hönninger, S. Development and

Evaluation of a Leaf Disease Damage Extension in Cropsim-CERES Wheat. *Agronomy* **2019**, *9*, 120, doi:10.3390/agronomy9030120.

195. Bastiaans, L. Ecology and Epidemiology Ratio Between Virtual and Visual Lesion Size as a Measure to Describe Reduction in Leaf Photosynthesis of Rice Due to Leaf Blast. *Phytopathology* 1991, *81*, 611–615.
196. Delécolle, R.; Maas, S. J.; Guérif, M.; Baret, F. Remote sensing and crop production models: present trends. *ISPRS J. Photogramm. Remote Sens.* **1992**, *47*, 145–161, doi:10.1016/0924-2716(92)90030-D.
197. Roerink, G. J.; Menenti, M.; Verhoef, W. Reconstructing cloudfree NDVI composites using Fourier analysis of time series. *Int. J. Remote Sens.* **2000**, *21*, 1911–1917, doi:10.1080/014311600209814.
198. Faivre, R.; Goffinet, B.; Wallach, D. Utilisation de Donnees Intermediaires pour Corriger la Prediction de Modeles Mecanistes. *Biometrics* **1991**, *47*, 1, doi:10.2307/2532490.
199. Bastiaanssen, W. G. M.; Ali, S. *Remote sensing in water resources management: The state of the art.*; International Water Management Institute: Colombo, Sri Lanka, 1998; ISBN 92-9090-363-5.
200. Nouvellon, Y.; Moran, M. S.; Seen, D. Lo; Bryant, R.; Rambal, S.; Ni, W.; Bégué, A.; Chehbouni, A.; Emmerich, W. E.; Heilman, P.; Qi, J. Coupling a grassland ecosystem model with Landsat imagery for a 10-year simulation of carbon and water budgets. *Remote Sens. Environ.* **2001**, *78*, 131–149, doi:10.1016/S0034-4257(01)00255-3.
201. Ritchie, J. T. Soil water balance and plant water stress. In *Understanding Options for Agricultural Production*; 1998; pp. 41–54.
202. Martre, P.; Wallach, D.; Asseng, S.; Ewert, F.; Jones, J. W.; Rötter, R. P.; Boote, K. J.; Ruane, A. C.; Thorburn, P. J.; Cammarano, D.; Hatfield, J. L.; Rosenzweig, C.; Aggarwal, P. K.; Angulo, C.; Basso, B.; Bertuzzi, P.; Biernath, C.; Brisson, N.; Challinor, A. J.; Doltra, J.; Gayler, S.; Goldberg, R.; Grant, R. F.; Heng, L.; Hooker, J.; Hunt, L. A.; Ingwersen, J.; Izaurralde, R. C.; Kersebaum, K. C.; Müller, C.; Kumar, S. N.; Nendel, C.; O'leary, G.; Olesen, J. E. J. E.; Osborne, T. M.; Palosuo, T.; Priesack, E.; Ripoche, D.; Semenov, M. A.; Shcherbak, I.; Steduto, P.; Stöckle, C. O.; Stratonovitch, P.; Streck, T.; Supit, I.; Tao, F.; Travasso, M.; Waha, K.; White, J. W.; Wolf, J.; Rötter, R. P.; Boote, K. J.; Ruane, A. C.; Thorburn, P. J.; Cammarano, D.; Hatfield, J. L.; Rosenzweig, C.; Aggarwal, P. K.; Angulo, C.; Basso, B.; Bertuzzi, P.; Biernath, C.; Brisson, N.; Challinor, A. J.; Doltra, J.; Gayler, S.; Goldberg, R.; Grant, R. F.; Heng, L.; Hooker, J.; Hunt, L. A.; Ingwersen, J.; Izaurralde, R. C.; Kersebaum, K. C.; M??ller, C.; Kumar, S. N.; Nendel, C.; O'leary, G.; Olesen, J. E. J. E.; Osborne, T. M.; Palosuo, T.; Priesack, E.; Ripoche, D.; Semenov, M. A.; Shcherbak, I.; Steduto, P.; St??ckle, C. O.; Stratonovitch, P.; Streck, T.; Supit, I.; Tao, F.; Travasso, M.; Waha, K.; White, J. W.; Wolf, J. Multimodel ensembles of wheat growth: Many models are better than one. *Glob. Chang. Biol.* **2015**, *21*, 911–925, doi:10.1111/gcb.12768.
203. Rötter, R. P.; Palosuo, T.; Kersebaum, K. C.; Angulo, C.; Bindi, M.; Ewert, F.; Ferrise, R.; Hlavinka, P.; Moriondo, M.; Nendel, C.; Olesen, J. E.; Patil, R. H.; Ruget, F.; Takáč, J.; Trnka, M. Simulation of spring barley yield in different climatic zones of Northern and Central Europe: A comparison of nine crop models. *F. Crop. Res.* **2012**, *133*, 23–36, doi:10.1016/j.fcr.2012.03.016.
204. Röll, G.; Memic, E.; Graeff-Hönninger, S. Multi-Model Approach for the Simulation of

Wheat Yields under different nitrogen application rates – implementation of an automatic calibration method for the DSSAT Wheat Models. *Am. Soc. Agron.* **2020**.

205. Wolf, J. Comparison of two potato simulation models under climate change. I. Model calibration and sensitivity analyses. *Clim. Res.* **2002**, *21*, 173–186, doi:10.3354/cr021173.
206. Gourdji, S. M.; Sibley, A. M.; Lobell, D. B. Global crop exposure to critical high temperatures in the reproductive period: Historical trends and future projections. *Environ. Res. Lett.* **2013**, *8*, doi:10.1088/1748-9326/8/2/024041.
207. Liu, C.; Allan, R. P. Observed and simulated precipitation responses in wet and dry regions 1850–2100. *Environ. Res. Lett.* **2013**, *8*, 034002, doi:10.1088/1748-9326/8/3/034002.
208. Porter, J. R.; Semenov, M. A. Crop responses to climatic variation. *Philos. Trans. R. Soc. B Biol. Sci.* **2005**, *360*, 2021–2035, doi:10.1098/rstb.2005.1752.
209. Lehmann, N.; Finger, R.; Klein, T. Optimizing Wheat Management towards Climate Change: A Genetic Algorithms Approach. In *Applied Simulation and Modelling*; ACTAPRESS: Calgary,AB,Canada, 2011.
210. Asseng, S.; Kheir, A. M. S.; Kassie, B. T.; Hoogenboom, G.; Abdelaal, A. I. N.; Haman, D. Z.; Ruane, A. C. Can Egypt become self-sufficient in wheat? *Environ. Res. Lett.* **2018**, *13*, doi:10.1088/1748-9326/aada50.
211. Asseng, S.; Martre, P.; Maiorano, A.; Rötter, R. P.; O'Leary, G. J.; Fitzgerald, G. J.; Girousse, C.; Motzo, R.; Giunta, F.; Babar, M. A.; Reynolds, M. P.; Kheir, A. M. S.; Thorburn, P. J.; Waha, K.; Ruane, A. C.; Aggarwal, P. K.; Ahmed, M.; Balkovič, J.; Basso, B.; Biernath, C.; Bindi, M.; Cammarano, D.; Challinor, A. J.; De Sanctis, G.; Dumont, B.; Eyshi Rezaei, E.; Fereres, E.; Ferrise, R.; Garcia-Vila, M.; Gayler, S.; Gao, Y.; Horan, H.; Hoogenboom, G.; Izaurralde, R. C.; Jabloun, M.; Jones, C. D.; Kassie, B. T.; Kersebaum, K. C.; Klein, C.; Koehler, A. K.; Liu, B.; Minoli, S.; Montesino San Martin, M.; Müller, C.; Naresh Kumar, S.; Nendel, C.; Olesen, J. E.; Palosuo, T.; Porter, J. R.; Priesack, E.; Ripoche, D.; Semenov, M. A.; Stöckle, C.; Stratonovitch, P.; Streck, T.; Supit, I.; Tao, F.; Van der Velde, M.; Wallach, D.; Wang, E.; Webber, H.; Wolf, J.; Xiao, L.; Zhang, Z.; Zhao, Z.; Zhu, Y.; Ewert, F. Climate change impact and adaptation for wheat protein. *Glob. Chang. Biol.* **2019**, *25*, 155–173, doi:10.1111/gcb.14481.
212. Wagner-Riddle, C.; Gillespie, T. J.; Hunt, L. A.; Swanton, C. J. Modeling a Rye Cover Crop and Subsequent Soybean Yield. *Agron. J.* **1997**, *89*, 208–218, doi:10.2134/agronj1997.00021962008900020010x.
213. Richardson, C. W.; Wright, D. A. WGEN: A Model for Generating Daily Weather Variables. *United States Dep. Agric. Agric. Res. Serv. ARS-8* **1984**, 83.
214. Geng, S. H. U.; Penning de Vries, F. W. T.; Supit, I. A simple method for generating daily rainfall data. *Agric. For. Meteorol.* **1986**, *36*, 363–376.
215. Soltani, A.; Hoogenboom, G. Assessing crop management options with crop simulation models based on generated weather data. *F. Crop. Res.* **2007**, *103*, 198–207, doi:10.1016/j.fcr.2007.06.003.
216. Hayhoe, H. Improvements of stochastic weather data generators for diverse climates. *Clim. Res.* **2000**, *14*, 75–87, doi:10.3354/cr014075.
217. Wallis, T. W. R.; Griffiths, J. F. An assessment of the weather generator (WXGEN) used in the erosion/productivity impact calculator (EPIC). *Agric. For. Meteorol.* **1995**, *73*, 115–133, doi:10.1016/0168-1923(94)02172-G.

218. Link, J.; Graeff, S.; Batchelor, W. D.; Claupein, W. Evaluating the economic and environmental impact of environmental compensation payment policy under uniform and variable-rate nitrogen management. *Agric. Syst.* **2006**, *91*, 135–153, doi:10.1016/j.agsy.2006.02.003.
219. Yost, M. A.; Kitchen, N. R.; Sudduth, K. A.; Massey, R. E.; Sadler, E. J.; Drummond, S. T.; Volkmann, M. R. A long-term precision agriculture system sustains grain profitability. *Precis. Agric.* **2019**, *20*, 1177–1198, doi:10.1007/s11119-019-09649-7.
220. Colaço, A. F.; Bramley, R. G. V. Do crop sensors promote improved nitrogen management in grain crops? *F. Crop. Res.* **2018**, *218*, 126–140, doi:10.1016/j.fcr.2018.01.007.
221. OECD Farm Management Practices to Foster Green Growth, OECD Green Growth Studies 2016.
222. Gandorfer, M.; Meyer-Aurich, A. Economic Potential of Site-Specific Fertiliser Application and Harvest Management. **2017**, 79–92, doi:10.1007/978-3-319-68715-5_3.
223. Lambert, D. M.; Lowenberg-DeBoer, J.; Malzer, G. L. Economic analysis of spatial-temporal patterns in corn and soybean response to nitrogen and phosphorus. *Agron. J.* **2006**, *98*, 43–54, doi:10.2134/agronj2005.0005.
224. Liu, Y.; Swinton, S. M.; Miller, N. R. Is Site-Specific Yield Response Consistent over Time? Does It Pay? *Am. J. Agric. Econ.* **2006**, *88*, 471–483, doi:10.1111/j.1467-8276.2006.00872.x.
225. Lukina, E. V.; Freeman, K. W.; Wynn, K. J.; Thomason, W. E.; Mullen, R. W.; Stone, M. L.; Solie, J. B.; Klatt, A. R.; Johnson, G. V.; Elliott, R. L.; Raun, W. R. NITROGEN FERTILIZATION OPTIMIZATION ALGORITHM BASED ON IN-SEASON ESTIMATES OF YIELD AND PLANT NITROGEN UPTAKE. *J. Plant Nutr.* **2001**, *24*, 885–898, doi:10.1081/PLN-100103780.
226. Link, J.; Graeff, S.; Batchelor, W. D.; Claupein, W. Evaluating the economic and environmental impact of environmental compensation payment policy under uniform and variable-rate nitrogen management. *Agric. Syst.* **2006**, *91*, 135–153, doi:10.1016/j.agsy.2006.02.003.
227. Alcoz, M. M.; Hons, F. M.; Haby, V. A. Nitrogen Fertilization Timing Effect on Wheat Production, Nitrogen Uptake Efficiency, and Residual Soil Nitrogen. *Agron. J.* **1993**, *85*, 1198–1203, doi:10.2134/agronj1993.00021962008500060020x.
228. Hamid, A. Efficiency of N uptake by wheat, as affected by time and rate of application, using N15-labelled ammonium sulphate and sodium nitrate. *Plant Soil* **1972**, *37*, 389–394, doi:10.1007/BF02139981.
229. Schulz, R.; Makary, T.; Hubert, S.; Hartung, K.; Gruber, S.; Donath, S.; Döhler, J.; Weiß, K.; Ehrhart, E.; Claupein, W.; Piepho, H.-P.; Pekrun, C.; Müller, T. Is it necessary to split nitrogen fertilization for winter wheat? On-farm research on Luvisols in South-West Germany. *J. Agric. Sci.* **2015**, *153*, 575–587, doi:10.1017/S0021859614000288.
230. Gerwing, J. R.; Caldwell, A. C.; Goodroad, L. L. Fertilizer Nitrogen Distribution Under Irrigation Between Soil, Plant, and Aquifer. *J. Environ. Qual.* **1979**, *8*, 281–284, doi:10.2134/jeq1979.00472425000800030003x.
231. P. Varshney; R. S. Kanwar; J. L. Baker; C. E. Anderson Tillage and Nitrogen Management Effects on Nitrate-Nitrogen in the Soil Profile. *Trans. ASAE* **1993**, *36*, 783–789, doi:10.13031/2013.28398.
232. Bly, A. G.; Woodard, H. J. Foliar nitrogen application timing influence on grain yield and

protein concentration of hard red winter and spring wheat. *Agron. J.* **2003**, *95*, 335–338, doi:10.2134/agronj2003.0335.

233. Müller, S.; Ansorge, H.; Weigert, I. Einfluß der Stickstoffdüngung auf Ertrag, Ertragsstruktur und N-Verwertung von Winterweizen - Möglichkeiten und Grenzen der Bestandesführung. *Zeitschrift für Pflanzenernährung und Bodenkd.* **1991**, *154*, 115–119, doi:10.1002/jpln.19911540207.
234. Beaudoin, N.; Saad, J. K.; Van Laethem, C.; Machet, J. M.; Maucorps, J.; Mary, B. Nitrate leaching in intensive agriculture in Northern France: Effect of farming practices, soils and crop rotations. *Agric. Ecosyst. Environ.* **2005**, *111*, 292–310, doi:10.1016/j.agee.2005.06.006.
235. Šima, T.; Nozdrovický, L.; Krištof, K.; Dubeňová, M.; Krupička, J. Impact of the quality of work of fertiliser spreader on nitrous oxide emissions released from soil to the atmosphere. *Agron. Res.* **2014**, *12*, 171–178.
236. Noh, H. K.; Zhang, Q.; Han, S. Sensor based variable rate application of nitrogen by using a multi-spectral image sensor. *ASAE Annu. Int. Meet. 2004* **2004**, *0300*, 963–979, doi:10.13031/2013.17063.
237. Chan, C. W.; Schueller, J. K.; Miller, W. M.; Whitney, J. D.; Cornell, J. A. Error sources affecting variable rate application of nitrogen fertilizer. *Precis. Agric.* **2004**, *5*, 601–616, doi:10.1007/s11119-004-6345-2.
238. Koch, B.; Khosla, R.; Frasier, W. M.; Westfall, D. G.; Inman, D. Economic Feasibility of Variable-Rate Nitrogen Application Utilizing Site-Specific Management Zones. *Agron. J.* **2004**, *96*, 1572–1580, doi:10.2134/agronj2004.1572.
239. Khongnawang, T.; Zare, E.; Zhao, D.; Srihabun, P.; Triantafilis, J. Three-Dimensional Mapping of Clay and Cation Exchange Capacity of Sandy and Infertile Soil Using EM38 and Inversion Software. *Sensors* **2019**, *19*, 3936, doi:10.3390/s19183936.
240. Kelley, J.; Higgins, C. W.; Pahlow, M.; Noller, J. Mapping Soil Texture by Electromagnetic Induction: A Case for Regional Data Coordination. *Soil Sci. Soc. Am. J.* **2017**, *81*, 923–931, doi:10.2136/sssaj2016.12.0432.
241. Heil, K.; Schmidhalter, U. Characterisation of soil texture variability using the apparent soil electrical conductivity at a highly variable site. *Comput. Geosci.* **2012**, *39*, 98–110, doi:10.1016/j.cageo.2011.06.017.
242. Jones, J. W.; Antle, J. M.; Basso, B.; Boote, K. J.; Conant, R. T.; Foster, I.; Godfray, H. C. J.; Herrero, M.; Howitt, R. E.; Janssen, S.; Keating, B. A.; Munoz-Carpena, R.; Porter, C. H.; Rosenzweig, C.; Wheeler, T. R. Brief history of agricultural systems modeling. *Agric. Syst.* **2017**, *155*, 240–254, doi:10.1016/j.agsy.2016.05.014.
243. Robert, C.; Fournier, C.; Andrieu, B.; Ney, B. Coupling a 3D virtual wheat (Triticum aestivum) plant model with a Septoria tritici epidemic model (Septo3D): a new approach to investigate plant-pathogen interactions linked to caonpy architecture. *Funct. Plant Biol.* **2008**, *35*, 997–1013.
244. He, W.; Yang, J. Y.; Zhou, W.; Drury, C. F.; Yang, X. M.; Reynolds, W. D.; Wang, H.; He, P.; Li, Z. T. Sensitivity analysis of crop yields, soil water contents and nitrogen leaching to precipitation, management practices and soil hydraulic properties in semi-arid and humid regions of Canada using the DSSAT model. *Nutr. Cycl. Agroecosystems* **2016**, *106*, 201–215, doi:10.1007/s10705-016-9800-3.

Acknowledegements / Danksagung

Ganz herzlich möchte ich mich bei Frau **Prof. Dr. Graeff – Hönninger** für die Möglichkeit bedanken, dieses Forschungsthema in Ihrer Arbeitsgruppe im Rahmen meiner Promotion zu bearbeiten. Ebenfalls bedanke ich mich für die Unterstützung in allen fachlichen Fragen sowie in allen Herausforderungen im Zeitraum der Promotion.

Besonderen Dank ebenfalls an Herrn **Prof. Dr. Hans-Peter Kaul** für die Übernahme des Zweitgutachtens, sowie bei Herrn **Prof. Dr. Torsten Müller** für die Bereitschaft als Drittgutachters dieser Arbeit.

Further, I want to thank **Prof. Dr. William D. Batchelor** for the pleasant stay and the productive work at the Auburn University.

Ein weiteres Dankeschön an die gesamte Arbeitsgruppe, für die angenehme Zeit und die tatkräftige Unterstützung. Insbesondere an Herrn **Dr. Sebastian Munz** und Herrn **Emir Memic** für die Hilfestellung bei Modellierungsfragen. Weiterhin richte ich einen ganz besonderen Dank an Frau **Andrea Richter**, die mich in allen Versuchen unermütlich unterstützt hat. Weiteren Dank an Frau **Birgit Beierl**, Frau **Yasha Auer** und Frau **Martina Pertsch** für die Unterstützung.

Ebenfalls bedanke ich mich beim ganzen Team des Ihinger Hofs für die Unterstützung für die Mitorganisation der Feldversuche. Ganz besonders Herrn **Markus Pflugfelder**, **Sebastian Böckle, Martin Zahner, Marianne Häfner**, **Andreas Lohrer** und **Stefan Knapp**.

Weiterhin danke ich dem Fachgebiet Biostatistik von Herrn **Prof. Dr. Piepho**, ganz besonders Herrn **Dr. Jens Hartung** für die Unterstützung und für ein allzeit offenes Ohr.

Zusätzlich bedanke ich mich bei Herrn **Sebastian Schwabe** für die konstruktiven Gespräche während des Genusses orientalischer Köstlichkeiten.

Ein ganz herzliches Dankeschön an meine ganze Familie für den tatkräftigen Beistand, in allen Lebenslagen ohne die diese Dissertation nicht möglich geworden wäre. Ganz besonders danke ich meiner Freundin für die Unterstützung in schwierigen Zeiten.

Zum Schluss bedanke ich mich bei der **Deutschen Bundesstiftung Umwelt** (**DBU)** für die Finanzierung dieses interessanten Forschungsthemas.

Eidesstattliche Erklärung

Eidesstattliche Versicherung über die eigenständig erbrachte Leistung

gemäß § 18 Absatz 3 Satz 5 der Promotionsordnung der Universität Hohenheim für die Fakultäten Agrar-, Natur- sowie Wirtschafts- und Sozialwissenschaften

1. Bei der eingereichten Dissertation zum Thema

Combining Remote Sensing and Crop Modeling Techniques to Derive a Nitrogen Fertilizer Application Strategy

handelt es sich um meine eigenständig erbrachte Leistung.

2. Ich habe nur die angegebenen Quellen und Hilfsmittel benutzt und mich keiner unzulässigen Hilfe Dritter bedient. Insbesondere habe ich wörtlich oder sinngemäß aus anderen Werken übernommene Inhalte als solche kenntlich gemacht.

3. Ich habe nicht die Hilfe einer kommerziellen Promotionsvermittlung oder -beratung in Anspruch genommen.

4. Die Bedeutung der eidesstattlichen Versicherung und der strafrechtlichen Folgen einer unrichtigen oder unvollständigen eidesstattlichen Versicherung sind mir bekannt.

Die Richtigkeit der vorstehenden Erklärung bestätige ich. Ich versichere an Eides Statt, dass ich nach bestem Wissen die reine Wahrheit erklärt und nichts verschwiegen habe.

Ort, Datum

Unterschrift

CV

Georg Roell

E-mail: georg.roell@hotmail.de

PROFESSIONAL EXPERIENCE

04.2020 – present	**Customer Consultant** **Amphasys AG (CH)** Main Focus: International Customer Consulting and Training and Project Management in Single Cell Analysis
05.2016 – 03.2020	**Scientific worker and Doctoral Student at University of Hohenheim (DE)** Main Focus: Optimizing of Nitrogen Application in Wheat by using Precision Farming (Remote Sensing) and Crop Modeling (CERES, CropSim, NWheat)

Dissertation: Development of Model-based Nitrogen Application Strategy by Integration of Nitrogen Sensor Data into a Site-specific Crop Model.

03.2015 - 11.2015/ 03.2014 - 11.2014	**KWS SAAT SE breeding station, Seligenstadt (DE); Working student** Main Focus: Field trials in breeding (Establishing and leading field trials Breeding in Sugar Beet, Maize and Oilseed Rape)
02.2012 - 06.2012	„**Landwirtschaftlicher Betrieb Darnstedt“, Darnstedt (DE)** **Agricultural manager** Farm Management and Business Administration (Crops: Wheat, Barley, and Oilseed Rape)
03.2010 - 07.2010	**Internship Bayer CropScience Deutschland GmbH, Langenfeld (DE)** Main Focus: Field trials in plant protection (Establishing and leading field trials in Sugar Beet, Maize, Wheat, Rye, Oilseed Rape, and Viticulture)

INTERNATIONAL EXPERIENCE

03.2018	**Maricopa phenotyping workshop at University of Arizona, AZ, USA**

02.2017 - 03.2017	**Guest Researcher, Department Biosystems Engineering Auburn University, Al, USA** Extension of CSM-CERES Wheat Modell to simulate the effect of plant diseases
07.2012 - 10.2012	**Internship at „Levke & Peter Eggers“ farm, Kanada (Alberta)** Main Focus: Farming und Pasture Farming (cattle, sheep)

EDUCATION

WS 2012/2013 - WS 2015/2016	**Masters degree in Agricultural Science at Universität Hohenheim** (final grade: 1.6) Main Focus: Plant production and agricultural trials

Master Thesis: Simulation of Germination Conditions of Sugar Beet by using Different Soil Temperature Models. (Grade 1.0)

WS 2007/08 – WS 2011/2012	**Diploma in agriculture (agricultural engineering graduate), University of applied sciences Weihenstephan** – Triesdorf (DE) (final grade: 2.5) Main Focus: Plant Production, Animal Produktion, Agricultural Economics and Renewable Energy

Diploma Thesis: Influence of Plant Growth Regulator „Carax“ on different Oilseed rape varieties. (Grade 1.0)

08/2005 – 07/2007	**Technical college, Weihenstephan-Triesdorf (DE),** advanced technical college certificate

SKILLS

Language:	German (frist language), Englisch (fluent)
Computer:	MS Office (very good) Fortran (good) Python (basic) QGIS (good) SAS (good) R (basic)

_____ _____

Place, date Signature